SAN099-2100 J

To be submitted to Macromol. Chem. & Phys. (Invited Feature Article)

A quantitative study of tethered chains in various solution conditions using Langmuir diblock copolymer monolayers

M.S. Kent

Sandia National Laboratories, Albuquerque, NM.

ABSTRACT

This article summarizes our investigations of tethered chain systems using Langmuir monolayers of polydimethysiloxane-polystyrene (PDMS-PS) diblock copolymers on organic liquids. In this system, the PDMS block adsorbs to the air surface while the PS block dangles into the subphase liquid. The air surface can be made either repulsive or attractive for the tethered PS chain segments by choosing a subphase liquid which has a surface tension lower or greater than that of PS, respectively. The segment profile of the PS block is determined by neutron reflection as a function of the surface density, the molecular weights of the PS and PDMS blocks, and the solution conditions. We cover the range of reduced surface density (Σ) characteristic of the large body of data in the literature for systems of chains tethered onto solid surfaces from dilute solution in good or theta solvent conditions ($\Sigma < 12$). We emphasize quantitative comparisons with analytical profile forms and scaling predictions. We find that the strong-stretching limit invoked in analytical SCF and scaling theories is not valid over this Σ range. On the other hand, over a large portion of this range ($\Sigma < 5$) tethered layers are well described by a renormalization group theory addressing weakly interacting or noninteracting chains. Simultaneous with the study of the profile form, the free energy of the chains is examined through the surface tension. A strong increase in the surface pressure is observed with increasing surface density which determines the maximum surface density which can be achieved. This apparently nonequilibrium effect is attributed to steric interactions and limited lateral interpenetration. This effect may explain several outstanding discrepancies regarding the adsorption of end-functionalized chains and diblock copolymers onto solid surfaces.

This work was supported by the U.S. Department of Energy under contract DE-AC04-94AL85000. Sandia is a multiprogram laboratory operated by Sandia Corporation, a Lockheed Martin Company, for the United States Department of Energy.

I. Introduction.

Tethered polymer chains are a class of polymer microstructures distinguished by the fact that chain molecules are anchored by only one end to a surface or an interface.[1,2] The fact that the polymer chains are only attached by one end to the tethering surface leads to segment profiles which differ from those obtained for the more common case in which all the segments can adsorb at the surface. These structures have been investigated largely for their potential to impart important properties to surfaces. However, tethered chains also occur in various microphases of block copolymers. In addition, they provide an interesting system to examine the balance of enthalpic and entropic contributions to free energy in confined geometries. Our focus is on layers of tethered chains in contact with a low molecular weight solvent. This is the case for many practical applications of tethered chains. In addition, while there are also important applications where tethered chains are in contact with a medium other than a solvent, the layers are often formed from solution. Practical uses of tethered chains include controlling adhesion,[3-9] lubrication,[10-12] or wetting[13,14] properties of surfaces, controlling flocculation in colloidal dispersions,[15,16] inhibiting protein adsorption,[17-22] extending lifetimes of drug delivery vehicles in the blood stream,[23-25] immobilization of enzymes in biosensors,[26] and controlling solvent flow through filters.[27]

cell detachment Biomaterials 16(1995)2

The segment density distribution within the layer strongly influences many important properties. For example, adhesive strength between a tethered layer and a polymer melt is maximized with an intermediate surface density and high molecular weight which allows for interpenetration and entanglement with matrix chains.[4-6,9] To inhibit flocculation in colloidal dispersions, particles must be kept from approaching to a distance where the interparticle attractive forces are high.[15,16] Lubrication is best achieved with short chains at very high packing density such that little energy dissipation occurs when contacting a sliding surface.[12] For inhibiting protein adsorption, high

DISCLAIMER

DISCLAIMER

Portions of this document may be illegible in electronic image products. Images are produced from the best available original document.

grafting density is most effective for small proteins, whereas increased layer thickness is most effective for large proteins.[17]

In order to design layers which are optimized for particular desired properties, one must understand how the segment density distribution varies with molecular parameters, solution conditions, and geometry as well as the free energy changes which occur upon deformation. Important factors include the surface density of chains (σ), the average chain length, the distribution of chain lengths, the quality of the solvent medium for the tethered chain segments, the nature of the interaction of the segments with the tethering surface (attractive, neutral , or repulsive), the presence of free chains in the solution, and the geometry of the surface. A further important consideration is the role of nonequilibrium effects during the tethering process.

Tremendous work has been undertaken in the last ~20 years to understand this class of polymer structures.[1,2,10,16,28,29] Much is understood about the equilibrium structure of tethered layers, yet some important questions remain. At sufficiently low σ such that tethered chains do not interact with their neighbors, their dimension is roughly comparable to that for a free chain in dilute solution. As σ increases and the tethered chains come into contact, they stretch normal to the surface to reduce unfavorable interactions between segments. The stretching of the chains normal to the surface is limited by the elastic restoring force arising from the entropic penalty for configurations which deviate from a random walk. Theoretical work has provided analytical forms for the tethered chain segment density profiles in the limit of high surface density such that the chains are strongly-stretched,[1] and also in the limit of low surface density such that the chains are weakly interacting or noninteracting.[30] However, often these analytical expressions have been invoked without precise knowledge of the region of parameter space for which they are valid. One important goal of this work has been to determine the region of parameter space for which these limiting cases may be applied. Therefore, in the following we emphasize quantitative comparisons. We also address the degree of

interpenetration of free chains with tethered chains, which is important for controlling the interactions of polymers with surfaces.

Another challenging feature of tethered chain systems is to understand the factors which limit the maximum surface density which can be achieved. Interestingly, all systems of chains which are tethered from dilute solution in good or theta solvent conditions are limited to a similar range of reduced surface density Σ ($=\sigma\pi R_g^2$ where R_g is the dilute solution free chain radius of gyration), despite the fact that the anchoring energy among these systems varies by almost two orders of magnitude.[31-52] The case of chains tethered from dilute solution is particularly important for practical applications since specialized polymers are typically expensive. We seek to understand why layers prepared under these conditions are limited to this particular range of surface density. Moreover, there is a strong dependence of the resulting surface density on the concentration of chains in the solution from which they are tethered (concentrated regime).[53-56] To our knowledge there is no quantitative understanding of this limit on σ in dilute solution or of the strong concentration dependence of σ in the concentrated regime. These are some of the main points addressed in this article.

A number of theoretical approaches have been applied to the study of tethered chain systems. These include scaling approaches,[57-60] analytical[2,62-66] and numerical[65-74] self-consistent field (SCF) calculations, a single-chain mean field statistical mechanical approach,[28] renormalization group theory,[30] and Monte Carlo (MC) and Molecular Dynamics (MD) simulations.[29] In the limit of high molecular weight and sufficiently high surface density such that fluctuations of a chain about its lowest free energy configuration can be neglected, SCF theory has provided analytical forms for the segment density profiles and free energy, as well as scaling relations of the profile characteristics with the molecular parameters in various geometries. The power law relations are equivalent to those derived previously using scaling arguments.[58,59] Following conventional terminology in this field, we refer to the regime of applicability of the

analytical SCF theory as the "strong-stretching" regime. While it is clear that $\Sigma >> 1$ for this regime, the precise range of Σ at which this limit is reached must be determined by experiment. We show below that this limit is not attained for the range of Σ achieved for chains tethered from dilute solution in good or theta solvents. In the limit of noninteracting chains ($\Sigma \leq 1$), the segment profile is independent of σ. We will refer to this limit as the "noninteracting" regime. For noninteracting or weakly interacting systems, analytical expressions for segment density profiles and the free energy have been derived using renormalization group theory.[30] Again, the theory does not specify the precise range of Σ for which this treatment applies. We show below that this limit is a good description of the layers for $\Sigma \leq 5$, which covers most of the data in the literature for chains tethered onto substrates from dilute solution.

Several approaches have been used to address regimes of surface density intermediate to these limiting cases. Numerical SCF calculations[65-74] and a single chain mean field statistical mechanical approach[29] are two principle theoretical methods. Molecular dynamics and Monte Carlo simulations[30] have also addressed the intermediate surface density regime.

For a complete understanding of tethered layers and to rigorously examine theoretical predictions, one would like to measure the detailed segment profile normal to the surface, the in-plane structure, the free energy of layers at equlilbrium, the free energy change upon deformation of the layers both parallel and normal to the surface, and the energy anchoring the chains to the surface. A number of experimental techniques have been employed to gather this information. Force-distance profiles for tethered layers compressed normal to the surface have been measured with the surface forces apparatus (SFA)[10,11,31-34,75-77] and atomic force microscope (AFM).[42,78,79] Segment profiles have been studied by neutron scattering and neutron reflection, using deuterium substitution to provide contrast between the tethered chain and the organic medium.[33,35-37,43-51,80-85] In-plane structure has been probed by AFM, both dry and in solution.[42,78,79,86-89]

In our approach to studying tethered chain systems we employ Langmuir monolayers of highly asymmetric polydimethysiloxane-polystyrene (PDMS-PS) diblock copolymers on the surface of an organic liquid.[44-52] This system is illustrated in Figure 1. The PDMS block anchors the copolymer to the surface, while the PS block dangles into the solvent. The magnitude of the surface tension of the subphase liquid relative to the surface tension of the PDMS block determines the anchoring energy, while the surface tension of the subphase liquid relative to that of the PS block detemines the nature of the interaction of the submerged block with the air surface. The surface tensions of the subphase liquids used in this study are shown in Figure 2 along with the surface tensions of PS and PDMS. Very high anchoring energies, reaching hundreds of kT, arise from the low surface tension of PDMS relative to the subphase liquid. Thus while the chains have translational mobility in the plane of the surface, they are very strongly attached to the surface. Regarding the interaction of the submerged block with the surface, we have investigated cases in which the air surface is strongly repulsive (EB and DOP) and weakly attractive (BrEB) for the PS block.

As the surface density increases, the copolymers interact with their neighbors on the surface. Depending upon the asymmetry of the copolymer (N_{PS} / N_{PDMS}, where N_i are the degrees of polymerization of the respective blocks), the interactions can occur either through the surface blocks ($N_{PDMS} >> N_{PS}$), through the submerged blocks ($N_{PDMS} << N_{PS}$), or through both blocks ($N_{PDMS} \cong N_{PS}$).

There are several advantages to studying tethered chains at the liquid-air interface. First, the free energy of the layer can be probed through surface tension measurements simultaneous with measurements of the structure of the layer by neutron reflection. We note that the neutron scattering length density of the PDMS block is nearly matched with that of air, and does not contribute to the reflectivity. Second, the surface density can be varied independently of the molecular weight (M) by compression in a Langmuir trough. This allows a detailed investigation of the onset of chain stretching, as well as a rigorous

test of scaling predictions. Third, the interaction of the submerged block with the surface can be controlled through the subphase surface tension.

Following a description of the experimental details, the results are presented in two sections. In section III.1 the detailed segmental profiles obtaiend by neutron reflection are examined for various solution conditions and molecular parameters. In section III.2, the free energy of interacting tethered layers is examined through surface tension measurements. The article ends with a summary of the most important conclusions from this work in section IV.

II. Experimental

Materials

The PDMS-PS diblock copolymers, and PS and PDMS homopolymers used in this work are described in Table 1. For the block copolymers, the sample code corresponds to the molecular weights (in kg/mol) of the PDMS and PS blocks, respectively. In most PDMS-PS samples, GPC traces typically reveal a small amount (< 5%) of PS-PDMS-PS triblock material. The subphase liquids ethyl benzoate, bromoethyl benzoate, and dioctyl phthalate were obtained from Aldrich and vacuum distilled before use. Deuterated ethyl benzoate was also used as a subphase, and was specially synthesized for this work by J. P. Roque (USTL, Montpellier, France). This material was also vacuum distilled just prior to use. Chloroform obtained from Aldrich was used as received for spreading the copolymer monolayers.

Procedures

Two methods of spreading the copolymer monolayers were used. For nearly all copolymer/subphase combinations, the copolymers spread from a dry grain deposited onto the surface of the subphase. However, spreading by this method was very slow on DOP due to its greater viscosity. For that reason, and to provide better control over the

surface density, spreading was also accomplished using dilute solutions of the copolymers in chloroform. Somewhat higher maximum pressures could be obtained using the former method than by spreading from a chloroform solution.

The surface density was typically varied by successive additions of spreading solution, or by aspiration of the surface, rather than by compresssion and expansion of the surface area with a movable barrier. The reason for this was the difficulty in obtaining a high miniscus, as required to obtain a clean reflection, while avoiding leakage around the Teflon barrier. Stability over a period of 2-6 hrs was required to collect the reflectivity data. Leakage around the barrier is a much more difficult problem with organic liquids than with water. A few such experiments were performed, but for the vast majority of the reflectivity experiments a movable barrier was not used. For the few experiments performed with a movable barrier, the isotherm and reflectivity data were in agreement with data obtained by the other method of varying coverage.

Surface tension was measured using the Wilhelmy plate technique. Although in some of our earliest work the surface pressure increased slightly during the reflectivity measurements for low σ due to an excess of copolymer in the subphase.[44] the surface pressure was never observed to decrease significantly during the experiments. This indicates that the surface pressure is not affected by short term relaxation within the monolayers. This is important with respect to understanding the large values of surface pressure which are observed, as discussed in Section 2.b. Detailed information regarding the spreading of the copolymers and the reproducibility and stability of the isotherms specific to each experiment can be found in the earlier articles.[44-52]

Neutron reflectivity was performed on the DESIR (Saclay), SPEAR (Los Alamos), and NG7 (NIST) reflectometers. The first two operate in the time of flight mode, while NG7 operates at fixed wavelength. The procedure used to fit the reflectivity data involved approximating the model profiles by a series of 2 Å thick slabs of constant concentration. and then calculating the reflectivity from the stack of layers using the

Fresnel equations with a Debye-Waller factor to describe the effect of roughness at the air surface.[90] The resolution, $\Delta q/q$ where Δq is the standard deviation of a Gaussian function, varied from 0.02 to 0.03. The precise value used for each data set was determined by fitting the reflectivity data for the pure solvent surface. As discussed in the results section, the data were analyzed using both theoretical and empirical profile forms. Best fit parameters were determined by the minimization of $\chi^2 = \Sigma((R_{exp}-R_{calc})^2/\sigma_{std}^2))/(N_{pts}-N_{param})$ using the Marquardt algorithm. Our goal in the fitting was to include the minimum amount of complexity demanded by the data. As a consequence, sharp corners and flat steps appear in certain segment concentration profiles which are clearly only approximations.

III. Results

III.1. Segment profile

Several important aspects of the segment concentration profiles can be obtained from neutron reflectivity. We focus on the following characteristics of the profile: the height of the layer (h), the location of the maximum in segment concentration, and the form of the fall-off in concentration with depth. As mentioned in the Introduction, the layer height has a strong influence on a number of important properties. In addition, the scaling of the layer height with σ and M can identify where experimental systems fall with respect to the limiting regimes described earlier. The location of the maximum has been a topic of interest, with numerical SCF,[65-72] SCMF,[29] and simulation[30] studies indicating a maximum at a depth well into the liquid for chains tethered to a repulsive, hard wall, whereas a number of experimental studies[35,36,53,54,80-83] have reported a maximum at the surface. Obtaining definitive results on this subject at a solid/liquid interface is challenging due to the difficulty of achieving a truly repulsive or noninteracting surface for the tethered chain (typically there is a weak attraction). The present experimental system provides good sensitivity to this feature, and the surface can be made unambiguously attractive or repulsive for the segments of the dangling block. Therefore, we pay special attention to this aspect in the discussion below. We begin with a discussion of the profile of the tethered PS blocks in a subphase liquid which is a good solvent and which also affords a repulsive surface for the PS segments. Following this we examine the influence of various solution conditions and molecular parameters on the profile.

III.1.a Good solvent, repulsive surface

EB is a good solvent for the submerged PS block,[91] and the air surface is repulsive for the PS block based on the surface tensions in Figure 2. For this case the magnitude of

the reflectivity signal is rather limited due to the low segment concentration in the swollen layer. Thus, while h can be obtained accurately over a wide range of σ (discussed further in section III.1.d.1), the detailed form of the profile can be determined only for the higher σ values. The profile form can be probed over a much wider range of σ at the theta temperatures (T_θ), as described in section III.1.c.

Figure 3a shows reflectivity data for a monolayer of 4.5-60 on EB for $\Sigma = 5.3$. The data are expressed as the ratio of the reflectivity from the monolayer-covered surface to the calculated reflectivity for the bare DOP surface with 3 Å roughness. This ratio indicates the magnitude of the signal from which the shape of the d-PS segmental profile is obtained. Roughly speaking, the peak position is a function of layer height. The decrease of R/R_o with q at higher q can be due to either a depletion layer or to roughness at the air surface. Much evidence, reviewed below, supports the depletion layer as the correct interpretation. Among the copolymers used in this study, the reflectivity for the 4.5-60 copolymer provides the greatest sensitivity to the depletion layer in good solvent conditions.[92] The magnitude of the oscillations in R/R_o with q is determined by the form of the body of the profile and the smoothness of the foot or tail.

The data in Figure 3a are compared to the best-fit curve obtained using the analytical SCF profile valid in the strong-stretching limit (dashed curve).[2,61,62] In this limit, the profile is described by $\phi = \phi_o[1-(z/L_o)^2$, where z is the depth from the surface. As observed in Figure 3a, the best-fit using this profile form is poor. Relative to the calculated curve, the data show weaker oscillations and a decrease in R/R_o with q beyond the main peak. The addition of a depletion layer and a smooth tail provides these features, and improves the fit substantially. However, still further significant improvement in the quality of the fit (χ^2 values reduced by roughly a factor of 2) can be obtained if the exponent is allowed to vary in the regression. In that case, the best fit is obtained with an exponent of 1.9. This suggests that the asymptotic strong-stretching limit is not obtained at this Σ, but requires higher Σ. Much more conclusive evidence for

this will be presented in the following sections. The solid curve in Figure 3a corresponds to the empirical profile described above, and is shown in Figure 3b.

The above comparison suggests that much of the accessible Σ range for the tethered layers on EB falls intermediate between the noninteracting and strongly-stretched regimes. Therefore, we have also compared empirical profiles derived fom the reflectvity data with profiles resulting from numerical SCF calculations using parameters corresponding to the experimental conditions.[70a] An example is given in Figure 3b for the 4.5-60 copolymer (dashed curve). Extensive comparison of experimental data with numerical and analytical SCF profiles indicates that the analytical SCF profile is not an adequate representation for the range of Σ accessible with this system ($\Sigma < 12$ in good solvent conditions).[70a]

We now discuss the effects of various molecular parameters and solution conditions on the tethered chain segment profile.

III.1.b Surface interaction

With the Langmuir monolayer system, the nature of the interaction of the PS segments with the air surface varies with the surface tension of the subphase liquid. The surface tension of BrEB is comparable to, but slightly greater than, that of PS. This makes the surface slightly attractive to the PS segments, and contrasts with the case of EB for which the air surface is strongly repulsive for the PS segments. Figure 4a shows reflectivity data for the 4.5-60 copolymer on BrEB for Σ from 4.8 to 9.9. Data for the bare BrEB suphase are also shown. We note that precise agreement between the reflectivity for the bare BrEB subphase and the calculated Fresnel curve was not obtained with BrEB, as shown in Figure 4a. Among the subphase liquids used, this occurrence was unique to BrEB. The slightly increased reflectivity for the bare subphase indicates a higher scattering length density near the air surface, apparently due to a bromine-containing contaminant. The pure solvent reflectivity curve shown in Figure 4a was

obtained repeatedly for different batches of freshly vacuum distilled BrEB. Therefore, a profile was fit to the reflectivity from the pure subphase and the fitted solvent profile was superimposed on the profile of the d-PS block in the analysis of data with the copolymer monolayer present.

The reflectivity for $\Sigma = 4.8$ in Figure 4a can be compared to the data in Figure 3a since the monolayers are at comparable surface densities. After accounting for the small effect of the contaminant, the reflectivity for 4.5-60 on BrEB differs in several aspects from the data on EB in Figure 3a: the peak is slightly broader and occurs at higher q in BrEB, no shoulder occurs following the main peak, and R/R_o is nearly independent of q beyond the main peak. The best-fit empirical profiles from the data in Figure 4a are shown in Figure 4b. In contrast to the profile in EB in Figure 3b, the maximum occurs at the surface. However, the segment concentration at the surface is relatively low, consistent with the fact that the surface tensions in Figure 2 indicate that the surface of BrEB is only weakly attractive to the PS segments. A segment volume fraction near unity would be expected in the case of a sufficiently strong attraction of the segments to the surface. In addition to the location of the maximum, there is an important difference in the curvature of the body of the profile. In Figure 4b, the curvature is negative within the body of the profile up to the maximum in contrast to the profile in EB.

Another signficant difference between the profiles in EB and BrEB for the 4.5-60 copolymer is that the layer heights are reduced in BrEB relative to the layer heights in EB. This is shown in Figure 4c, where the layer heights in BrEB and EB are compared for a range of Σ for the 4.5-60 and 20-170 copolymers. The layer heights are roughly 20 % reduced in BrEB relative to the values in EB for the 4.5-60 copolymer. The layer heights for the 4-30 copolymer (not shown) are also reduced in BrEB relative to that in EB. On the other hand, the layer heights are nearly the same in BrEB and EB for both the 20-170 and 28-330 (not shown) copolymers. Apparently the layer height is

sufficiently large for the latter two copolymers that the effect of the perturbation in the profile near the surface is insignificant.

Thus Figures 3 and 4 demonstrate that the maximum can occur either at the surface or at a depth into the subphase depending upon the nature of the segment-surface interaction. It is quite common for polymers in a solvent medium to have a slight attraction to a solid surface. This likely explains the lack of a depletion layer in a number of such studies[35,36,53,54,80-83]

III.1.c Solvent quality

The solvent quality can be varied either by choice of subphase liquid or by changing temperature. As the solvent quality becomes poorer, segment-segment interactions are increasingly favored with respect to segment-solvent interactions. This causes a contraction of the tethered layers. In this work, DOP was used to attain theta solvent conditions for the PS block (T_θ = 22 °C). In addition, solvent conditions better than theta and poorer than theta were achieved with DOP by varying the temperature.

Reflectivity data for the 20-170 copolymer in DOP over the temperature range from T_θ to T_θ - 56 °C are shown in Figure 5a. Reflectivity data for T_θ and T_θ + 58 °C are shown in Figure 5b. The monolayers in Figure 5a and 5b are at slightly different σ, but are both close to the maximum attainable values. Profiles obtained from the data at T_θ and T_θ - 56 °C are shown in Figure 5c along with a profile obtained in good solvent conditions (in EB) for comparable σ.[93] This figure demonstrates the large variation in layer height which results for different solvent conditions. Profiles obtained from the data at T_θ and T_θ + 58 °C are shown in the inset to Figure 5c. Comparison with the main figure demonstrates that the solvent quality varies only weakly with temperature above T_θ, in contrast to the strong variation with temperature just below T_θ. The variation in rms layer height (normalized by the rms layer height at T_θ) over the T range from T_θ - 56 °C to T_θ + 58 °C is shown in Figure 6. These data can be compared to the ratios in EB

(1.82) and in the fully collapsed state (0.12).[94] The solvent condition at T_θ + 58 °C is still quite far from the good solvent condition achieved at room temperature in EB. Likewise, the solvent condition at T_θ - 52 °C is still quite far from the fully collapsed nonsolvent limit. Thus, while solvent quality varies significantly with T, the extremes of solvent quality are not generally accessible by this method for systems in which van der Waals interactions dominate. This is true for free chains in solution as well,[95] and contrasts with the contraction to nearly full collapse over a narrow temperature range observed with poly(N-isopropylacrylamide) in water,[96] which involves hydrogen bonding interactions between the chain segments and water molecules.

Despite the fact that the tethered layers contract with decreasing solvent quality, the maximum in segment concentration remains at a depth into the liquid for the case of a strongly repulsive surface. In fact, we observe that the depletion layer actually increases slightly with decreasing solvent quality. Examples are given in Figure 7a and 7b. Figure 7a shows a comparison between best-fit profiles (near-surface region only) in good (EB, 22 C) and theta (DOP, 22 C) solvent conditions for the 4.5-60 copolymer. The depletion layer is noticeably greater in theta solvent conditions. We note that the air surface of EB is somewhat more repulsive for the d-PS segments than the air surface of DOP. However, since the surface is strongly repulsive for the PS segments in both solvents, we attribute the difference in Figure 7a to the difference in solvent quality. A comparison of the depletion layer in theta (DOP, 22 C) and poor (DOP, 30 C) solvent conditions for the 20-170 copolymer is shown in Figure 7b. Here the same subphase liquid is employed at both conditions, and so the increase in the depletion layer can be unambiguously assigned to the decrease in solvent quality. This trend has been observed in numerical SCF calculations.[66, 68]

III.1.d Surface density and molecular weight

The tethered chain segment profile is a strong function of both surface density and molecular weight. The variation of profile characteristics with σ and M can be used to determine where systems fall with respect to the limiting cases of strong-stretching ($\Sigma >> 1$) and noninteracting chains ($\Sigma \leq 1$). Indeed, an important advantage of the Langmuir monolayer system is the ability to vary both σ and M independently over a wide range. We consider variation both in the form of the profile and in the scaling of the layer height with σ and M.

III.1.d.1 Variation in profile form with σ and M

Earlier (Figure 3a) we compared data for the 4.5-60 copolymer in the good solvent EB at a relatively high surface density (Σ=5.3) with the analytical SCF form valid for the limiting case of strongly-stretched chains. In theta solvent conditions, a much stronger reflectivity signal results and therefore a detailed comparison can be made with both analytical SCF[62c,63] and RG[30] profiles over a wide range of surface density. This comparison has been made for M_{PS} ranging from 30,000 to 330,000.

We begin by comparing the reflectivity data with best-fits using the RG profile valid for weakly interacting or noninteracting chains. Figure 8a shows data for the 20-170 copolymer on DOP at 22 °C over a range of Σ from 1 to 8.4 along with the best-fit curves. Excellent agreement is obtained at the lower surface densities, but the fits become poor at the higher surface densities. This result holds true for the 4-30, 4.5-60, and 28-330 copolymers as well. For all four PS molecular weights, we determine that the RG profile is appropriate for $\Sigma \leq 5$ in theta conditions. Note that this covers a large portion of the data in the literature for chains tethered onto substrates from dilute solution.

Next we compare data at the maximum attainable surface density (Σ = 8.4) with the analytical SCF form valid in the strong stretching limit ($\Sigma >> 1$) given by $\phi = \phi_o[1-$

$(z/L_o)^2]^{1/2}$. This is shown in Figure 8b. The very high reflectivity signal allows very detailed information about the profile shape to be extracted. In this comparison we have modified the analytical SCF profile by adding a depletion layer and an exponential tail. The agreement is still poor near the peak as well as in the range of q from 0.02 to 0.04 $Å^{-1}$. Better agreement is obtained if the profile exponent is allowed to deviate from the predicted value of 1/2. Even further significant improvement is obtained with the addition of a step of constant ϕ following the depletion layer. Only with the addition of the step does the calculated curve agree well with the shoulder of the peak from 0.02 to 0.04 $Å^{-1}$. The best-fit empirical profile is shown in the inset to Figure 8b along with the best-fit modified SCF profile. An exponent of 2.0 +/- 0.02 results for the best-fit empirical profile. For all four molecular weights, the best-fit profile exponents are > 2 at low σ and decrease to roughly 2 at the highest σ. This indicates that the profiles are approaching the strong-stretching limit, but that this limit is not obtained for Σ up to 11. The best-fit empirical profiles for the entire range of σ for the 20-170 copolymer are shown in Figure 8c. Note that no systemmatic variation in the size of the depletion layer is detected over this range of σ in theta conditions.

Reflectivity for a range of M at T_θ is shown in Figure 9a. In each case the data were obtained near the highest attainable Σ. The corresponding best-fit profiles are shown in Figure 9b. The shift in the peak position in Figure 9a indicates a strong dependence of the layer height on M, which will be discussed in Section III.1.d.2. In addition, the depletion layer varies significantly with molecular weight at T_θ. The variation of the depletion layer with M at T_θ is shown in the inset in Figure 9b for the 4.5-60, 20-170 and 28-330 copolymers. (The q range is insufficient for a precise determination of the depletion layer for the 4-30 copolymer.) Defining the depletion layer as the distance from the air surface to the beginning of the step, values of 39 Å, 51 Å, 63 Å are obtained for these three copolymers, respectively. The absolute magnitude

of the depletion layer depends somewhat on the precise model form, whereas the trend of increasing magnitude with M is model independent.

III.1.d.2 Variation in layer height with σ and M

Detailed predictions have been made for the dependence of layer height on σ and M for the two limiting cases of strongly-stretched and noninteracting chains.[1,2,58-62] For the case of noninteracting tethered chains, the chain dimension varies with M as for a free chain in dilute solution. Thus $h \sim \sigma^0 M^{0.6}$ in good solvent conditions and $h \sim \sigma^0 M^{0.5}$ in theta solvent conditions. As the chains crowd each other they stretch normal to the surface. In that case, the dimension normal to the surface is no longer described by the statistics of isolated chains, but rather the dependence of layer height on M increases. In the strong-stretching limit, $h \sim \sigma^{1/3} M$ in good solvent conditions and $h \sim \sigma^{1/2} M$ in theta solvent conditions.

We have measured the layer heights in good and theta solvent conditions over an order of magnitude variation in σ and M. The data are shown in Figures 10a (good solvent) and Figure 10b (theta solvent). The degree of chain stretching is quantified in Figure 11 for both solvent conditions. The chains stretch by up to a factor of 1.5 over this range of Σ, with stronger stretching observed in good solvent conditions. Note that $(h_{RMS}/R_g)_{\sigma \to 0} \cong 1.45$ in both good and theta solvents. For comparison, values obtained by MC simulation for good solvent conditions fall in the range of 1.40 - 1.43.[97] Linear regressions of the data in Figure 11 give $h_{RMS}/R_g = 1.39 + 0.0763\ \Sigma$ (good solvent) and $h_{RMS}/R_g = 1.40 + 0.0565\ \Sigma$ (theta solvent). Numerical SCF calculations using parameter values corresponding to the present system are in reasonably close agreement with these data.[98] On the other hand, the dependencies of h on σ and M over this Σ range are not consistent with the predictions in the strong-stretching limit, as shown in Figures 12a and 12b, but rather both dependencies are much weaker ($h \sim \sigma^{0.22} M^{0.86}$ - good solvent, h ~

$\sigma^{0.18}M^{0.74}$ - theta solvent). From the exponent values, we observe that over a similar range of Σ the tethered layer in theta solvent conditions is further from the strong-stretching limit than is the tethered layer in good solvent conditions. Chain stretching is caused by higher order interactions in a theta solvent, and therefore a greater degree of chain overlap is required to reach the strong-stretching limit. The variation of layer height with σ and M thus supports the conclusion derived from analysis of the profile form that the asymoptotic limit is not reached for Σ up to 11. This covers the entire range reported in the literature for chains tethered from dilute solution in good or theta solvents.

We have also examined the importance of σ and M on the contraction of the layer below T_θ. This was accomplished by forming monolayers at T_θ and then decreasing the temperature. In the following we refer to a reduced temperature defined as $\tau = (T- T_\theta)/T$. The decrease of $h_{rms} / h_{rms,\theta}$ with $|\tau|$ depends upon both σ and M, as observed in Figure 13a. These data can be considered with respect to the limits of strongly-stretched[62c] and noninteracting chains.[99-101] First, the data clearly do not follow the dependence predicted for the asymptotic strong-stretching limit, as demonstrated in Figure 13b. This is expected, since our study of the profile form and layer height in good and theta solvent conditions indicates that this limit is only reached for $\Sigma >> 11$ at T_θ. Moreover, Σ decreases with decreasing T as the dangling PS chains contract.

The other limiting case is that for isolated, noninteracting chains ($\Sigma \leq 1$). In this limit the contraction of the layer is expected to be analogous to that of free chains in dilute solution. For isolated free chains, $R_g / R_{g,\theta}$ is a function of $|\tau| M^{1/2}$.[99-101] For $\tau << 0$, $R_g / R_{g,\theta} \propto (|\tau| M^{1/2})^{-1/3}$, which is termed the "collapsed" regime although the chains may still be quite expanded relative to the fully collapsed, nonsolvent limit. Our data are compared to this limiting behavior in Figure 13c. In this figure the rms layer heights are normalized by the rms layer heights at T_θ in the limit of $\Sigma \leq 1$. This representation shows that the layers are stretched normal to the surface at T_θ, due to interactions between the chains. However, as the temperature decreases the degree of overlap among neighboring

chains becomes weaker and the dependence on Σ diminishes. At the lowest temperatures, the data approach the scaling predicted for isolated tethered chains in a poor solvent. The remaining small dependence on Σ is likely due to the fact that the noninteracting regime is not quite reached at the lowest T for the higher Σ monolayers. Thus, while the chains are strongly overlapped at T_θ (but not in the strongly-stretched limit), they approach the noninteracting limit at the lowest T investigated. The contraction behavior below T_θ thus further supports the conclusion that the layers are far from the strong-stretching limit for the present range of Σ. We note that the contraction of the tethered layer with decreasing temperature is continuous over the experimental range of Σ in all cases.

III.1.e Free chains in bulk

Next we examine the influence of free chains in solution on the tethered layer. In particular, we focus on the perturbation of the tethered chain profile due to the presence of free chains, and the degree of penetration of free chains into the tethered layer. The degree of penetration of free chain segments into the layer and their access to the near surface region has important implications for systems involving free chains which interact strongly with a surface, such as for protein adsorption onto biosurfaces. In addition, the degree of penetration of free chains into the tethered layer is another test of the applicability of the strong-stretching limit.

In order to directly assess the degree of penetration of free chains into the layer formed by the submerged PS blocks, we have employed two contrast schemes in the reflectivity study. In the first contrast scheme, the free PS chains are deuterated and the PS blocks are protonated. Protonated PS has a neutron scattering length density which is very close to that of EB, and so this contrast scheme allows the profile of the free PS chains to be obtained. In the second scheme, the tethered blocks are deuterated and the free PS chains are protonated, which allows the segmental profile of the tethered PS blocks to be obtained. The molecular weights are nearly the same in the two contrast

schemes, enabling a direct comparison of the tethered and free chain profiles. The profiles are obtained as a function of the surface density of the tethered chains at a fixed concentration of free chains. The comparison of tethered and free chain profiles has been made for both $P < N$ and $P > N$, where P and N are the degrees of polymerization of the free and tethered chains, respectively.[50] Only the former case will be shown here.

Representative reflectivity curves from the first contrast scheme for the case of $P < N$ (40K deuterated free chains at volume fraction of 0.056, 166 K protonated tethered chains) are shown in Figure 14a. The data are presented as the ratio of the reflectivity from the monolayer-covered surface to the calculated Fresnel reflectivity for a subphase of uniform composition equal to that of the EB/free chain solution. Curves are shown for Σ ranging up to 12.

The segment profiles of the free d-PS chains obtained from this contrast scheme are shown in Figure 14b. With no copolymer present, the free PS chain segments are depleted from the surface over a distance of ~ 60 Å. This effect is due to the entropic penalty for chains which reside near a repulsive wall, and has been examined in detail previously.[102] With increasing Σ, the depth of the depleted zone increases and the shape of the free chain profile changes dramatically. At low Σ, the free PS chain profile is primarily affected at depths greater than 100 Å, while the region of the profile adjacent to the surface is largely unaffected. This indicates that free chain segments are first expelled from the body of the tethered layer rather than the near surface region. At higher Σ, the gradient in the free chain profile at the surface becomes strongly affected, decreasing rapidly toward zero at the highest Σ values examined. In addition, with increasing Σ the shape of the profile changes from concave to convex, tending toward the exponential form predicted in the asymptotic strong-stretching limit.[62A,62B] The depth of the depleted zone becomes nearly independent of Σ at the highest values examined, saturating at roughly 600 Å. Thus, these results clearly show free chain penetration at low Σ, and progressive exclusion of mobile chains from the body of the brush with increasing

Σ. However, to test the predictions of the analytical SCF theory in the strong-stretching limit, direct comparison with the tethered chain profile is required.

Corresponding tethered chain profiles have been obtained using the second contrast scheme (deuterated tethered PS chains). A comparison of tethered layer heights in the presence of free chains and in pure EB is shown in Figure 15 for the full range of Σ. The layer heights, defined by extrapolation of the body of the profile to zero volume fraction, are found to be nearly the same in the 43K and 400K solutions (both at 6%) at all Σ values. This is not surprising since both solutions are beyond the chain overlap concentration, and the characteristic length or mesh size of a semidilute solution is determined only by the concentration of free chain segments.[103] At low Σ, the layer height is substantially reduced in the presence of free chains compared to the height in pure EB. This effect diminishes with increasing Σ, and at the highest Σ we find that the layer height in the presence of free chains is nearly the same as that in pure EB. However, some noticeable differences in the profiles still remain at the highest Σ. Figure 16 shows reflectivity at the highest Σ in the presence of the free 400K protonated PS chains along with the reflectivity in pure EB. Best-fit profiles are shown in the inset. The principle difference is that the tail of the tethered chain profile is less pronounced in the 400 K free PS solution than in pure EB, and the body of the tethered chain profile is slightly more rounded. Similar, but less pronounced, effects are observed with the 43 K free PS chains

Direct comparison of the profiles for the tethered blocks and the free PS chains for $\Sigma \cong 12$ are displayed in Figure 17 for 40 K free chains. While the free chains are largely excluded from the near-surface region, there remains significant penetration of free chains into the brush. The degree of penetration of free chains into the brush is greater for the 40K free chains than for 400K free chains (not shown). Profiles calculated from the analytical SCF theory of Zhulina, et al.[62a,62b] in the asymptotic limit are also displayed in Figures 17 for comparison. The degree of free chain penetration into the brush in the

experimental profiles is much greater than is predicted in the asymptotic strong-stretching limit. The concentration falls off more gradually in the experimental profiles, in contrast to more step-like profiles predicted in the strong-stretching limit. On the other hand, numerical SCF calculations modeling the conditions of the 40K free chain solution (Σ=12) have shown a degree of penetration similar to that in Figure 17.[104] The significant penetration of free chains into the layer at $\Sigma \leq 12$ is further evidence that such systems are far from the asymptotic regime, and that numerical SCF calculations are required for an accurate description.

1.f Bimodal molecular weight distributions within the layer

All the data described in the previous sections involved layers composed of monodispersed tethered chains. The final aspect of the profile which we address is the effect of a bimodal molecular weight distribution. In certain cases, it may not be possible to optimize desirable properties within the range of segment profiles obtainable with single component tethered layers. This motivates the study of mixed layers, for which a much larger range of segment profiles is possible. In addition, the structure within bimodal layers offers another opportunity to test the applicability of the strong-stretching limit.

Figure 18 shows sample reflectivity data for 11-66/20-170, 11-66/28-330, and 4-30/28-330 mixed monolayers. The two peaks in each curve indicate the presence of two characteristic length scales within the monolayers. The curves through the data in Figures 18a-18c are best fits obtained from least squares regression using the following model profile comprised of the sum of two parabolas:

$$\phi(z) = \phi_{o,1}\,[1-(z/h_1)^2] + \phi_{o,2}\,[1-(z/h_2)^2] \qquad \text{for } z < h_1 < h_2$$

$$\phi(z) = \phi_{o,2}\,[1-(z/h_2)^2] \qquad \text{for } h_1 < z < h_2 \qquad (1)$$

The best-fit profiles are shown in Figures 19a-19c. The model profile in eqn 1 is adequate to describe the main features of the reflectivity curves as shown by the comparisons in Figure 18. This profile is the simplest functional form (fewest adjustable parameters) from which these large-scale features can be accurately extracted. No monomodal profile will describe the data from the mixed monolayers, as is clear from the presence of two peaks in each curve in Figure 18. Whereas our previous work on single component monolayers has indicated the presence of a depletion layer near the surface and a smooth tail away from the surface, these more detailed features are difficult to extract from a mixed monolayer. We note that the profiles obtained from the reflectivity represent an average in the plane of the surface. Thus, no information is obtained regarding the distribution of the copolymers in the plane of the surface.

Our data from bimodal monolayers have been analyzed largely in terms of the two characteristic dimensions and the component surface densities (obtained from the integral of the profile).[51] We focus here on the data for the 11-66/20-170 mixed monolayers in Figure 18a. The degree of interaction among the submerged blocks in the mixed monolayer can be inferred from the value of the total reduced surface density:

$$\Sigma = \sigma_{20\text{-}170}\,\pi R_{g,\,20\text{-}170}{}^{2} + \sigma_{11\text{-}66}\,\pi R_{g,\,11\text{-}66}{}^{2} \qquad (2)$$

The effect of the 66K blocks on the dimension of the 170K blocks is shown in Figure 20a. In this figure, the layer heights for the 170 K submerged blocks (h_{170}) in the 11-66/20-170 mixed monolayers are shown along with data obtained previously for the single component 20-170 monolayer. The curve through the single component data is a guide to the eye. The surface density of the 20-170 copolymer is plotted on the abscissa for both the single component and the mixed monolayers in order to allow a direct assessment of the affect of the 66K blocks on the dimension of the 170K blocks. The Σ

values for the three mixed monolayers are 2.9, 8.2, and 10.1 At the lowest Σ, the value of h_{170} in the mixed monolayer is within experimental error of that obtained at the same surface density of 20-170 chains in the single component monolayer. In this case, there is only weak interaction among the submerged blocks and the dimension of the 170 K blocks is unaffected by the presence of the 66k blocks. However, at higher surface densities where the submerged blocks interact strongly, the layer heights for the 170 K blocks are larger in the presence of the 11-66 copolymers than in their absence at the same $\sigma_{20\text{-}170}$. The additional stretching amounts to roughly 30% at the highest total surface density.

Figure 20b compares the layer heights for the 66 K PS blocks in the same mixed monolayers with data for the single component 11-66 monolayers. In contrast to Figure 20a, little or no variation in the dimension of the shorter chains is observed due to the presence of the longer chains.

Thus, the presence of the smaller PS blocks leads to additional stretching of the larger PS blocks relative to their dimension in a single component monolayer, while the dimension of the smaller PS blocks is largely unaffected by the presence of the larger blocks. Comparing this effect for the three molecular weight ratios, we find that the stretching of the larger chains induced by the shorter chains is greatest for $N_2 \cong 3\ N_1$, smaller for $N_2 \cong 5\ N_1$, and negligible for $N_2 \cong 11\ N_1$.[51] This trend is expected, since the perturbation of the profile of the longer chains due to the shorter chains must become negligible in the limit of $N_2 >> N_1$. The trends in the results described above are qualitatively consistent with the predictions of analytical[61b,64] and numerical[105] SCF calculations, and suggest that the longer chains are stretched in the inner region of the brush.

In a further study we determined the detailed profiles of the individual components of a bimodal brush consisting of PS chains of roughly 30K and 170K. Figure 21a shows reflectivity data for a mixed monolayer in which both chains were

deuterated, and also a mixed monolayer in which only the longer chains were deuterated. The monolayers were spread using nearly identical solutions in which the concentration of each copolymer was ~ 2.5 x 10^{-7} mol/ 5 ml $CHCl_3$. Reflectivity data to higher q values and better statistics than in the previously described mixed monolayer experiments were obtained to enable more detailed infomation to be extracted.

For the monolayer in which both PS blocks were deuterated, the best-fit using eqn 1 is shown in Figure 21a (dashed curve) along with a curve obtained with an empirical profile comprised of a stack of layers with Gaussian smearing at each interface (solid curve). The simple two-parabola profile is slightly inadequate as shown by the dashed curve in Figure 21a, whereas the empirical profile provides a much better fit to the data. The two profiles are compared in Figure 21b. While the dimensions of each component are accurately obtained with eqn 1, precise agreement with the reflectivity data requires a more step-like layer near the surface and slight oscillations in the profile of the longer chains. A small (20-25 Å) depletion layer might be expected based on the profiles of single component monolayers in good and theta solvents. However, a determination cannot be made from these data since a good fit can be obtained with or without such a layer.

For the bimodal monolayer in which only the longer chains were deuterated, there is a rather sharp minimum in R/R_o at q = 0.023 $Å^{-1}$ which is quite distinctive of the profile shape. This minimum is not obtained with a parabolic profile, as shown in Figure 21a. Since reflectivity data from single component monolayers of 20-170 in EB are well described with a parabolic profile,[106] the minimum in Figure 21a indicates a significant perturbation in the profile due to the presence of the smaller chains. The best-fit empirical profile is shown in Figure 21c along with the parabolic profile. The mimumum in Figure 21a, along with the slightly increased value of R/R_o at higher q, indicates a region depleted of d-PS segments near the surface yet with a maximum immediately at

the surface. Weak oscillations are also present in the profile of the longer chains as for the bimodal profile in Figure 21b.

The inset to Figure 21b shows a parameter-free comparison between the profile of the longer chains and the profile predicted by the analytical SCF theory of Birshtein, et al.[64] The principle observation is that there is less stratification in the experimental system than is predicted for the strong-stretching limit. The same result has been reported previously in a more extensive comparison by Levicky, et al involving bimodal layers of PVP-PS copolymers adsorbed onto silicon substrates.[55] This is further evidence that the strong-stretching limit is not valid for such experimental systems.

2. Free energies and anchoring energies

In addition to enabling a study of the segment profile by reflectivity, the Langmuir monolayer system also provides a unique opportunity to probe the free energy and anchoring energy of tethered chains through surface tension measurements.[107]

The free energy of the monolayer (F_M) is related to the surface pressure ($\Pi = \gamma_o - \gamma$, where γ_o and γ are the surface tensions of the pure solvent and monolayer-covered surface, respectively) by $\Pi = -(\partial F_M/\partial A)_{n,T,P}$, where A is the surface area, and n is the number of copolymer molecules in the monolayer. The surface pressure is a 2-dimensional analogue of the osmotic pressure of bulk solutions, and reflects the extent and nature of interactions among the copolymers within the monolayer. As mentioned in the Introduction, the copolymers can interact either through the surface blocks ($N_{PDMS} >> N_{PS}$), through the submerged blocks ($N_{PDMS} << N_{PS}$), or through both blocks ($N_{PDMS} \cong N_{PS}$), depending upon the asymmetry.

The anchoring energy per chain (F_{anch}) is related to the interfacial tensions and the molecular weight of the PDMS block by $F_{anch} = a^2NS$,[46] where a is the length of a PDMS monomer, N is the number of monomers per PDMS block, and S is the spreading parameter ($S = \gamma_{air/L} - \gamma_{air/PDMS} - \gamma_{PDMS/L}$, where $\gamma_{air/L}$, $\gamma_{air/PDMS}$, and $\gamma_{PDMS/L}$ are the interfacial tensions and the designation L stands for subphase liquid). For the present systems, very high anchoring energies per chain (~ 20kT to 500kT) arise from large positive values of the spreading parameter.[46,47] The fact that the anchoring energies are much larger than thermal energy of order kT accounts for the stability of the monolayers.

The discussion below focusses on the form of the Π versus σ isotherms. This relationship provides an interesting contrast with the force-distance profiles in SFA or AFM experiments for compression normal to the tethering surface. We find that the dependencies of Π on σ and M are quite different than predicted by either scaling or mean-field theories. The discussion focuses on the origin of the pressure, and why the

isotherms deviate strongly from predictions. In addition, we discuss how these observations may relate to adsorption of chains from solution into a brush.

III.2.a Results

The degree of interaction among the surface or submerged blocks can be deduced by comparing the copolymer isotherms with the surface pressure isotherm of PDMS.[107] This is shown in Figure 22a-22c, where isotherms for a number of copolymers with varying asymmetry are compared to that for PDMS on EB, BrEB, and DOP, respectively. The surface pressure is plotted against the surface concentration of PDMS (ϕ_{PDMS}) in order to indicate the contribution due to the PS blocks. If the PS blocks contributed negligibly to the surface pressure, the isotherms for the copolymers would fall on top of the PDMS isotherm in this representation. However, for all samples on each subphase liquid a large deviation from the PDMS isotherm is observed. Consider the copolymer isotherms on EB in Figure 22a. For the nearly symmetric copolymer 25-35 ($N_{PS} \cong N_{PDMS}$), the deviation from the PDMS isotherm occurs at relatively high ϕ_{PDMS} where the pressure in the PDMS isotherm is nonzero. In that case, interactions among both PDMS and PS blocks contribute to the surface pressure. On the other hand, for the most asymmetric copolymers ($N_{PS} >> N_{PDMS}$), we infer from the PDMS isotherm that interactions among the PDMS blocks are weak and contribute negligibly to the pressure. In that case the pressure is due entirely to interactions among the PS blocks. Since our interest is primarily in studying the free energy of the tethered PS layers, we define an excess surface pressure ($\Delta\Pi$) as the difference in pressure for the PDMS-PS and PDMS monolayers at a given ϕ_{PDMS}. The free energy of the tethered PS layer (F_{PS}) is then related to the surface pressure excess by $\Delta\Pi = -(\partial F_{PS}/\partial A)_{n,T,P}$.

The $\Delta\Pi$ isotherms for the 4-30, 4.5-60, 20-170 and 28-330 copolymers in good and theta solvent conditions are compared in Figures 23a and 23b. These samples are sufficiently asymmetric that the PDMS blocks contribute only a small fraction of the total

pressure in each case. For all samples the isotherm is shifted to higher σ in theta solvent conditions relative to good solvent conditions. The shifts in the isotherms observed in Figure 23 can be generally accounted for by the weaker segment-segment interactions of the dangling chain in a theta solvent. Weaker intramolecular segment-segment interactions lead to a contraction of the tethered coil in a theta solvent relative to a good solvent. Thus, overlap of the PS blocks is achieved at higher σ. In addition, only higher order segment interactions generate pressure in a theta solvent. Both of these effects contribute to the shift in the isotherm to higher σ.

While the shifts in the isotherms from good to theta conditions are easily understood, the form of the isotherms deviate sharply from prediction. It was shown in Section III.1 that these systems are not in the strong-stretching limit, and therefore the dependence of $\Delta\Pi$ on σ should be weaker than predicted in that limit ($\Pi \sim M\sigma^x$, where x takes the value of 5/3 (SCF) and 11/6 (scaling) in a good solvent, and 2 (both theories) in a theta solvent).[108] However as shown in Figure 24a and 24b, the dependence of $\Delta\Pi$ on σ is much stronger than predicted by scaling and SCF theory in the strong-stretching limit. A quantitative comparison with analytical SCF theory given in Reference 44 for the 10.5-40 copolymer showed that $\Delta\Pi$ reaches values which are an order of magnitude greater than predicted by this theory. Even more significant than the sharp increase of $\Delta\Pi$ with σ, Figure 23 and Figure 24 show that the rise in $\Delta\Pi$ occurs at lower σ for increasing M. This is observed for all three subphase liquids (EB, BrEB, and DOP). This strong dependence on M is a radical departure from theoretical prediction.

Both of these observations suggest a pseudo hard-core interaction among the submerged PS blocks, which contrasts with the assumption of laterally uniform layers in the SCF and scaling theories. In particular, the isolated chain dimension apparently remains a characteristic length within the layer even for $\Sigma >> 1$. However, the value of σ at which the sharp rise in $\Delta\Pi$ occurs does not scale precisely with R_g. Figure 25 demonstrates that in both good and theta solvents, chains of higher molecular weight can

be compressed to a smaller fraction of R_g before the hard-core-like behavior occurs. Nevertheless, Figures 23-25 provide strong evidence that the isolated ($\Sigma < 1$) tethered chain dimension remains an important characteristic length within the tethered layer even for $\Sigma >> 1$.

Limited isotherm data have also been obtained in poor solvent conditions.[48] This was accomplished by spreading the copolymer monolayers on DOP at 22 °C and then decreasing the temperature. At -30 °C, negative pressures are observed at low σ which indicate metastability toward in-plane phase separation. This has been discussed elsewhere.[48] The change in $\Delta\Pi$ with T at higher σ is shown in Figure 26 along with the isotherms for good and theta solvent conditions from Figure 23. Surprisingly, only a small decrease in $\Delta\Pi$ is observed upon cooling from 22 °C to -30 °C despite the fact that the layer height decreases dramatically over this range (see Figure 13a). Indeed, based on the degree of contraction and the isotherms obtained in good and theta solvents, we would expect negligible pressure to result if the poor solvent conditions of Figure 26 were obtained by increasing σ isothermally at -30 °C rather than by spreading the monolayer at 22 °C and then cooling to -30 °C. We conclude that the measured pressure is pathway dependent, and that nonequilibrium (steric) effects play an important role in the pressure isotherms. However, we emphasize that no relaxation of the pressure is observed on experimental time scales (several days) even for the highest pressures in Figure 23.

The effect of subphase surface tension on the surface pressure isotherms has also been examined. Figure 27 compares the surface pressure isotherms for the 20-170 and 28-330 copolymers on BrEB and EB. The subphase surface tension differs by ~ 7 dyn/cm for these two subphase liquids (Figure 2) whereas both liquids are good solvents for PS. Figure 28 shows that the value of σ at which the strong increase in $\Delta\Pi$ with σ occurs is nearly the same on EB and BrEB. The dependence of $\Delta\Pi$ on σ is similar, being perhaps slightly stronger on EB. While the form of the isotherms are quite similar, much

higher values of surface pressure are reached on BrEB. This is due to the greater anchoring energy arising from the increased value of S. The strong similarity in the isotherms is consistent with the interpretation of the isotherms as due to the interaction of the submerged PS blocks. Earlier it was shown (Figures 3 and 4) that the form of the segment profile of the dangling block in the near-surface region is different in these two liquids. However, in Figure 4c the effect of weak adsorption of PS to the BrEB surface was shown to have a negligible effect on the layer height for the higher M samples. Figure 28 shows that the small perturbation in the profile also has little effect on the surface pressure for the higher M samples.

III.2.b Discussion

Since the surface pressure isotherms are strongly contrary to predictions, we have considered other effects which might contribute to the surface pressure, in addition to interactions among the submerged blocks. However, a number of evidences confirm that the rise in pressure is indeed due to interactions among the submerged blocks. First, when the molecular weight of the PS block is held nearly constant while that of the PDMS block is varied, the data fall onto a single curve when plotted as $\Delta\Pi$ against σ.[44] This supports the assertion that $\Delta\Pi$ is the contribution of the dangling PS blocks. Second, as shown in Figure 23, the value of σ at which $\Delta\Pi$ increases rapidly depends upon the molecular weight of the submerged PS block. There is no correlation with the molecular weight of the surface PDMS block.[46] Third, the shift in the isotherms on EB and DOP in Figure 23 are consistent with the difference in solvent quality for the submerged PS block. Fourth, Figure 28 shows that the isotherms are nearly independent of the surface tension of the subphase liquid (higher M samples) when constant solvent quality for the submerged block is maintained. This is consistent with the interpretation of the isotherms as due to the interactions of the submerged blocks.

While the above evidences confirm that the strong increase in $\Delta\Pi$ with σ is due to interactions among the submerged blocks, the $\Delta\Pi$ isotherms cannot be described by osmotic interactions arising from the laterally-averaged local segment concentration $\phi(z)$, as modeled in current theories of tethered chains. The clearest indication of this is the strong M dependence of the σ value where $\Delta\Pi$ increases sharply. The failure of the data to collapse in Figure 24 indicates an effect in the data which is entirely absent from current theories. Also, as mentioned earlier the dependence of $\Delta\Pi$ on σ is much stronger than can be accounted for by osmotic interactions calculated from $\phi(z)$. Furthermore, the comparisons in Figure 27 indicate that the pressure depends upon the pathway to the final state, and thus that nonequilibrium (steric) effects are important.

The surface pressure isotherm data suggest that the submerged blocks interact in a manner more like soft-spheres with hard-cores than the picture assumed in existing theories in which the pressure is due to the laterally-averaged local segment concentration. We suggest that the M-dependence of the isotherms, the apparent hard-core-like behavior, arises from limited interpenetration of coils. Limited interpenetration may be a result of steric effects. The sharp rise in pressure can be due to either higher order osmotic interactions or to distorted chain configurations (entropic chain elasticity), both of which would result from limited lateral interpenetration. Regarding the former, the SCF and scaling treatments are based on only second (good) or third (theta) virial interactions. The importance of including higher order interactions has been demonstrated by Grest et al[108] and Szleifer et al[109] for short chains. However, it appears unlikely with the relatively high M and low segment concentrations in the present tethered layers that higher order osmotic interactions alone could be strong enough to account for the entire discrepancy. Moreover, if the high surface pressures were due entirely to higher order osmotic interactions, one would expect much greater stretching normal to the surface than is actually observed. Therefore, we suspect that entropic

effects plays an important role. Other evidence of configurational constraints correlated with Σ has been reported recently.[56]

While the present work is the first to reveal a sharp rise in pressure with increasing σ, this observation gives insight into important outstanding discrepancies between theoretically predicted adsorption behavior and experimental observations. Several workers have explored the equilibrium adsorption isotherms and kinetics of end-adsorbing chains which follow from either the analytical SCF (or scaling) treatment of chain free energy (f) in the strong-stretching limit or a numerical SCF description.[110-112] These analyses indicate a strong dependence of σ_{eq} on binding energy (Δ). For $\Delta >> kT$, $f_{eq} \approx \Delta$, and chain adsorption is predicted to continue until the chains become strongly-stretched. In addition, the analyses predict a strong (and smooth) increase of σ with the concentration of chains in the bulk from the very dilute regime through the concentrated regime.

Experimentally, it is observed that chains with strongly interacting end-groups ($\Delta >> kT$) do not continue to adsorb from dilute solution until they are strongly-stretched, but rather adsorption stops at much lower coverage. The vast majority of the data in the literature for chains tethered from dilute solution in good or theta solvents fall in the range of $\Sigma \leq 5$.[34,36-39,41,42] In a few cases the range extends to $\Sigma \cong 7$.[32,35] We have shown that chains stretch by only a factor of ~ 1.4 over the range from $1 \leq \Sigma \leq 7$ (Figure 11), and that this range of Σ is far removed from the strong-stretching limit. Osmotic interactions account for only a few kT/chain for these systems, far lower than the anchoring energies in most cases. In addition, the predicted strong dependence of σ on Δ is not observed experimentally, but rather all data for chains tethered from dilute solution in good and theta solvents fall into the *same* range of Σ despite widely different anchoring energies. For example, the present data have anchoring energies ranging up to ~ 350 kT,[46,47] PS chains tethered onto silicon via reaction of chlorosilane groups with silanol groups on silicon oxide have anchoring energies ranging of ~ 370 kT,[113] thiol terminated PS chains

end-grafted onto gold have an anchoring energy of ~ 170 kT,[113] asymmetric PVP-PS diblock copolymers adsorbing onto mica have estimated anchoring energies ranging from 15 - 32 kT,[114] and zwitterion end-functionalized PS chains have an anchoring energy estimated at 6-8 kT,[32] yet the range of maximum Σ is very comparable for all these cases when adsorption (or increase in σ for the Langmuir monolayer system) occurs in dilute solution. The surface density clearly depends upon the anchoring energy when anchoring energy is very low.[32,115] However, similar M-dependent upper limits of Σ occur for all systems tethered from dilute solution in good or theta solvents regardless of Δ. Figure 28 shows that in the Langmuir monolayer system the limiting Σ value is not dependent upon anchoring energy.

The observed dependence of the final (time-independent) surface density (σ_{final}) on ϕ is also contrary to prediction. Adsorbed amount is observed to depend strongly on solution concentration for extremely low concentrations, but reaches a well-defined plateau at concentrations which are still very dilute.[41] This plateau extends from the dilute regime well into the semidilute regime.[41,82] In the concentrated regime, σ again increases with ϕ.[82] This strong dependence on σ in the concentrated regime extends up to solvent free melt conditions. This general behavior appears to be independent of anchoring energy. Thus the large regime of intermediate concentration where σ is independent of ϕ is contrary to prediction.

Adsorption data thus indicate that the maximum surface density for chains tethered from a wide range of solution concentration from dilute to semidilute is determined by the molecular weight of the tethered chain and is largely independent of solution concentration and anchoring energy.

The pressure isotherm data from the Langmuir monolayer system shed light on these discrepancies. As mentioned above, there is a remarkable correspondance between the maximum surface density (σ_M) achieved in the Langmuir monolayer system and σ_{final} observed for tethering from dilute solution onto solid substrates. Moreover, the

dependence on molecular weight is strikingly similar as well. For highly asymmetric PEO-PS diblock copolymers adsorbing onto silicon from toluene, Motshmann, et al, have observed $\sigma_{final} \alpha M^{-1.18}$,[41] whereas in the present Langmuir monolayer systems with copolymers of comparable asymmetry and over a similar molecular weight range, $\sigma_M \alpha M^{-0.97}$.[46] We suggest that the same steric effects, distorted configurations, and large potential barriers as represented by the $\Delta\Pi$ isotherms occur when chains adsorb into a tethered layer from solution. Regarding the very strong dependence of σ_{final} on solution concentration in the concentrated regime,[82,83] we suggest that the large potential barrier to chain insertion as represented by the $\Delta\Pi$ isotherms may be circumvented by tethering chains from a matrix in which the chains are already interpenetrated.

We reiterate that scaling arguments based on an energy of kT per blob[103] cannot account for the high chain energies observed in present isotherm data. There is some limited support for anomalously high chain energies in highly confined geometries. In one SFA study, it was reported that the force-distance relation could not be described using the experimental relationship for osmotic pressure from semidilute solution, but rather the chain energy exceeded that by roughly a factor of 2 at the highest compressions.[34] In another SFA study, force data appeared to begin to deviate sharply (toward higher force) from the SCF prediction at the highest compressions examined.[32] We note that the compressions in the present work exceed that in the SFA work. Finally, direct force-distance measurements on single grafted chains and polymer brushes at high compressions have been reported recently using AFM.[78,79] The data indicate very high chain energies at high compression. For example, integrating the force-distance curve of Ortiz and Hadziioannou for compression of a single tethered poly(methacrylic acid) chain in water we obain an energy of roughly 1300 kT.[79] However, this value includes electrostatic repulsion between negatively charged –COO groups along the polymer chain, in addition to osmotic interactions, lateral chain stretching, and confinement

effects. No data are yet available for compression of a single uncharged coil in a good solvent.

An important outstanding issue with the above interpretation of the $\Delta\Pi$ isotherms is the absence of confirmation in MD simulations to date. Grest has performed constant surface pressure MD simulations of tethered chains in which the surface pressure was fixed at an imposed value by allowing the surface area per unit cell to vary.[108] The simulations yielded pressure isotherms which can be compared with the present experimental isotherms. In the simulations (chains with 50 to 200 statistical segments), the isotherms in theta solvent conditions were shifted to higher σ relative to those in good solvent conditions, and the magnitude of the shift was comparable to that observed in Figure 23. In addition, the simulations showed a stronger dependence of Π on σ ($\Pi \sim \sigma^{2.5}$ in a good solvent, $\Pi \sim \sigma^{3.0}$ in theta solvent) than predicted by the SCF and scaling theories.

While the simulations and the present experiments both reveal a shift in the isotherm from good to theta conditions and an increased dependence of Π on σ, the form of the dependence of Π on σ and M observed in the simulations is significantly different than in the present data. In particular, plots of $\Pi/M\sigma^x$ versus σ from the simulations were nearly linear in contrast to the present data in Figure 24. In addition, in the simulations the isotherms for chains varying over roughly an order of magnitude in M nearly collapsed onto a single curve in that representation, the dependence on M being slightly greater than $\Pi \sim M$. Although the collapse was noticably poorer in a theta solvent than in a good solvent, the behavior still contrasts sharply with that in Figure 24. Thus, while several features of the present data are consistent with these simulations, the dependence of Π on σ is much stronger in the present data and the M dependence of the σ value where the sharp rise occurs is not reproduced. In addition, no evidence of limited interpenetration has been observed.[116] It may be that such effects do not occur with the same magnitude in simulations of shorter chains.

IV. Summary and significance

We have used Langmuir monolayers of diblock copolymers as a model tethered chain system. We have determined detailed concentration profiles of the tethered chain segments by neutron reflection as a function of solvent quality, surface interaction, surface density, molecular weight, free chains in solution, and bimodal molecular weight distributions. We have emphasized quantitative comparison with analytical theories over the range of Σ which is common to all systems tethered from dilute solution in good or theta solvents. For practical applications this range has great importance due to the high cost of specialty polymers.

We find that the analytical SCF theory for the strong-stretching limit is not valid over this range. The profile forms of analytical SCF theory in the strong-stretching limit (good or theta solvents) are not approached for $\Sigma \leq 11$, but require substantially greater Σ. In addition, analytical SCF and scaling in the strong-stretching limit predict dependencies of layer height on σ and M which are substantially stronger than the dependencies which are observed in this range of Σ. Moreover, the amount of stratification predicted in bimodal layers in the strong-stretching limit is much greater than is observed. Even more important differences occur in the degree of penetration of free chains into tethered layers in this regime.

On the other hand, we find that the renormalization group theory of Adamuti-Trache, et al[30] addressing the case of weakly interacting and noninteracting chains describes well the segment profiles for $\Sigma \leq 5$ (comparison made for theta solvent conditions). This covers a large portion of the range which can be achieved by tethering from dilute solution in good or theta solvents. Numerical SCF or SCMF describe well the segment density profiles over the entire experimental Σ range, including free chain penetration into tethered layers.

Our conclusion regarding the inapplicability of the strong-stretching limit for layers of chains tethered from dilute solution in good or theta solvents is in contrast with

previous conclusions based largely on analyses of force-distance profiles measured in the surface forces apparatus.[32,34,117] Comparisons were reported in which the force-distance profiles agreed well with the analytical SCF prredictions with no adjustable parameters. Furthermore, force-distance profiles for a range of molecular weights and surface densities collapsed to a universal curve using scaling variables predicted by the theory. These results were taken as support for the applicability of the strongly-stretched tethered chain models. However, in those studies the highest reduced surface density was only 7.4. The universal scaling of the force-distance profiles occurred for Σ ranging from 1.7 to 5.1. Our results (Figure 11) show that tethered layers are far from the strong-stretching limit for $\Sigma = 7.4$. In addition, Figure 11 shows that there is virtually no chain stretching for $\Sigma = 1.7$. Thus we find the curious result that the analytical SCF theory, whose primary assumption is that of strongly-stretched chains, describes quantitatively with no adjustable parameters the force-distance relationship for systems far from the strong-stretching condition, including a system in which chain stretching is entirely absent.

Insight has been provided recently through numerical SCF calculations.[68,74] Numerical SCF calculations using parameters characteristic of the experimental systems deviate substantially from the force-distance relation of the asymptotic theory. One key difference is the degree of interdigitation between opposing brushes. Models invoking strongly-stretched chains predict no interdigitation, as retraction would be more energetically favorable for strongly-stretched chains than interdigitation. Numerical SCF calculations indicate that significant interdigitation does indeed occur, which follows directly from the result that chains are not strongly-stretched in this Σ range. Interdigitation was shown to reduce the force by up to an order of magnitude.[74] Even though the theoretical force-distance curves are much different in the two cases, both could be brought into agreement with the same experimental data within the uncertainty of the parameter values. We conclude that comparison with force-distance profiles is of little value in validating the applicability of the strongly-stretched tethered chain models.

The Langmuir monolayer system offers an opportunity to test predictions regarding the relation between the segment-surface interaction and the segment concentration in the near surface region, since the surface can be made unambiguously attractive or repulsive to the dangling chain segments depending on the subphase surface tension. A depletion of segments at the surface is observed for a repulsive surface, in agreement with prediction from theory and simulation. The depletion layer increases with molecular weight, is nearly independent of surface density, and increases with decreasing solvent quality. These trends and the magnitudes are in excellent agreement with numerical SCF calculations. No depletion layer is observed for a surface which is slightly attractive to the dangling PS segments. The lack of a depletion layer in many studies at solid-liquid interfaces is apparently due to a slight attraction of the segments to the surface.

One important aspect of tethered chain systems not reproduced by any theoretical treatment to date is the upper limit of Σ experienced for all systems tethered from dilute solution in good or theta solvents. This limit occurs despite widely differing anchoring energies, and occurs for both end-grafted chains and asymmetric block copolymer systems as well as for the present Langmuir system. Rather than being dependent upon anchoring energy as predicted thoretically, the upper limit of Σ is determined primarily by the molecular weight of the tethered chain. Another unresolved issue is the strong dependence of the resultant surface density on the concentration of chains in the solution from which they are tethered in the concentrated regime, which follows a large plateau in the adsorption isotherm. The surface tension of Langmuir monolayers of diblock copolymers provides insight into these observations. Our study has revealed a strong increase in surface pressure with surface density which restricts the Σ range. Strong evidence indicates the sharp rise in pressure is due to interactions among the submerged blocks. The magnitude of Π and the dependencies on σ and M are not consistent with existing theories. Evidence has been presented indicating this is nonequilibrium (steric)

effect. We suggest that this effect is due to limited interpenetration of neighboring chains, and the resulting distorted configurations or higher order osmotic interactions. A strong correspondance exists between the maximum σ in the Langmuir system and σ_{eq} in adsorbing systems. Moreover, a similar M dependence is also observed. We conclude that the nonequilibrium (steric) effect may be general to chains tethered from dilute solution and explain the common upper limit to Σ which is experienced for a wide number of systems.

This upper limit of Σ restricts potential applications of tethered chains. It has been well-demonstrated that much higher surface densities can be achieved by tethering from a highly concentrated solution or melt. However, cost may prohibit this method for some applications. A very promising alternative is the "grafting from" method, wherein chains are polymerized from active sites on the surface.[118-129] A further possible alternative is adsorption from chains in the collapsed state, that is from a nonsolvent, perhaps using a micellar microstructure.

ACKNOWLEDGMENTS

This work was supported by the U.S. Department of Energy under contract CE-AC04-94AL85000. Sandia is a multiprogram laboratory operated by Sandia Corporation, a Lockheed Martin Company, for the United States Department of Energy.

REFERENCES AND NOTES

1) A. Halperin, M. Tirrell, T.P. Lodge, *Adv. Polm. Sci.*, **100**, 31, (1992)
2) S. T. Milner, *Science* **251**, 905, (1991)
3)(a) E. Raphael, P. G. de Gennes, *J. Phys. Chem.* **96**, 4002, (1992); (b) H. Ji, and P. G. de Gennes *Macromolecules* **26**, 520, (1993)
4) (a) M. Deruelle, L. Lé ger, M. Tirrell, *Macromolecules* **28**, 7419, (1995).; (b) M. Deruelle, M. Tirrell, Y. Marciano, H. Hervet, L. Leger, *Faraday Disc.* **98**, 55 (1994)
5) F. Brochard-Wyart, P. G. de Gennes, *J. Adh.*, **57**, 21, (1996).
6) F. Brochard-Wyart, P. G. de Gennes, L. Leger, Y. Marciano, E. Raphael, *J. Phys. Chem.*, **98**, 9405, (1994).
7) J. Duchet, J. P. Chapel, B. Chabert, J. F. Gerard, *Macromolecules* **31(23)**, 8264 (1998)
8) C. Ligoure, *Macromolecules* **29**, 5459 (1996)
9) C. Creton, H. R. Brown, K. R. Shull, *Macromolecules* **27**, 3174 (1994)
10) J. Klein, *Annu.Rev. Mater. Sci.* **26**, 581, (1996)
11) J. Klein, D. Perahia, S. Warburg, *Nature* **352**, 143, (1991)
12) S. A. Gupta, H. D. Cochran, P. T. Cummings, *J. Chem. Phys.* **107**, 10316 (1997)
13) J. I. Martin, Z. G. Wang, M. Shick, *Langmuir* **12**, 4950 (1996)
14) G. Reiter, P. Auroy, L. Auvray, *Macromolecules* **29(6)**, 2150 (1996)
15) D. H. Napper, *"Polymeric Stabilization of Colloid Dispersions"*, Academic Press, New York, 1983
16) G. J. Fleer, M. A. Cohen Stuart, J. M.H. M. Scheutjens, T. Cosgrove, B. Vincent, *"Polymers at Interfaces"*, Chapman and Hall, London, 1993
17) A. Halperin, *Langmuir* **15**, 2525 (1999)
18) I. Szleifer, *Biophys. J.*, **72**, 595 (1997)
19) D. L. Elbert, J. A. Hubbell, *Ann. Rev. Mater. Sci.*, **26**, 365 (1996)
20) H. Lee, H. B. Lee, J. D. Andrade, *Prog Polym. Sci.* **20**, 1043 (1995)
21) M. Malmsten in Biopolymers at Interfaces, M. Malmsten Ed., Surfactant Science Series; Marcel Dekker: New York, in press
22) W. Muller, *Eur. J. Biochem.* **155**, 213 (1986)
23) D. Lasic, F. Martin "Stealth Liposomes"; CRC Press, Boca Raton, (1995).
24) A. Halperin, *Euro. Phys. J. B* **3**, 359 (1998)
25) D. Papahadjopoulos, T. M. Allen, A. Gabizon, E. Mayhew, K. Matthay, S. K. Huang, K. D. Lee, M. C. Woodle, D.D. Lasic, C. Redemann, F. Martin, Proc. *Natil. Acad. Sci.* **88**, 11460 (1991)
26) T. D. Gibson, J. R. Woodward, "Biosensors & Chemical Sensors", P. G. Edelman and J. Wang, Ed.; ACS Symposium Series 487, (1992).
27) Y. S. Park, Y. Ito, Y. Imanishi, *Macromolecules* **31**, 2606, (1998).
28) Szleifier, I Adv. Chem. Phys., **94**, 165, (1996)
29) G.S. Grest, and M. Murat, *"Monte Carlo and Molecular Dynamics Simulations in Polymer Science"*; K. Binder, Ed.; Clarendon Press: Oxford, 1994
30) M. Adamuti-Trache, W. E. McMullen, J. F. Douglas, *J. Chem. Phys.* **105**, 4798 (1996)
31) S. Patel, G. Hadziioannou, S. Granick, M. Tirrell, *J. Am Chem. Soc.* **108**, 2869 (1996)
32) (a) . Taunton, C. Toprakcioglu, L. J. Fetters, J. Klein, *Nature* **332**, 712 (1988). H. (b) J. Taunton, C. Toprakcioglu, L. J. Fetters, J. Klein, *Macromolecules* **23**, 571 (1990)
33) T. Cosgrove, T. G. Heath, J. S. Phipps, R. M. Richardson, *Macromolecules* **25**, 434 (1992)
34) Watanabe, H.; Tirrell, *M. Macromolecules* **26**, 6455 (1993)
35) J. B. Field, C. Toprakcioglu, R. C. Ball, H. B. Stanley, L Dai, W. Barford, J. Penfold, G. Smith, and W. Hamilton, *Macromolecules* **25**, 434 (1992)

36) J. B. Field, C. Toprakcioglu, L Dai, G. Hadziioannou, G. Smith, and W. Hamilton, *J. Phys. II (Paris)* **2**, 2221 (1992)
37) T. Cosgrove, T. G. Heath, J. S. Phipps, R. M. Richardson, *Macromolecules* **24**, 94, (1991)
38) Guzonas, D. A.; Boils, D.; Tripp, C.P.; Hair, M. L. *Macromolecules* **25**, 2434 (1992)
39) Parsonage, E.E.; Tirrell, M.; Watanabe, H.; Nuzzo, R.G. *Macromolecules* **24**, 1987 (1991)
40) J. F. Tassin, R. L. Siemens, W. T. Tang, G. Hadziioannou, J. D. Swalen, B. A. Smith, *J. Phys. Chem* **93**, 2106 (1989)
41) H. Motschmann, M. Stamm, C. Toprakcioglu, *Macromolecules* **24**, 3681 (1991)
42) (a)V. Koutsos, E. W. van der Begte, G. Hadziiooannou, *Macromolecules* **32**, 1233 (1999); (b) V. Koutsos, E. W. van der Vegte, E. Pelletier, A. Stamouli, G. Hadziioannou, *Macromolecules* **30**, 4719 (1997)
43) S. Satija (grafting from dilute solution)
44) M.S. Kent, L.T. Lee, B. Farnoux, F. Rondelez, *Macromolecules* **22**, 1449 (1989)
45) B. J. Factor, L. T. Lee, M. S. Kent, F. Rondelez, *Phys. Rev. E.* **48**, 2354 (1993)
46) M.S. Kent, L.T. Lee, B.J. Factor, F. Rondelez, G. Smith, *J. Chem. Phys.* **103(6)**, 2320 (1995)
47) M.S. Kent, J. Majewski, G. Smith, L.T. Lee, S. Satija, *J. Chem. Phys.* **108(13)**, 5635 (1998)
48) M.S. Kent, J. Majewski, G. Smith, L.T. Lee, S. Satija, *J. Chem. Phys.* **110(7)**, 3553, (1999)
49) L.T. Lee, B.J. Factor, M.S. Kent, F. Rondelez, *J. Chem. Soc., Faraday Discuss.* **98**, 139 (1994)
50) L. T. Lee and M. S. Kent, *Phys. Rev. Lett* **13**, 2899 (1997)
51) M. S. Kent, B. J. Factor, S. Satija, P. Gallagher, G. S. Smith, *Macromolecules* **29**, 2843 (1996)
52) F. E. Runge, M. S. Kent, H. Yu, *Langmuir* **10**, 1962 (1994)
53) (a) Auroy, P.; Auvray, L.; Lé ger, L. *Macromolecules* **1991**, *24*, 5158; (b) Auroy, P.; Auvray, L.; Lé ger, *L. Physica A* **172**, 269 (1991)
54) A. Karim, S. K. Satija, J. F. Douglas, J. F. Ankner, L. J. Fetters, *Phys. Rev. Lett.* **73**, 3407 (1994)
55) R. Levicky, N. Koneripalli, M. Tirrell, S. Satija *Macromolecules* **31**, 2616 (1998)
56) R. Levicky, N. Koneripalli, M. Tirrell, *Macromolecules* **31**, 3731 (1998)
57) S. J. Alexander, *J. Phys. (Paris)* **38**, 977 (1977)
58) P. G. de Gennes, *Macromolecules* **13**, 1069 (1980)
59) A. Halperin, *Macromolecules* **20**, 2943, (1987)
60) A. Halperin, *J. Phys. France* **49**, 131, (1988)
61) (a) Milner, S.T.; Witten, T.A.; Cates, *M.E. Macromolecules* **21**, 2610, (1988); (b) Milner, S.T.; Witten, T.A.; Cates, *M. Macromolecules* **22**, 853 (1989)
62) (a)E.B. Zhulina, O.V. Borisov and V.A. Pryamitsin, *J.Coll. Interf. Sci.* **137**, 495 (1990); (b) E.B. Zhulina, O.V. Borisov, L. Brombacher, *Macromolecules* **24**, 4679 (1991); (c) E. B. Zhulina, O. V. Borisov, V. A. Pryamitsyn, T. M. Birshtein, *Macromolecules* **24**, 140 (1991)
63) D. F. K. Shim, M. E. Cates, *J. Phys. (Paris)* **50**, 3535, (1989)
64) Birshtein, T. M.; Liatskaya, Y.V.; Zhulina, E.B. *Polymer* **31**, 2185 (1990)
65) T. Cosgrove, T. Heath, B van Lent, F. Leermakers, J. Scheutjens *Macromolecules* **20**, 1692, (1988)
66) M. Muthukumar and J. S. Ho, *Macromolecules* **22**, 965, (1989)
67) S. T. Milner, *J. Chem Soc., Faraday Trans.* **86**, 1349, (1990)
68) M. D. Whitmore, J. Noolandi, *Macromolecules* **23**, 3321, (1990)
69) G. J. Fleer, Colloids Surf. **35**, 151, (1989)
70) (a) R. Baranowski, M. D. Whitmore, *J. Chem. Phys.* **103**, 2340 (1995);

(b) R. Baranowski, M. D. Whitmore, *J. Chem. Phys.* **108**, 9885 (1998)

71) C. M. Wijmans, J. M. H. M. Scheutjens, E. B. Zhulina, *Macromolecules* **25**, 2657 (1992)
72) J. I. Martin, Z. G. Wang, *J. Phys. Chem.* **99**, 2833 (1995)
73) C. Yeung, A. C. Balazls, D. Jasnow, *Macromolecules* **26**, 1914 (1993)
74) E. Ruckenstein, B. Li, *J. Chem. Phys.* **107,** 932 (1997)
75) S. Patel, M. Tirrell, *Annu. Rev Phys. Chem.* **40**, 597 (1989)
76) S. Patel, M. Tirrell, G. Hadziioannou, Colloids Surf. 31, 157, (1988)
77) J. Klein, Y. Kamiyama, H. Yoshizawa, J. N. Israelachvili, L. Fetters, P. Pincus, *Macromolecules* **25**, 2062 (1992).
78) T. W. Kelley, P. A. Schorr, K. D. Johnson, M. Tirrell, C. D. Frisbie, *Macromolecules* **31(13)**, 4297 (1998)
79) C. Ortiz, G. Hadziioannou, *Macromolecules* **32**, 780, (1999).
80) P. Auroy, L. Auvray, L. Lé ger, *Phys. Rev. Let.* **69(1)**, 93 (1992)
81) P. Auroy, L. Auvray, L. Lé ger, *Phys. Rev. Lett.* **66**, 719 (1991)
82) P. Auroy, L. Auvray, L. Lé ger, *Macromolecules* **24**, 2523 (1991)
83) A. Karim, J. F. Douglas, F. Horkay, L. J. Fetters, S. K. Satija, *Physica B* **221**, 331, (1996)
84) (a) P. Gallagher and S. Satija, Proceedings of the 5th Surface X-ray and Neutron Scattering Conference, Oxford, July 1997; (b) P. Gallagher S. Satija, Proceedings of the International Conference on Neutron Scattering, Toronto, August 1997
85) S. M. Baker, N. Melosh, E. Torgerson, G. Smith, C. Toprakcioglu, A. Vradis, (in preparation)
86) S. J. O'Shea, M. ER. Welland, T. Rayment, *Langmuir* **9**, 1826 (1993)
87) W. Zhao, G. Krausch, M. H. Rafailovich, J. Sokolov, *Macromolecules* **27**, 2933 (1994)
88) A. Karim, V. V. Tsukruk, J. F. Douglas, S. K. Satija, L. J. Fetters, D. H. Reneker, M. D. Foster, *J. Phys. II* **5**, 1441 (1995)
89) S. M. Baker, A. Callahan, G. Smith, C. Toprakcioglu, A. Vradis, (in preparation)
90) T. P. Russell, *Mater. Sci. Rep.* **5**, 171 (1990)
91) EB is good solvent
92) This is because this value of M_{PS} provides a fairly large increase in reflectivity relative to the bare subphase due to a relatively high segment concentration, but yet the experimentally accessible q range is still sufficient to examine the slope of R/R_o with q beyond the main peak. Copolymers with a higher M_{PS} give a weaker increase in reflectivity. Copolymers with a lower M_{PS} require a q range beyond that which can be achieved in a reasonable time scale
93) For the 20-170 copolymer in good solvent conditions, a conclusion regarding the depletion layer cannot be made from the reflectivity data. In Figure 5c the depletion layer for good solvent conditions was determined based on the magnitude observed in theta solvent conditions and the variation with solvent quality observed for the 4.5-60 sample
94) thickness in fully collapsed state from integral of the profile
95) P. Stepanek, C. Konak, B. Sedlacek, *Macromolecules* **15**, 1214, (1992)
96) (a) C. Wu, S. Zhou, *Macromolecules* **28**, 8381 (1995); (b) X. Wang, X. Qiu, C. Wu, *Macromolecules* **31**. 2972 (1998)
97) C. Sorenson, J. Kovac (private communication)
98) M. Whitmore, M. Pepin (private communication)
99) I. C. Sanchez, *Macromolecules* **12**, 980, (1979)
100) C. Williams, F. Brochard, H. Firsch, *Ann. Rev. Phys. Chem.* **32**, 433 (1981)
101) I. H. Park, Q. W. Wang, B. Chu, *Macromolecules* **20**, 1965 (1987)
102) L. T. Lee, O. Guiselin, A. Lapp, B. Farnoux, J. Penfold, *Phys. Rev. Lett.* **67**, 2838 (1991)

[103] P. G. de Gennes, "*Scaling Concepts in Polymer Physics*", Cornell Universiy, Ithaca 1979
[104] C. M. Wijmans, B. J. Factor, *Macromolecules* **29**, 4406 (1996)
[105] Dan, N.; Tirrell, *M. Macromolecules 26*, 6467 (1993)
[106] The magnitude of the reflectivity signal for the 20-170 copolymer in EB is insufficient to permit fine details of the profiles to be extracted. In particular, the presence of a depletion layer and slight deviations from a parabolic profile cannot be determined in this case, in contrast with the data for the 4.5-60 copolymer in Figure 3. Rather, a profile composed of a parabola with an exponential tail is sufficient to describe the reflectivity data for 20-170 in EB (see Figure 6a of Ref. 46)
[107] S. Granick, J. Herz, *Macromolecules* **18**, 460 (1985)
[108] G. S. Grest, *Macromolecules* **27**, 418 (1994)
[109] M. A. Carignano, I Szleifer, *J. Chem. Phys.* **100**, 3210 (1994)
[110] Ligoure and L. Leibler, *J. Phys. France* **51**, 1313 (1990)
[111] S. T. Milner, *Macromolecules* **25**, 5487 (1992)
[112] K. R. Shull, *Macromolecules* **29**, 2659 (1996)
[113] CRC Handbook of Chemistry and Physics, 61st Edition, R. Weast, Ed. CRC Press, Boca Raton,1980.
[114] S. Dhoot, M. Tirrell, *Macromolecules* **28**, 3692, (1995).
[115] E. Kumacheva, J. Klein, P. Pincus, L. J. Fetters, *Macromolecules* **26**, 6477, (1993).
[116] G. Grest (private communication)
[117] S. T. Milner, *Europhys. Lett* **7(8)**, 695 (1988)
[118] R. Maos, S. Matis, E. Dimasi, B. M. Ocko, J. Sagiv, *Nature* **384**, 150 (1996)
[119] A. Ulman, *Chem. Rev.* **96**, 1533 (1996)
[120] S. B. Roscoe, S. Yitzchaik, A. K. Kakkar, T. J. Marks, W. Lin, G. K. Wong, *Langmuir* **10**, 1337 (1994)
[121] S. Heid, F. Effenberger, *Langmuir* **12**, 2118 (1996)
[122] X. Huang and M. J. Wirth, *Macromolecules* **32(5)**, 1694 (1999)
[123] (a) O. Prucker, J. Ruhe, *Macromolecules* **31**, 592, (1998); (b) *ibid*, pg 602.
[124] D. Hritcu, W. Muller, D. E. Brooks, *Macromolecules* **32(3)**, 565 (1999)
[125] M. Musseman, E. E. Malmstrom, M. McNamara, M. Mate, D. Mecerreyes, D. G. Benoit, J. L. Hedrick, P. Mansky, E. Huang, T. P. Russell, C. J. Hawker, *Macromolecules* **32**, 1424 (1999)
[126] J. Habicht, M. Schmidt, J. Ruhe, D. Johannsmann, *Langmuir* **15(7)**, 2460 (1999)
[127] H. Iwata, I. Hiratia, Y. Ikada, Langmuir **13**, 3063 (1997)
[128] A. Roters, M. Schimmel, J. Ruhe, D. Johannsmann, *Langmuir* **14**, 3999 (1998)
[129] G. Tovar, S. Paul, W. Knoll, O. Prucker, J. Ruhe, *Supramolec. Sci.* **2**, 89 (1995)
[130] S. Wu, "*Polymer Interface and Adhesion*", Marcel Dekker, New York (1982)1.

Table 1. Description of polymer samples

Copolymer sample	M_w PDMS (kg/mol)	M_w PS (kg/mol)	Mw/Mn	Source
4-30	4	30 D	1.1	Polymer Labs (U.K.)
3-29	3	29 H	1.04	Polymer Source (Canada)
25-35	25	35 H	1.2	R. Jerome (Liege)
10.5-40	10.5	40 H	1.1	Y. Gallot (ICS Strasbourg)
4.5-60	4.5	60 D	1.1	Polymer Labs (U.K.)
11-66	11	66 D	1.1	Polymer Standards Service (FRG)
1.5-102	1.5	102 D	1.1	Polymer Labs (U.K.)
8-166	8	166 H	1.06	Polymer Source (Canada)
20-170	21	169 D	1.06	Polymer Standards Service (FRG)
28-330	28	330 D	1.08	Polymer Standards Service (FRG)

PDMS sample	M_w PDMS (kg/mol)	Mw/Mn	Source
PDMS-25	25	3.8	Alain Lapp (LLB, Saclay, FR)
PDMS-100	94	3.0	Aldrich
PDMS-26	25.8	1.03	Polymer Standards Service (FRG)

PS sample	M_w PS (kg/mol)	Mw/Mn	Source
PS-40	40 D	<1.1	Polymer Source (Canada)
PS-400	400 D	<1.1	Polymer Source (Canada)
PS-43	43 H	<1.1	Polymer Standards Service (FRG)
PS-400	400 H	<1.1	Polymer Standards Service (FRG)

Figure Captions

1. Illustration of the Langmuir monolayer system formed by PDMS-PS diblock copolymers on an organic liquid. A) symmetric copolymers, B) asymmetric copolymers ($M_{PS} >> M_{PDMS}$)

2. Surface tensions of the polymers and subphase liquids used in this work. Values for EB, BrEB, and DOP were measured by the Wilhelmy plate technique. Values for PS and PDMS were obtained from Ref 129.

3. a) Reflectivity from the monolayer covered surface for the 4.5-60 copolymer at Σ = 5.3 on EB. The data are divided by the calculated reflectivity for the pure EB subphase (R_o). The curves through the data are best fits using a parabolic profile as predicted by analytical SCF theory (dashed line) and an empirical profile (solid curve). The reflectivity data are not consistent with a parabolic form. b) Best-fit empirical profile corresponding to the solid curve in Figure 3a (solid line). The empirical profile from the reflectivity data compares favorably with a profile from the numerical SCF calculations of Baranowski and Whitmore[70a] using parameters corresponding to the experimental conditions.

4. a) Reflectivity from the monolayer covered surface for the 4.5-60 copolymer on BrEB at Σ = 4.8 (filled triangles), 5.9 (X), 7.9 (O), and 9.9 (●). The data are divided by the calculated reflectivity for the pure BrEB subphase (R_o). The measured reflectivity for the BrEB subphase is also shown (+). For the pure BrEB subphase the deviation of the measured reflectivity from the calculated reflectivity apparently indicates the presence of a contaminant. The effect of this contaminant has been accounted for in the data analysis as described in the text. The curves through the data for the monolayer-covered surfaces

are best-fits using empirical profiles. b) Best-fit empirical profiles corresponding to the curves in Figure 4a. These profiles contrast with the profile obtained for PS tethered to the air-EB interface in Figure 3b in that the maximum in segment concentration occurs at the surface in BrEB. This is due to the weak attraction of PS segments to the air surface of BrEB. c) Layer height for the 4-60 (triangles) and 20-170 (squares) samples on EB (filled symbols) and BrEB (open symbols). The decreased layer heights for the 4.5-60 sample in BrEB relative to the heights in EB is a result of the attraction of the PS segments to the air surface of BrEB. The importance of this effect diminishes with increasing PS block molecular weight and is negligible for the 20-170 sample.

5. a) Reflectivity data over temperatures ranging from 22 °C (T_θ) to -35 °C for 20-170 at $\sigma \cong 1.7 \times 10^{-4}$ Å^{-2}. Curves for different temperatures have been shifted on the vertical axis for clarity. Actual temperatures are given in Table I of Ref. 48. The data are divided by the calculated reflectivity for the pure DOP subphase (R_s). b) Reflectivity data for 20-170 at $\sigma \cong 1.9 \times 10^{-4}$ Å^{-2} at 22 °C (O) and at 80 °C (●). c) Best-fit empirical profiles corresponding to the curves in Figure 5a for 22 °C (T_θ) and -35 °C. Also shown is a profile obtained in good solvent conditions (EB) for comparable σ. The inset shows the best-fit empirical profiles corresponding to the curves in Figure 5b.

6. Variation in RMS layer height over the temperature range from T_θ + 58 °C to T_θ - 56 °C for $\sigma \cong 1.7 \times 10^{-4}$ Å^{-2}. The measured layer height at 80 °C was obtained for $\sigma \cong 1.9 \times 10^{-4}$ Å^{-2} and scaled to the lower σ using the data in Figure 10.

7. Variation of depletion layer with solvent quality. a) Near-surface region of best-fit profiles in good (EB) and theta (DOP, 22 °C) solvent conditions for the 4.5-60 copolymer. b) Near-surface region of best-fit profiles in theta (DOP, 22 °C) and poor (DOP, -30 °C) solvent conditions for the 20-170 copolymer.

8. a) Reflectivity from the monolayered-covered DOP surface at 22 °C for the 20-170 copolymer at reduced surface densities of 1.0, 2.2, 4.9, 6.5, and 8.4. Curves through the data are best-fits using the RG profile from Ref. 30. The RG profile describes the data reasonably well for $\Sigma \leq 5$. b) Reflectivity data at $\Sigma = 8.4$ compared with the best-fit obtained using the analytical SCF profile modified to include a depletion layer and an exponential tail (dashed curve). Much better agreement is obtained in the region from q = 0.02 to 0.04 Å-1 if the profile exponent is allowed to vary and a step of constant ϕ is added to the profile (solid curve). The inset shows the best-fit profiles corresponding to the curves through the data in b). c) Best-fit empirical profiles obtained from the data in a). No variation in the depletion layer is observed over this range of Σ.

9. Reflectivity for the 4-30 (+), 4.5-60 (♦), 20-170 (□), and 28-330 (•) copolymer monolayers near the maximum attainable surface densities. The solid curves represent the best-fits using the same profile form as in Figure 8c. b) Best-fit profiles corresponding to the reflectivity curves in a) for the 4-30 (short dashes), 4.5-60 (dot-dashed), 20-170 (long dashes), and 28-330 (solid curve) copolymers. The inset shows the depletion of d-PS segments in the near surface region. The arrows indicate the end of the depletion layer for each profile. The depletion layer increases with molecular weight.

10. a) The height of the tethered d-PS layer versus reduced surface density Σ for the 4-30 (Δ), 4.5-60 (open diamonds), 1.5-100 (∇), 20-170 (□), and 28-330 (O) copolymers at 22 °C in EB (good solvent). b) The height of the tethered d-PS layer versus reduced surface density Σ for the 4-30 (filled triangles), 4.5-60 (♦), 20-170 (■), and 28-330 (•) copolymers at 22 °C in DOP (theta solvent).

11. RMS layer heights scaled by the free chain dilute solution radii of gyration in good (open symbols) and theta (filled symbols) solvent conditions. Symbols have the same meaning as in Figure 10. Superposition of the data for the different molecular weights indicates that chain stretching is a universal function of the degree of chain overlap over the present range of Σ. Stronger chain stretching is observed in good solvent conditions.

12. a) Best-fit power law relation $h \sim \sigma^{0.22} M^{0.86}$ (solid curve) compared with the data from Figure 10a. The symbols have the same meaning as in Figure 10a. The dashed curve indicates $h \sim \sigma^{1/3}$ as predicted by scaling and SCF theories. b) Best-fit power law relation $h \sim \sigma^{0.18} M^{0.74}$ (solid curve) compared with the data from Figure 10b. The symbols have the same meaning as in Figure 10b. The dashed curve indicates $h \sim \sigma^{1/2}$ as predicted by scaling and SCF theories.

13. a) Variation of RMS layer height h_{rms} with reduced temperature τ for the 20-170 copolymer (open symbols) and the 28-330 copolymer (filled symbols). In each case, circles (squares) represent lower (higher) surface densities. For the 20-170 copolymer the surface densties are 5.8×10^{-5} Å^{-2} ($\Sigma = 2.6$ at T_θ) and 1.7×10^{-4} Å^{-2} ($\Sigma = 7.6$ at T_θ). For the 28-330 copolymer the surface densties are 5.2×10^{-5} Å^{-2} ($\Sigma = 4.5$ at T_θ) and 1.3×10^{-4} Å^{-2} ($\Sigma = 10.7$ at T_θ). The profile becomes weakly dependent on T below -20 °C ($\tau \cong -0.16$). b) Data for h_{rms} plotted according to the scaling prediction of the SCF theory of Birshtein, *et al.*[64] for the asymptotic limit of strongly-stretched ($\Sigma >> 1$,) infinite M chains. The symbols have the same meaning as in a). c) Data for h_{rms} plotted according to the scaling prediction in the limit of isolated chains ($\Sigma < 1$) The symbols have the same meaning as in a). The strong dependence on Σ at T_θ is due to the stretching of chains within the interacting tethered layers. The dependence on Σ decreases with decreasing T. At the lowest temperatures, the data approach the universal scaling predicted for the isolated chain limit.

14. a) Representative reflectivity data for 40 K deuterated free PS chains (~ 6 vol. %) and 170 K protonated tethered PS blocks. R_o is the calculated Fresnel reflectivity for a subphase of uniform composition equal to that of the EB/free chain solution. The copolymer surface density ranges up to $\Sigma \cong 12$. Open squares indicate reflectivity for $\Sigma = 0$. b) Segment concentration profiles for the 40 K free PS chains. The dashed curve indicates the free chain profile for $\Sigma = 0$. With increasing Σ, the free chains are progressively excluded from the surface region.

15. Tethered d-PS layer heights in pure EB (Δ) and in ~ 6 vol % solutions of 43 K (filled triangles) and 400 K (■) free PS chains.

16. Reflectivity data for tethered d-PS chains at $\Sigma = 11.0$ in pure EB (open circles) and at $\Sigma = 11.6$ in a 6 vol.% solution of 400 K protonated PS (filled circles). R_o is the calculated Fresnel reflectivity for the subphase in the absence of the copolymer. In contrast to the data in Figures 14a. only a small variation in seen in the reflectivity for different free chain lengths in this contrast scheme (reflectivity for the tethered d-PS chains in the 43 K PS solution not shown). The inset shows the segment concentration profiles of the tethered d-PS block in pure EB (dashed line) and in the 6 vol.% solution of 400 K protonated PS (solid line).

17. Comparison of the segment profiles for the 170 K tethered PS block at $\Sigma \cong 12$ and for the 40 K free PS chains. While the free chains are largely excluded from the surface region, there is more penetration of free chains into the tail of the brush than is predicted by SCF calculations in the asymptotic limit (dashed lines).

18. Reflectivity for the following bimodal monolayers: a) 11-66/20-170, b) 11-66,/28-330, and c) 4-30/28-330. R_0 is the calculated reflectivity for a bare EB surface. The solid curves through the data are best-fits calculated using the model profile in eqn 1 of the text. The corresponding best-fit profiles are shown in Figure 19.

19. Best-fit profiles corresponding to the solid curves in Figure 18 for the following bimodal monolayers: a) 11-66/20-170, b) 11-66,/28-330, and c) 4-30/28-330.

20. a) Comparison of the layer heights of the 170 K PS blocks in the mixed monolayers (solid circles) with those in the single component 20-170 monolayers (open squares) as a function of $\sigma_{20\text{-}170}$. In the strongly interacting regime ($\Sigma >> 1$), the 170 K blocks are more stretched in the bimodal monolayer than in the single component monolayers at fixed $\sigma_{20\text{-}170}$. The curve through the single component data corresponds to a power law dependence and is a guide to the eye. b) Comparison of the layer heights of the 66 K PS blocks in the 11-66/20-170 mixed monolayers (solid circles) with those in the single component 11-66 monolayers (open squares) as a function of $\sigma_{11\text{-}66}$. In the strongly interacting regime, the 66 K blocks have nearly the same dimension in the bimodal monolayer as in the single component monolayers. The curve through the single component data is a guide to the eye.

21. a) Reflectivity for bimodal tethered layers composed of 30 K and 170 K PS chains. Solid circles correspond to data for a 4-30/20-170 mixed monolayer, where both PS blocks are deuterated. Open squares correspond to data for 3-29/9-166 mixed monolayers, where the PS block for 9-166 is deuterated and the PS block for 3-29 is protonated. Solid curves through the data corresponding to best-fits using the empirical profiles shown in b) and c). Dashed curves correspond to best-fits using eqn 1 (4-30/20-170 mixed monolayer) and a parabola (3-29/9-166 mixed monolayer). b) Best-fit d-PS segmental profiles corresponding to the data for the 4-30/20-170 mixed monolayer in a)

using an empirical form (solid curve) and eqn 1 (dashed curve). c) Best-fit d-PS segmental profiles corresponding to the data for the 3-29/9-166 mixed monolayer in a) using an empirical form (solid curve) and a parabola (dashed curve). The inset shows a parameter-free comparison between the experimentally determined empirical profile for the longer chains and the profile predicted by the analytical SCF theory of Birstein, et al.[64] Stronger stratification is predicted in the strong-stretching limit than is observed in the experimental profile.

22. a) Comparison of surface pressure isotherms for the 4-30 (+), 4.5-60 (♦), 20-170 ( ), 28-330 (•), 10.5-40 (filled triangles) and 25-35 (■) copolymers with that for PDMS homopolymer (solid curve) on EB. The same isotherm resulted for two PDMS samples of molecular weight 25,000 and 100,000 g/mol. The difference in surface pressure ($\Delta\Pi$) at a given PDMS surface concentration indicates the effect due to the interaction of the submerged PS blocks. This difference in surface pressure is related to the free energy of the tethered PS layer as described in the text. b) Comparison of surface pressure isotherms for the 4-30, 4.5-60, 20-170, 28-330 copolymers with that for PDMS homopolymer (solid curve) on BrEB. Symbols have the same meaning as in a). c) Comparison of surface pressure isotherms for the 4-30, 4.5-60, 20-170, 28-330 copolymers with that for PDMS homopolymer (solid curve) on DOP. Symbols have the same meaning as in a).

23. Surface pressure excess versus surface density in good (open symbols) and theta (filled symbols) solvents for a) 4-30 (squares) and 20-170 (circles) copolymers, and b) 4.5-60 (squares) and 28-330 (circles) copolymers. The increase in $\Delta\Pi$ with σ in theta conditions is similar to that observed in a good solvent, but shifted to higher σ.

24. Comparison of experimental excess pressures with the dependencies predicted by SCF theory in a) good solvent and b) theta solvent conditions. Symbols have the same meaning as in Figure 22. SCF theory predicts that the data for different M should collapse onto a horizontal line in these representations.

25. Examination of the M dependence of the pseudo hard-core radii in a) good solvent and b) theta solvent conditions. The symbols have the same meaning as in Figure 22. If the hard core radius were directly proportional to the isolated rms tethered chain dimension (or R_g), the sharp rise in surface pressure would occur at the same value of Σ for each copolymer. However, the data indicate that larger tethered chains can be compressed to a greater degree before the hard-core-like behavior occurs.

26. Surface pressure isotherms for the 20-170 (■) and 28-330 (•) block copolymers and PDMS homopolymer (solid line) on DOP at a) 22 °C and b) -30 °C.

27. Decrease in excess surface pressure ($\Delta\Pi$) observed over the temperature range from $\tau = 0$ (□) to $\tau = -0.21$ (□) compared to the $\Delta\Pi$ isotherms in good (O) and theta (•) solvents for a) the 20-170 copolymer and b) the 28-330 copolymer. The decrease in $\Delta\Pi$ over this T range is smaller than expected based on the difference in the isotherms in good and theta solvent conditions. This seems to suggest a non-equilibrium or pathway dependent effect.

28. Comparison of $\Delta\Pi$ isotherms in EB (filled symbols) and BrEB (open symbols) for the 20-1 (circles) copolymers. The σ value where the rise in pressure occurs is nearly independent of sul constant solvent quality is maintained.

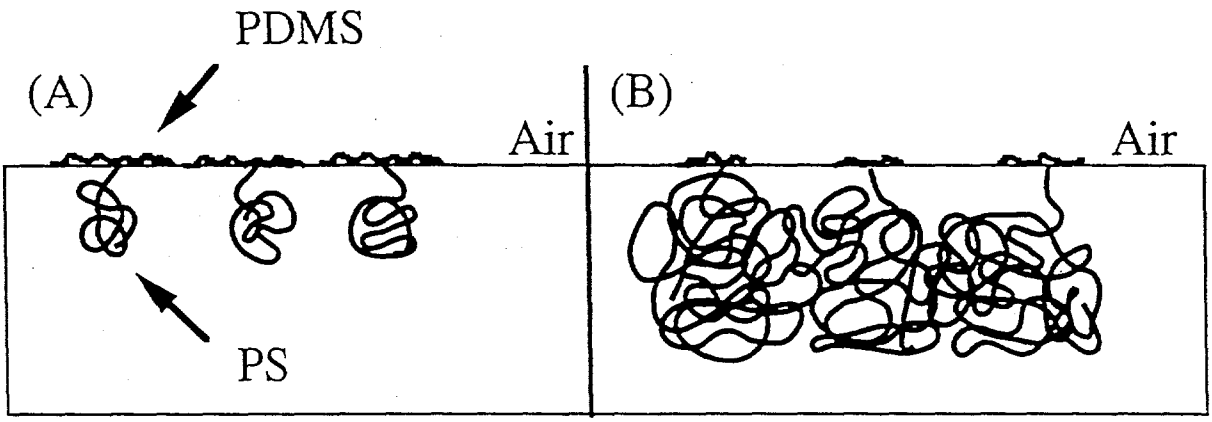
PDMS
(A)
Air
PS
(B)
Air

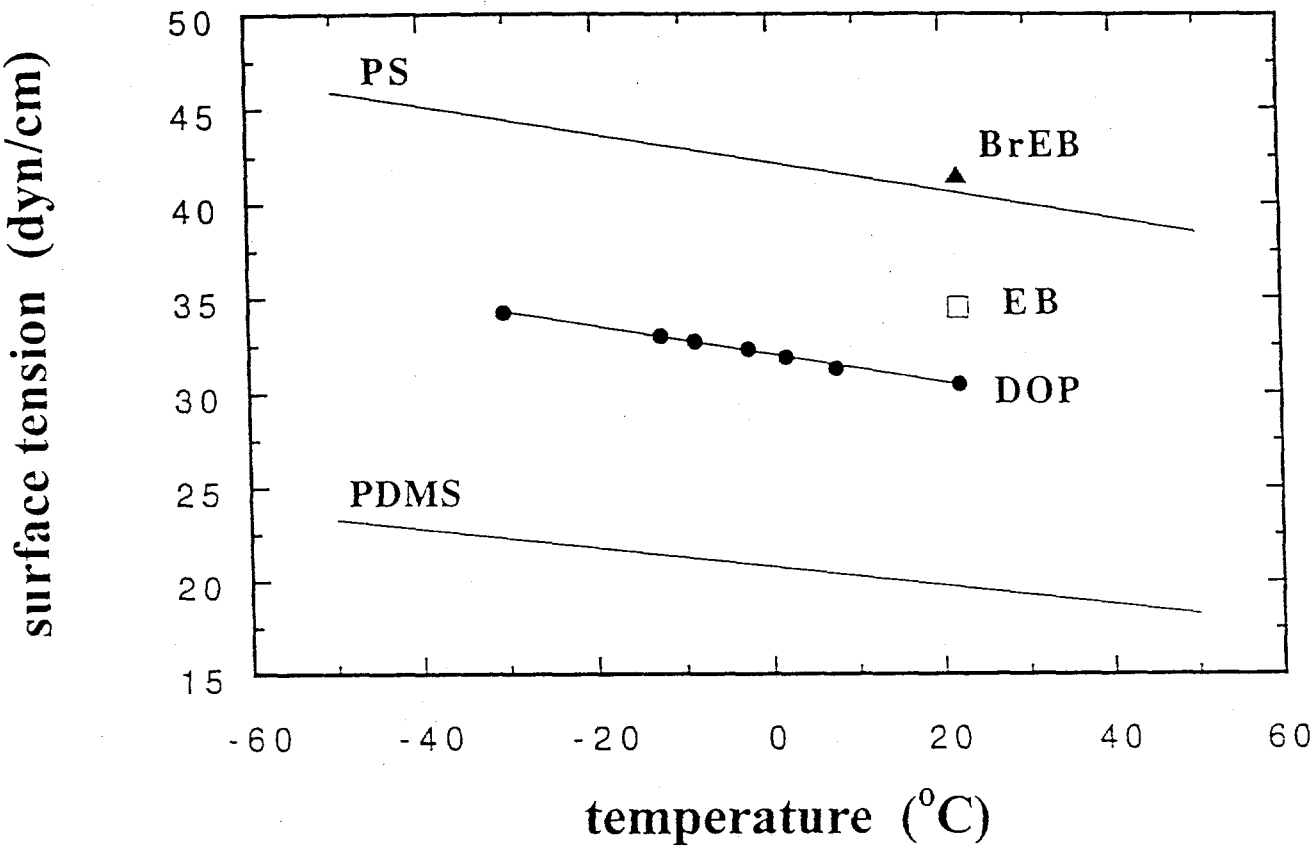
surface tension (dyn/cm)
50
45
40
35
30
25
20
15
PS
BrEB
EB
DOP
PDMS
-60
-40
-20
0
20
40
60
temperature (°C)

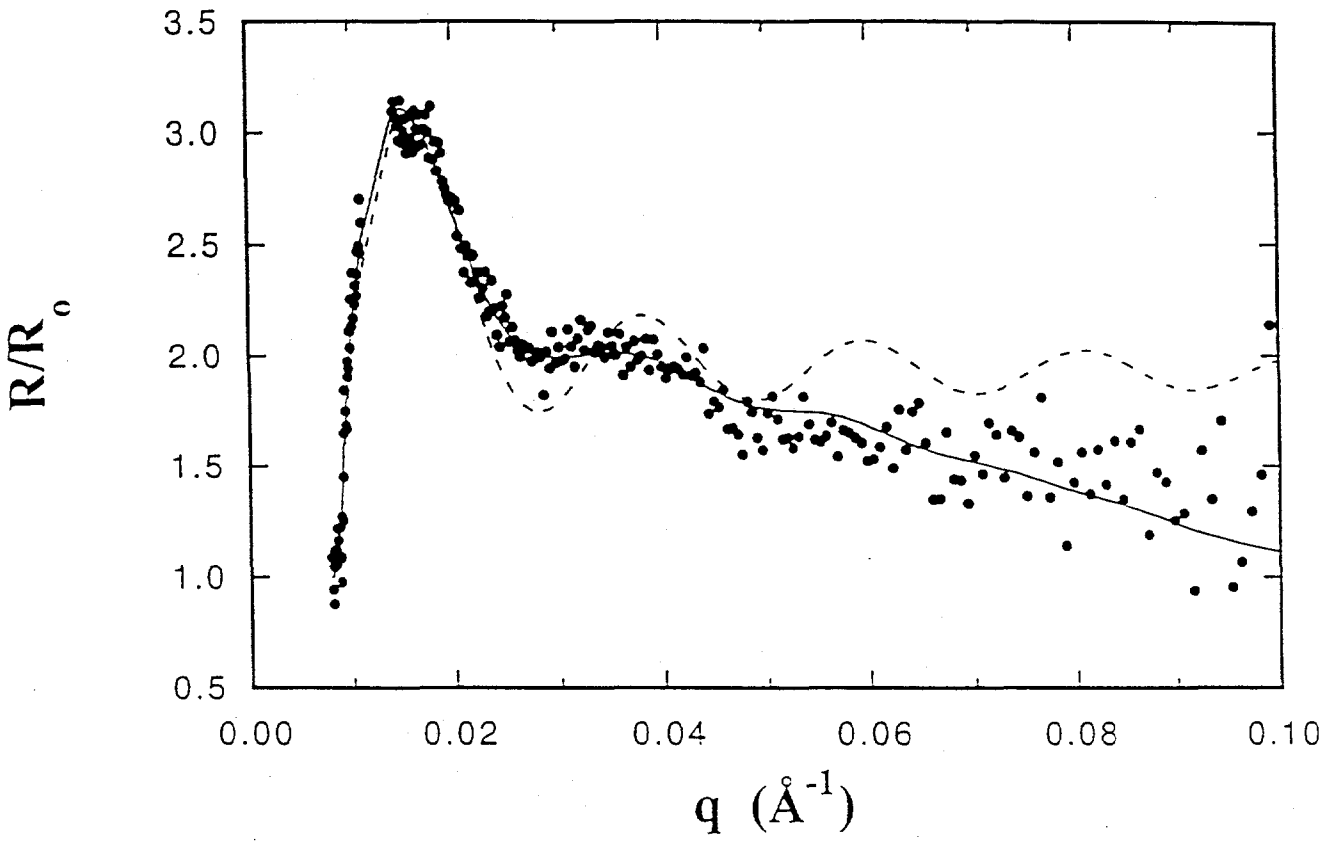
3.5
3.0
2.5
2.0
1.5
1.0
0.5
R/R$_o$
0.00
0.02
0.04
0.06
0.08
0.10
q (Å^{-1})

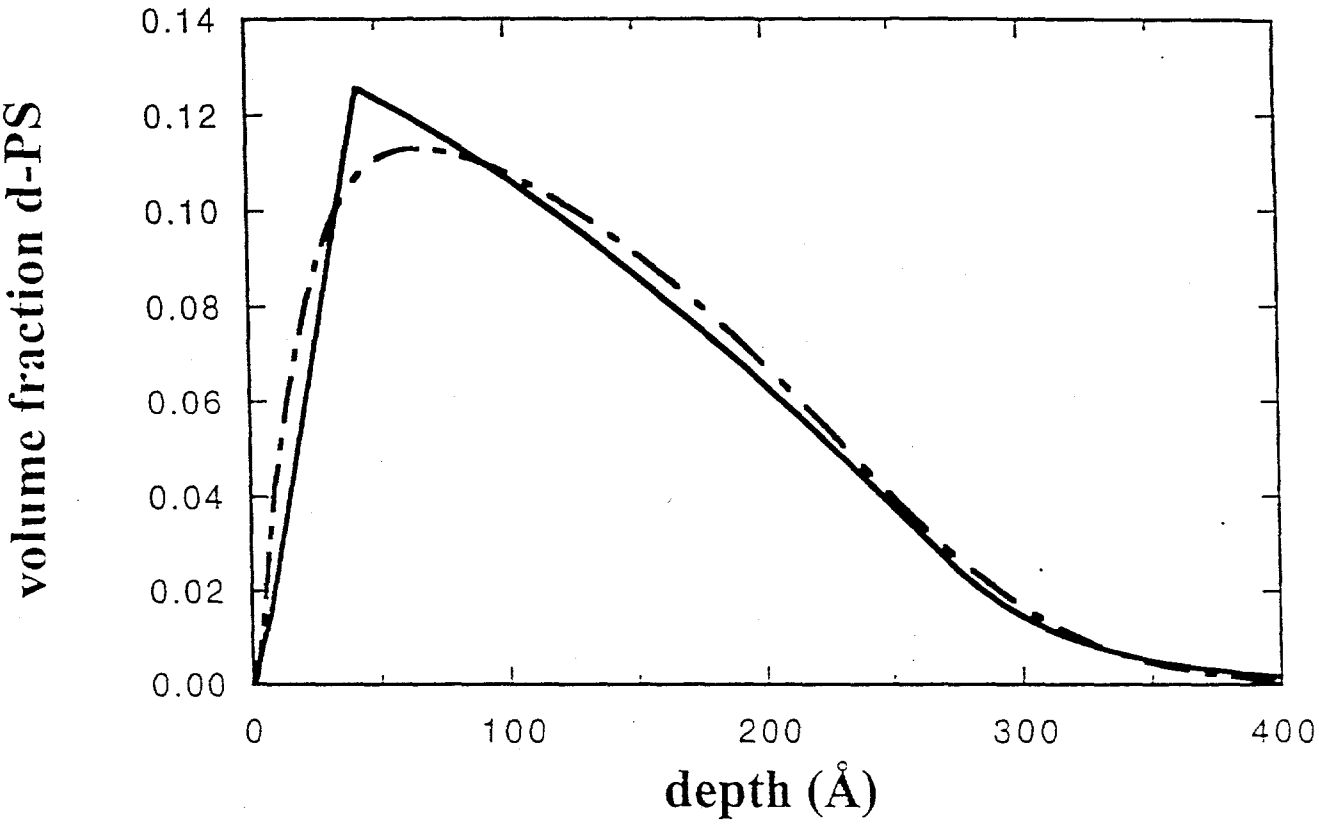
volume fraction d-PS
0.14
0.12
0.10
0.08
0.06
0.04
0.02
0.00
0
100
200
300
400
depth (Å)

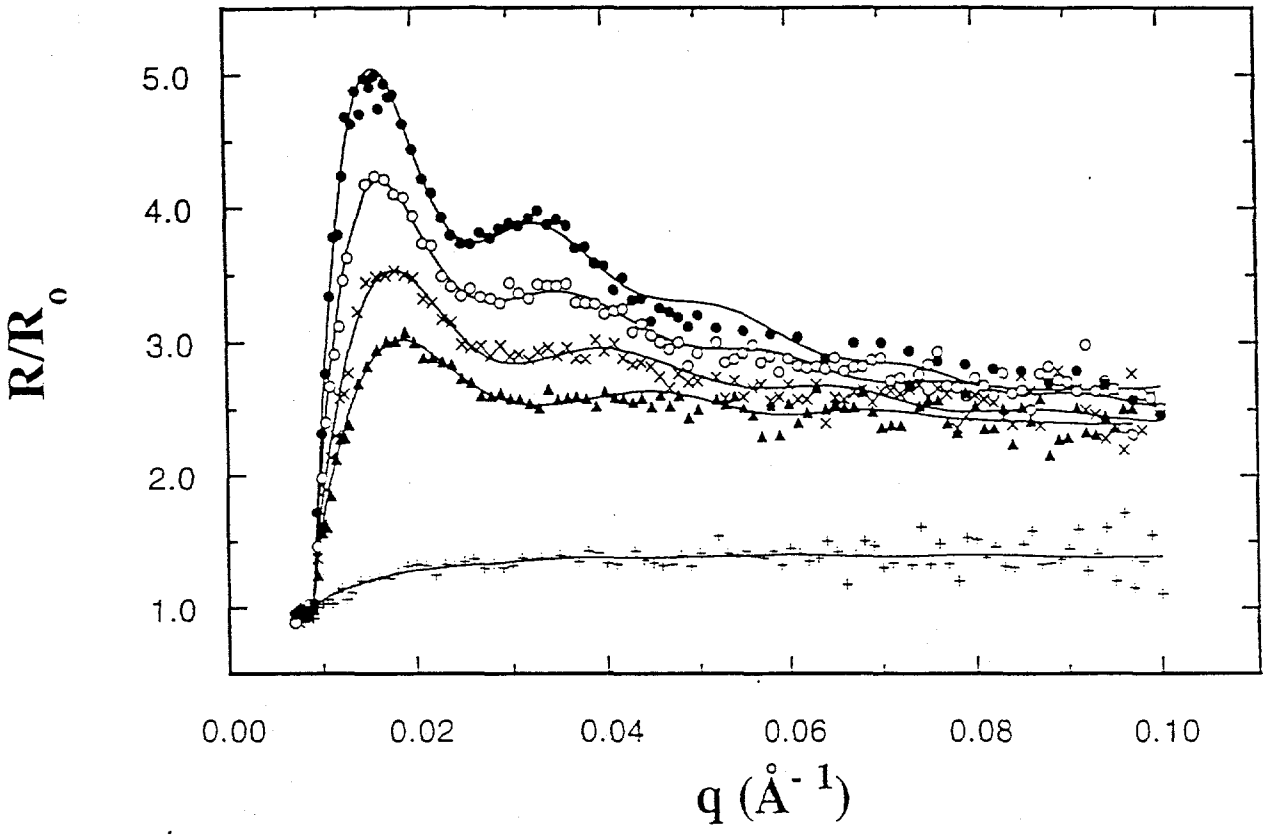
R/R0
5.0
4.0
3.0
2.0
1.0
0.00
0.02
0.04
0.06
0.08
0.10
q (Å-1)

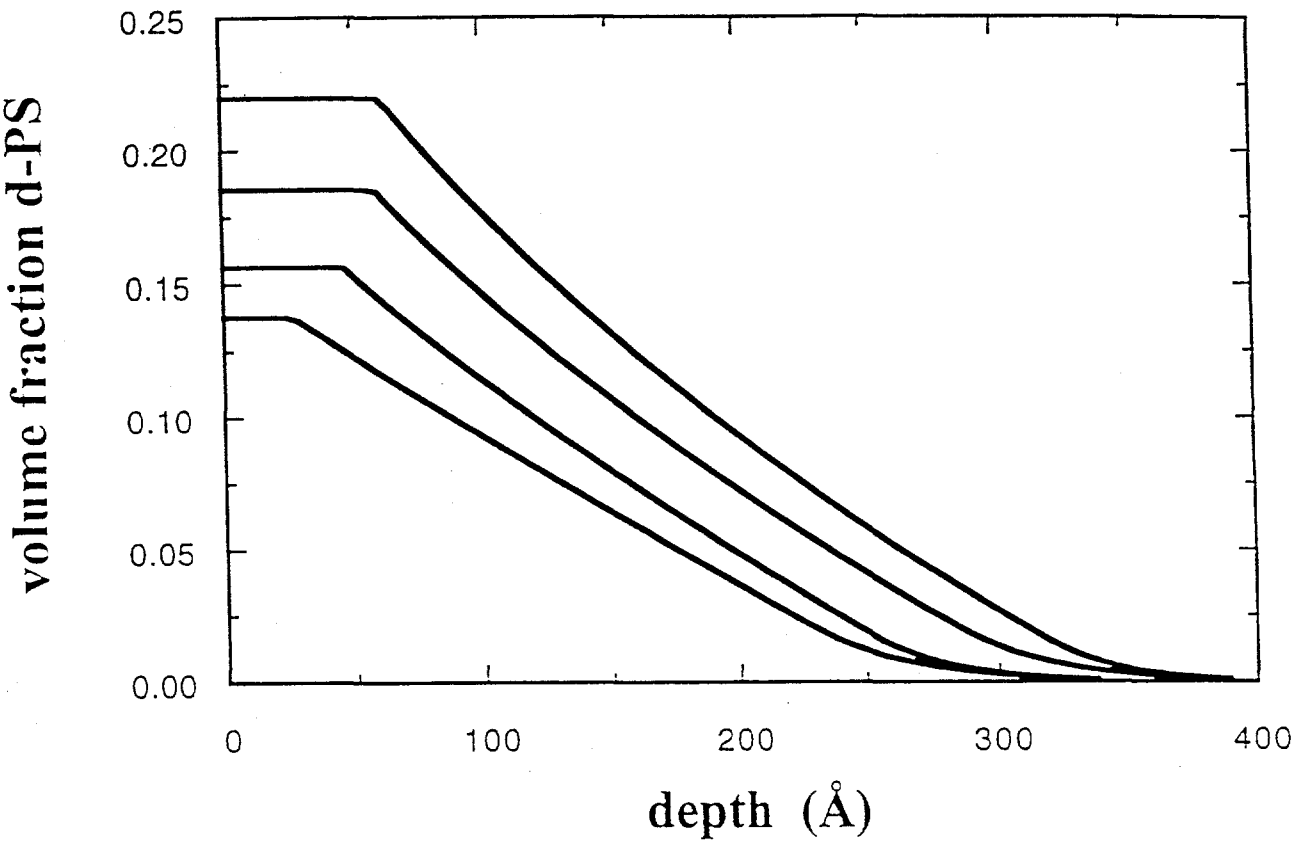
volume fraction d-PS
0.25
0.20
0.15
0.10
0.05
0.00
0
100
200
300
400
depth (Å)

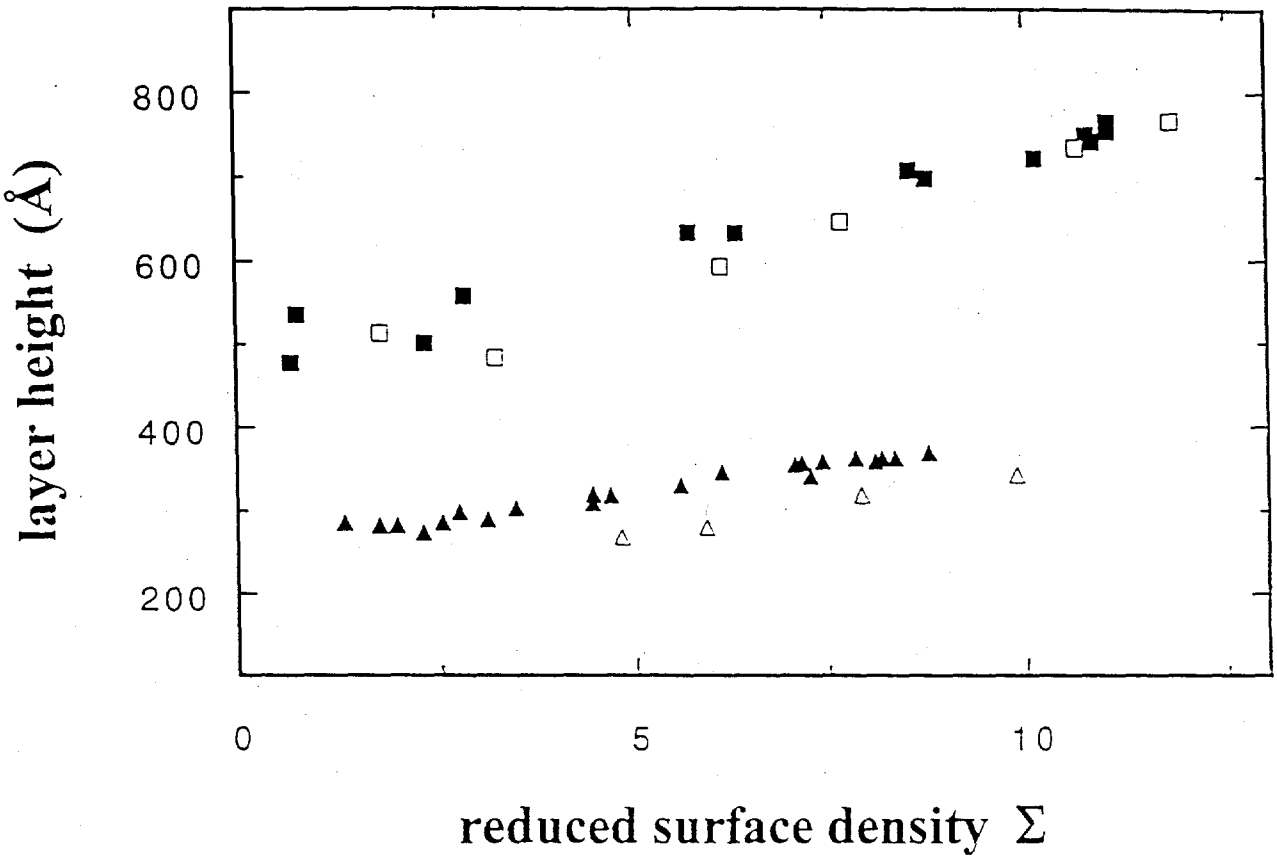
800
600
400
200
layer height (Å)
0
5
10
reduced surface density Σ

4c

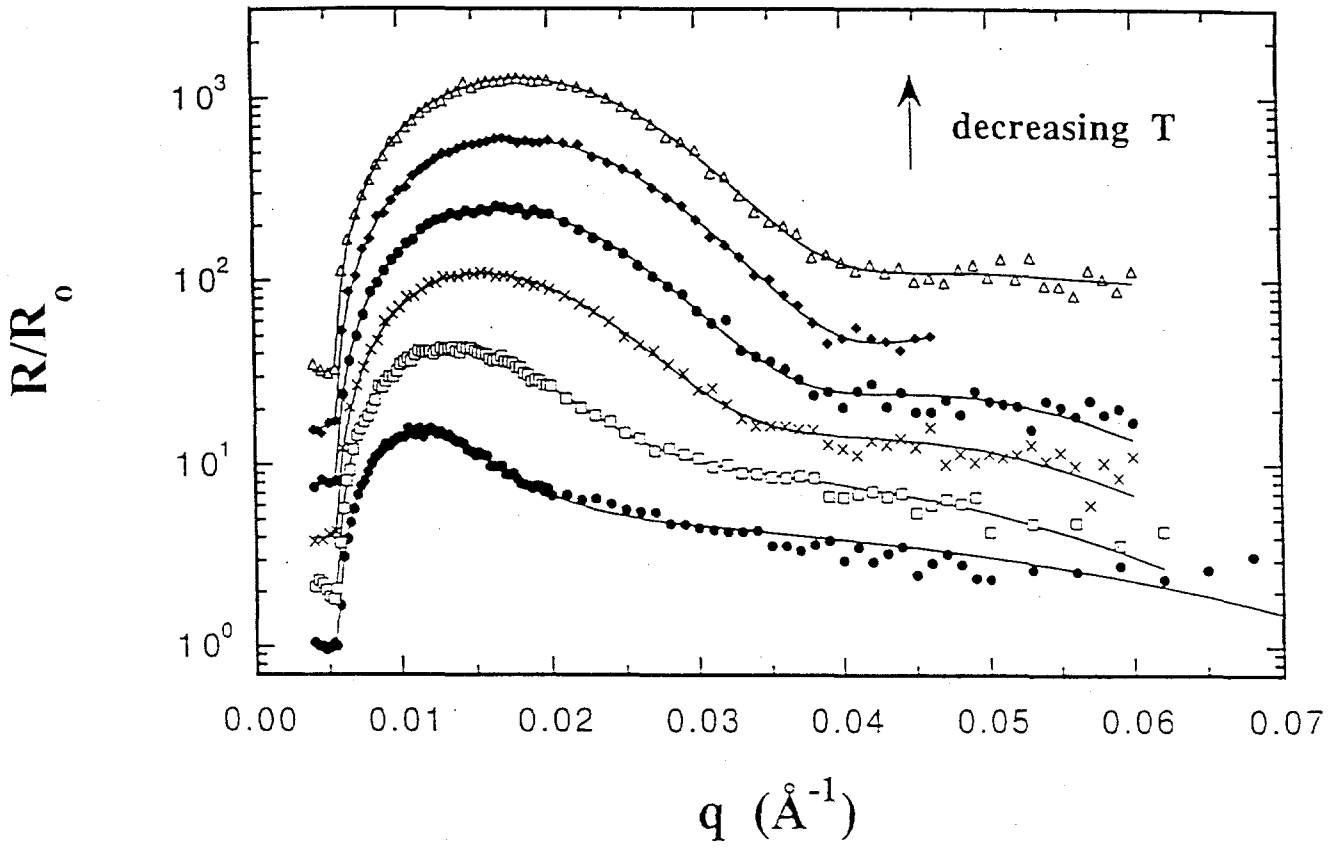
R/R0
10^3
10^2
10^1
10^0
decreasing T
0.00
0.01
0.02
0.03
0.04
0.05
0.06
0.07
q (Å^-1)

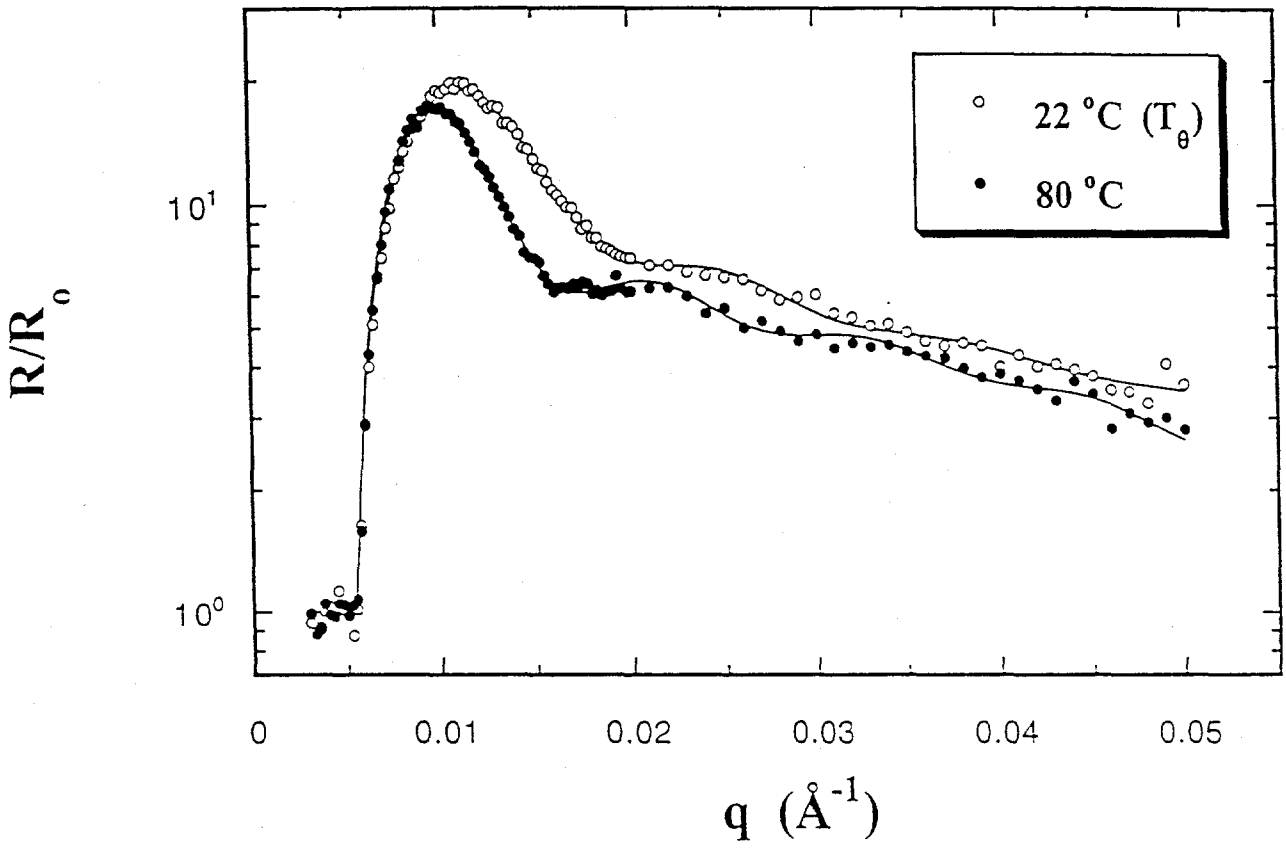
22 °C (T_θ)
80 °C
R/R_o
10^1
10^0
0
0.01
0.02
0.03
0.04
0.05
q (Å^-1)

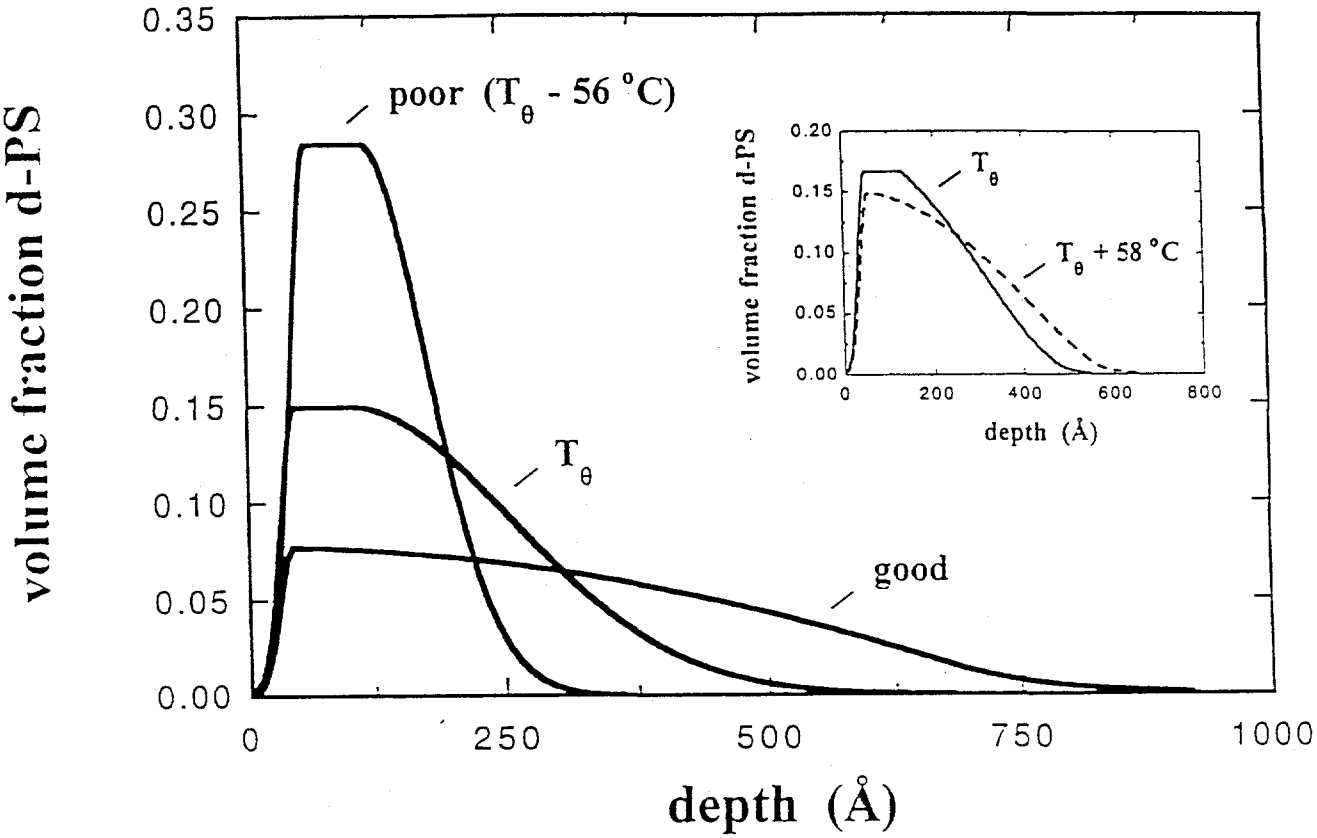
volume fraction d-PS
0.35
0.30
0.25
0.20
0.15
0.10
0.05
0.00
poor (T_θ - 56 °C)
T_θ
good
0
250
500
750
1000
depth (Å)
volume fraction d-PS
0.20
0.15
0.10
0.05
0.00
T_θ
T_θ + 58 °C
0
200
400
600
800
depth (Å)

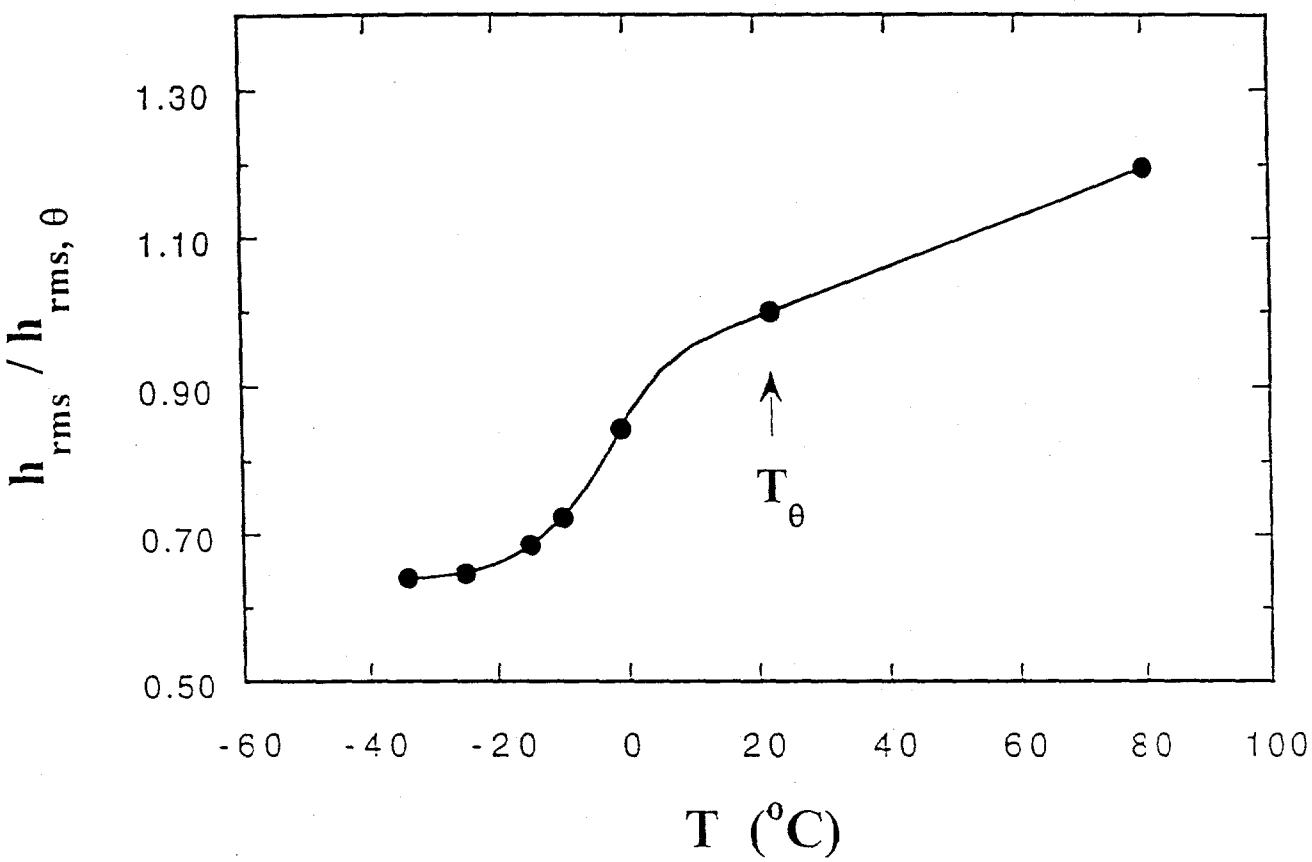
1.30
1.10
0.90
0.70
0.50
$h_{rms} / h_{rms,\theta}$
T_θ
-60
-40
-20
0
20
40
60
80
100
T (°C)

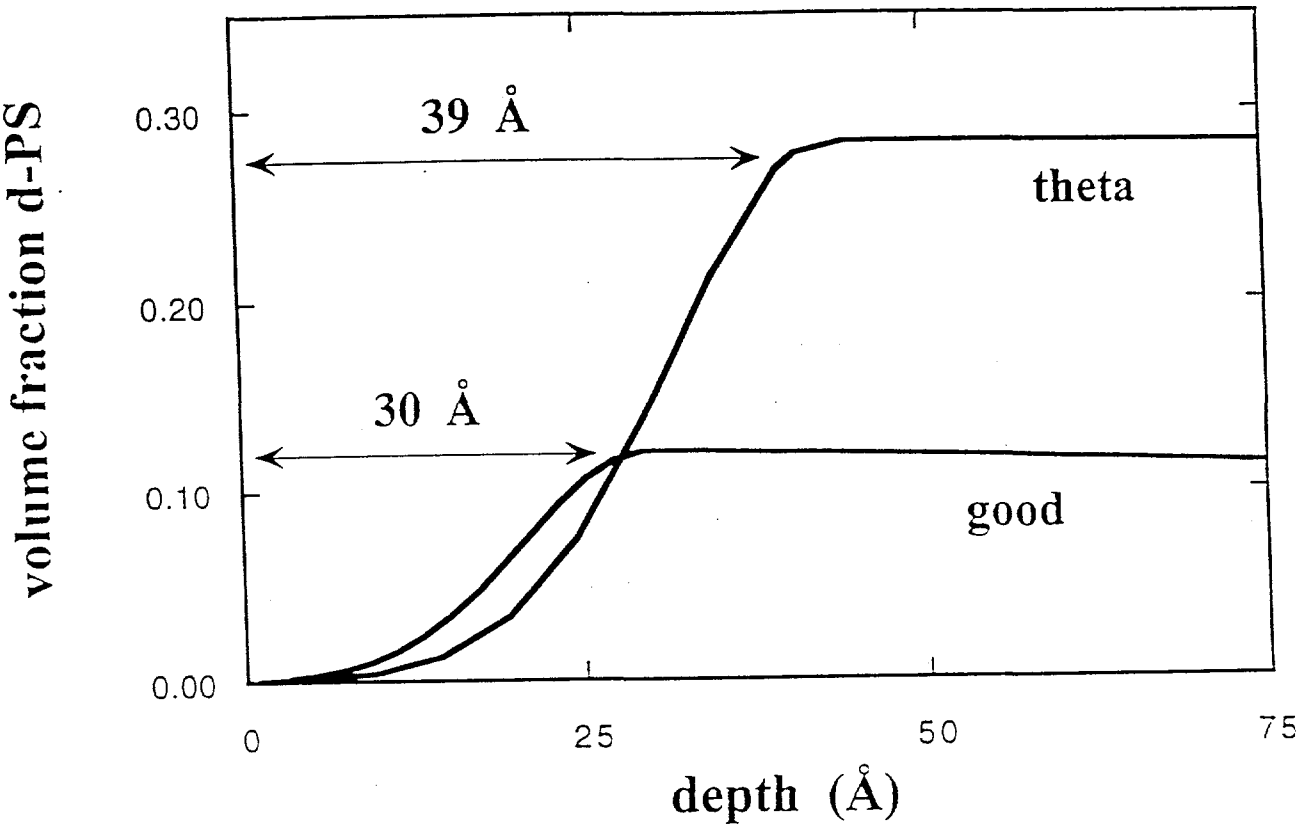
volume fraction d-PS
0.30
0.20
0.10
0.00
39 Å
30 Å
theta
good
0
25
50
75
depth (Å)

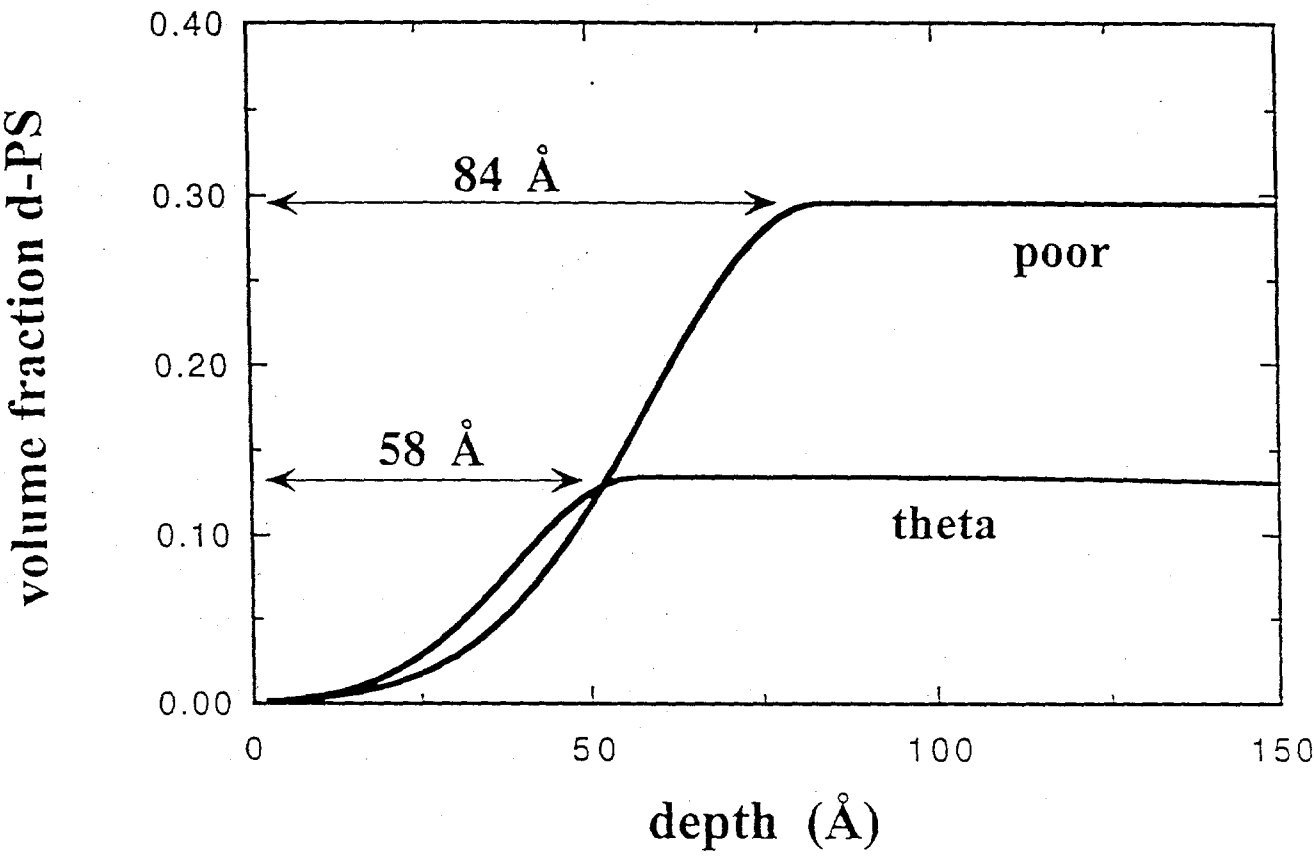
volume fraction d-PS
0.40
0.30
0.20
0.10
0.00
84 Å
58 Å
poor
theta
0
50
100
150
depth (Å)

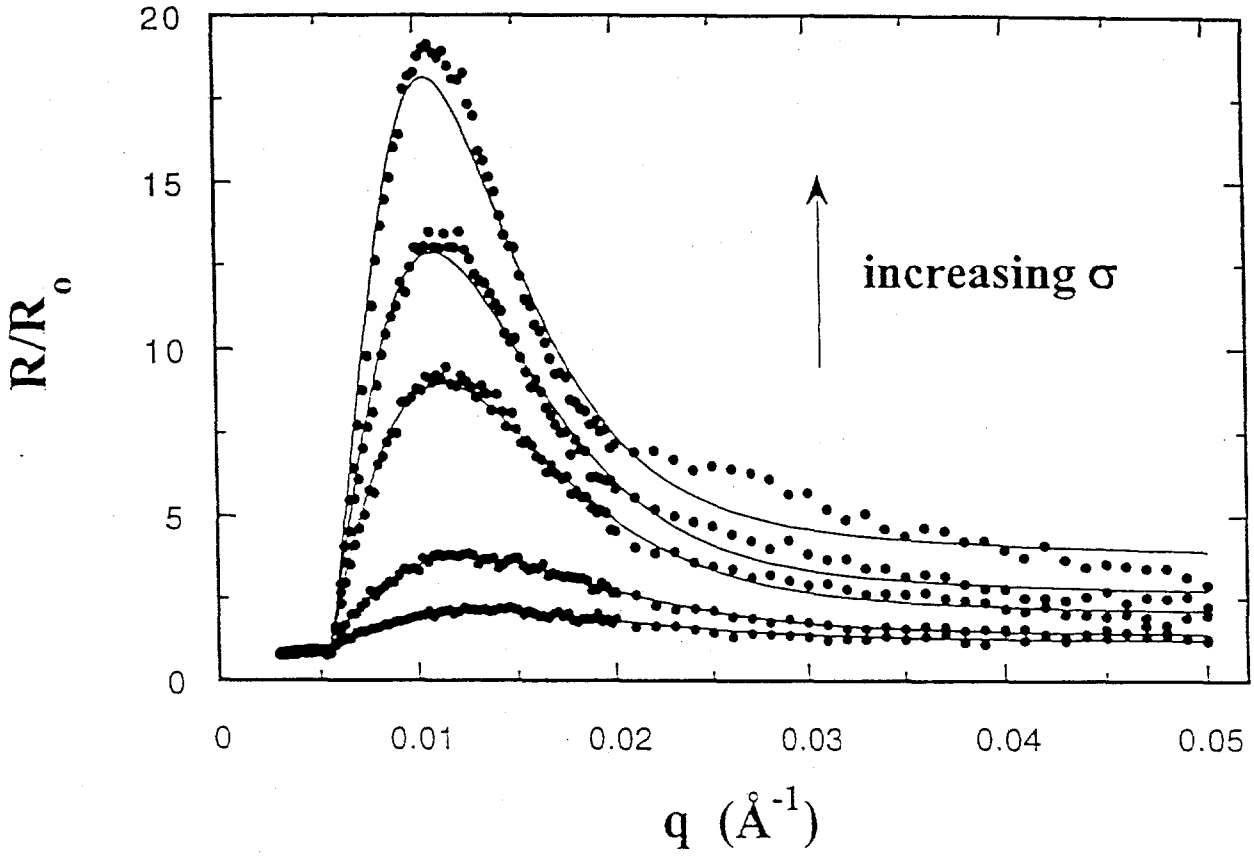
20
15
10
5
0
R/R$_o$
increasing σ
0
0.01
0.02
0.03
0.04
0.05
q (Å^{-1})

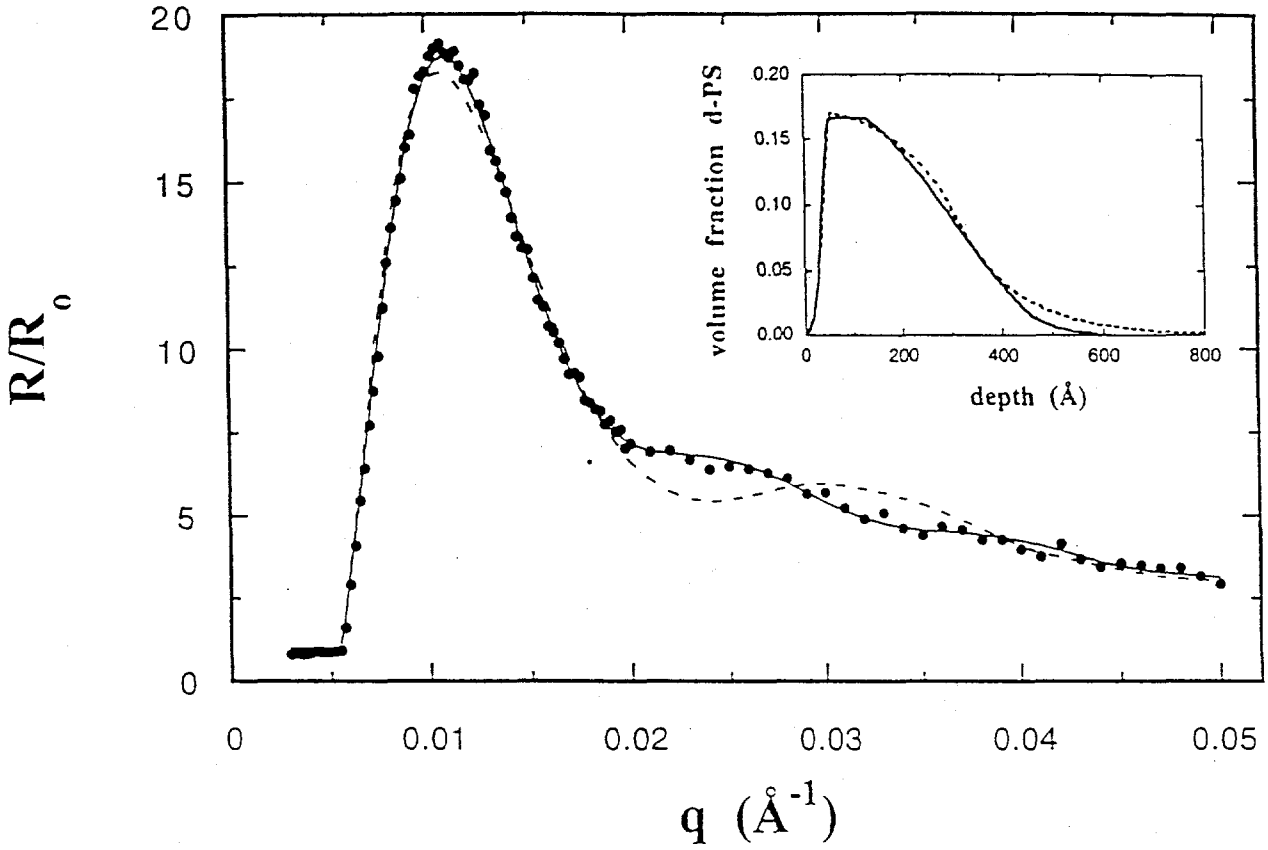
R/R0
20
15
10
5
0
0
0.01
0.02
0.03
0.04
0.05
q (Å-1)
volume fraction d-PS
0.20
0.15
0.10
0.05
0.00
0
200
400
600
800
depth (Å)

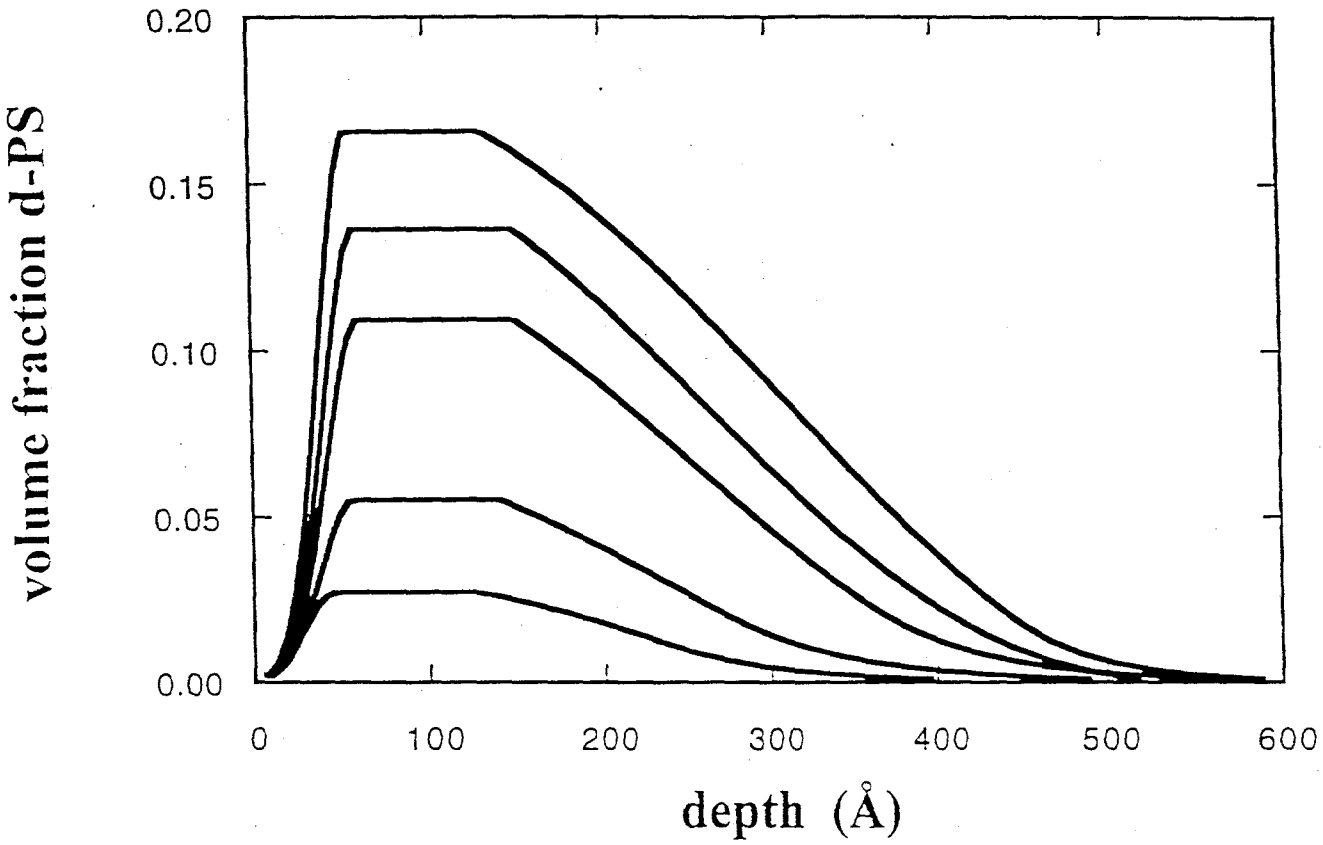
volume fraction d-PS
0.20
0.15
0.10
0.05
0.00
0
100
200
300
400
500
600
depth (Å)

8c

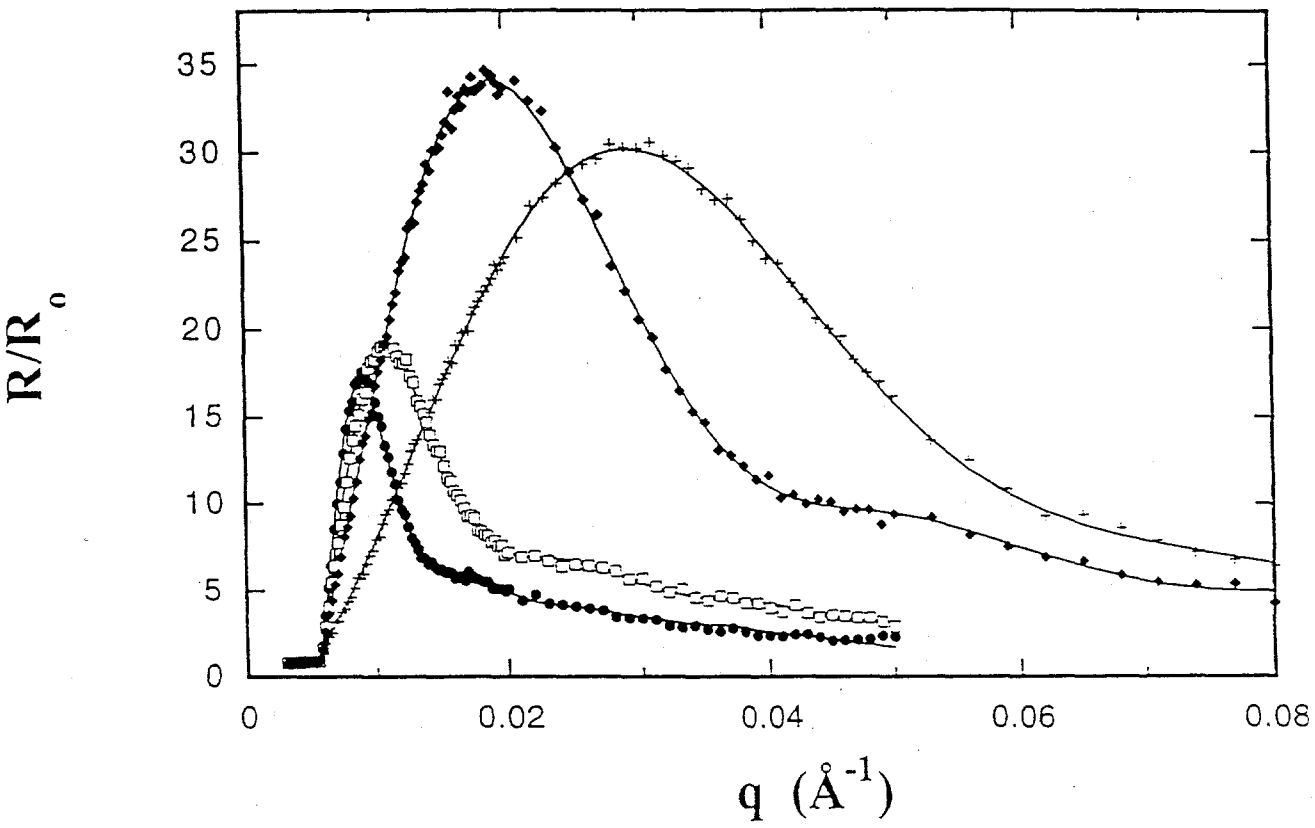
R/R0
35
30
25
20
15
10
5
0
0
0.02
0.04
0.06
0.08
q (Å-1)

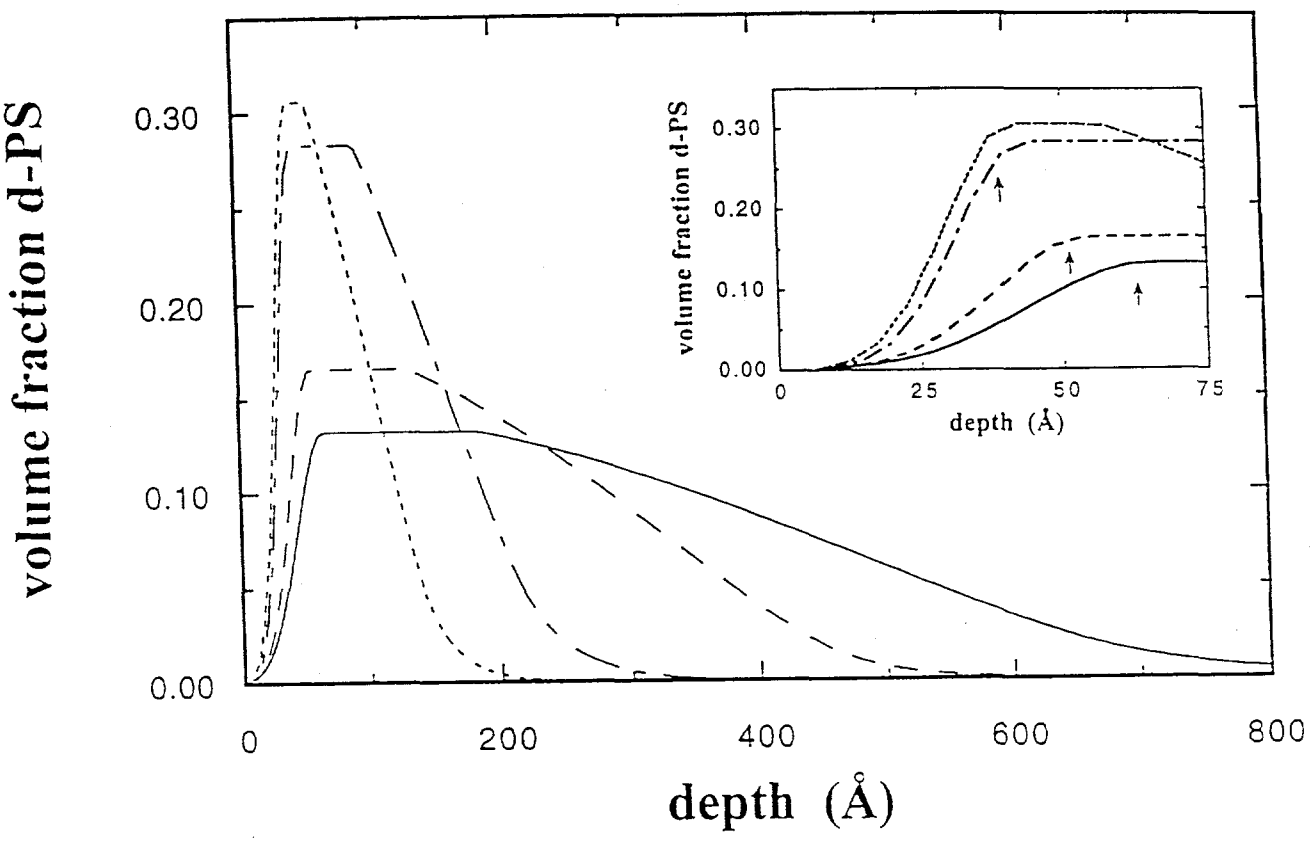
volume fraction d-PS
0.30
0.20
0.10
0.00
0
200
400
600
800
depth (Å)
volume fraction d-PS
0.30
0.20
0.10
0.00
0
25
50
75
depth (Å)

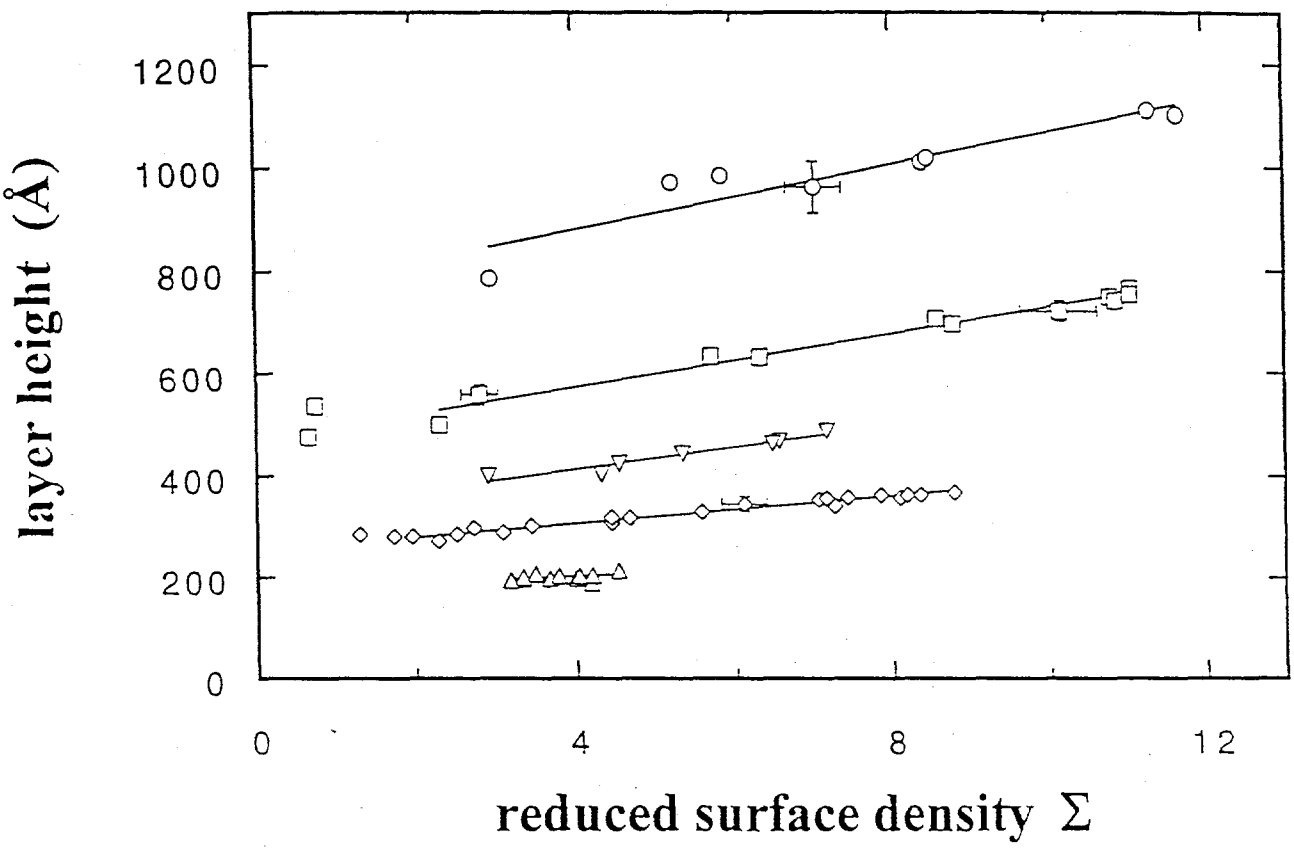
layer height (Å)
1200
1000
800
600
400
200
0
0
4
8
12
reduced surface density Σ

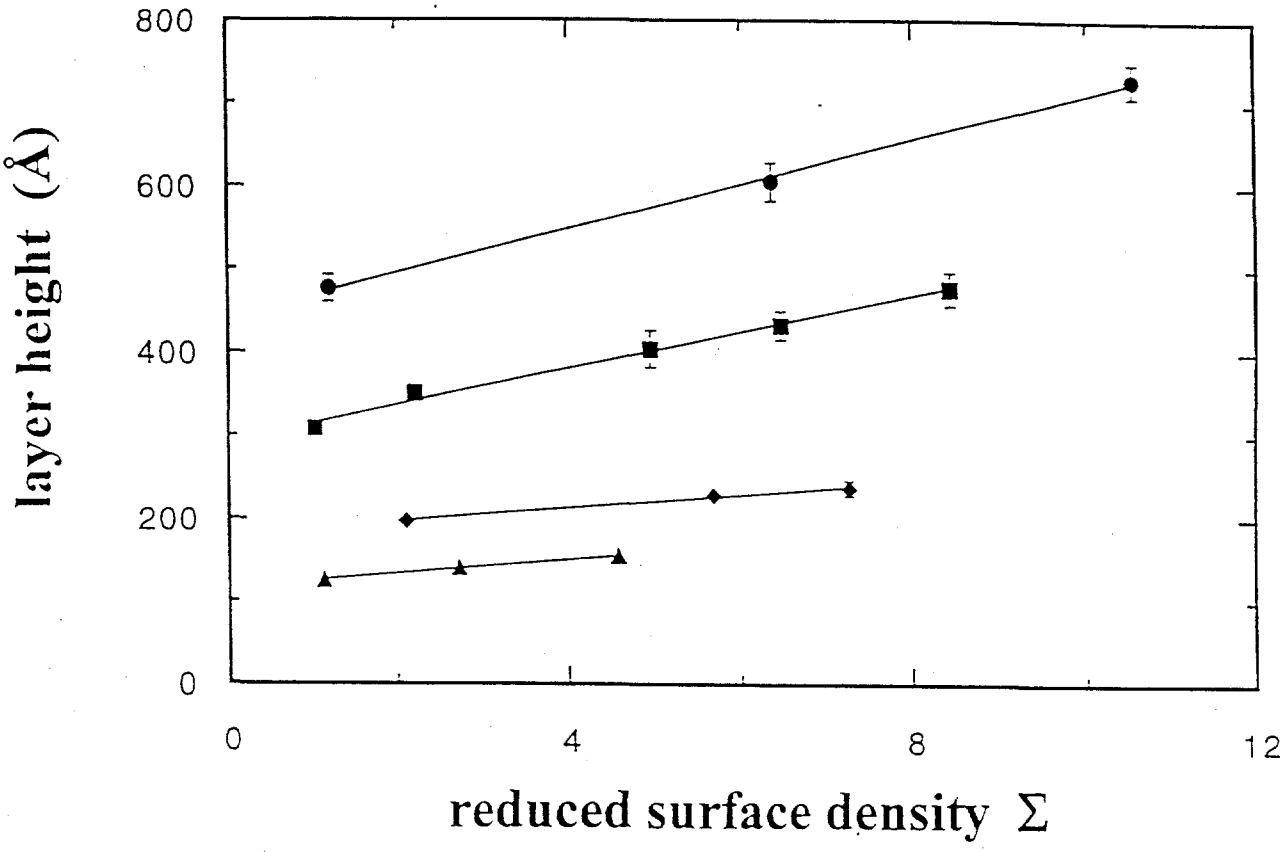
800
600
400
200
0
layer height (Å)
0
4
8
12
reduced surface density Σ

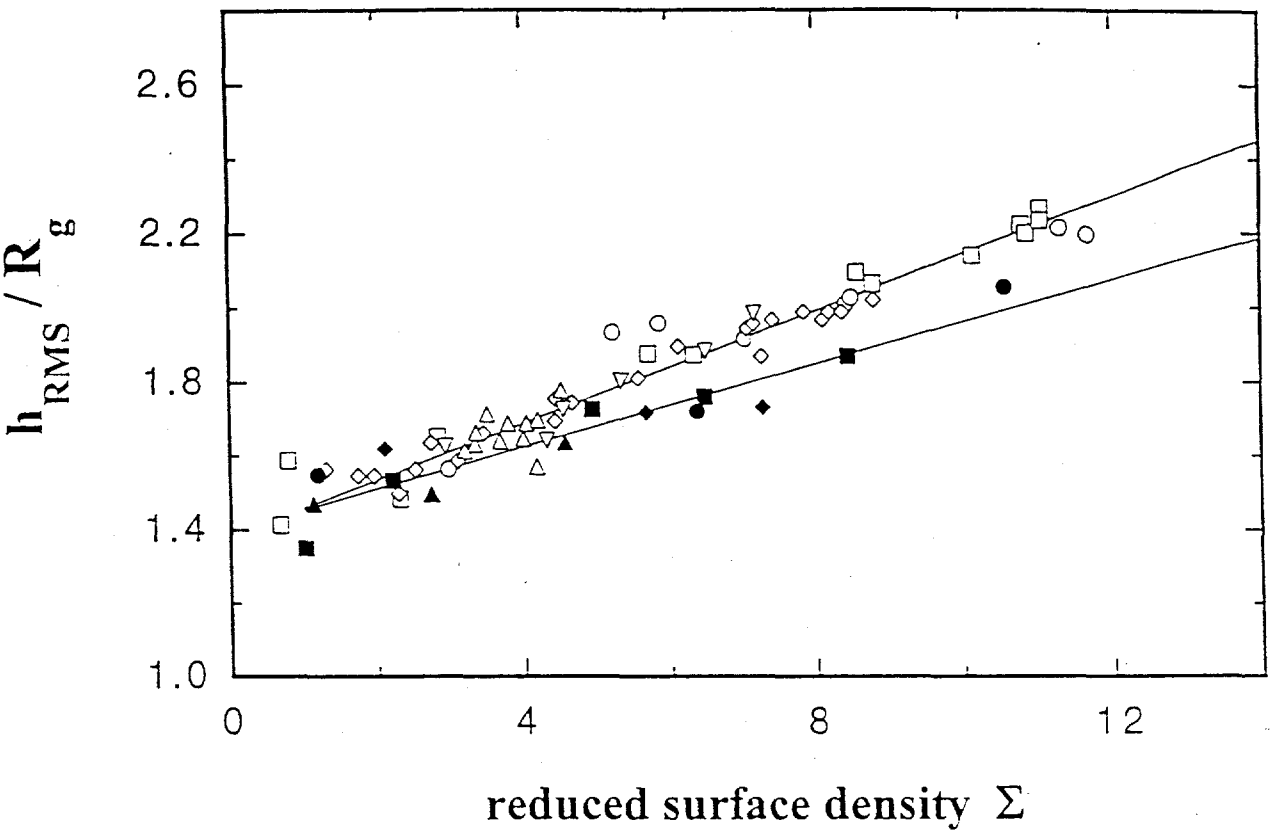
2.6
2.2
1.8
1.4
1.0
0
4
8
12
h_{RMS} / R_g
reduced surface density Σ

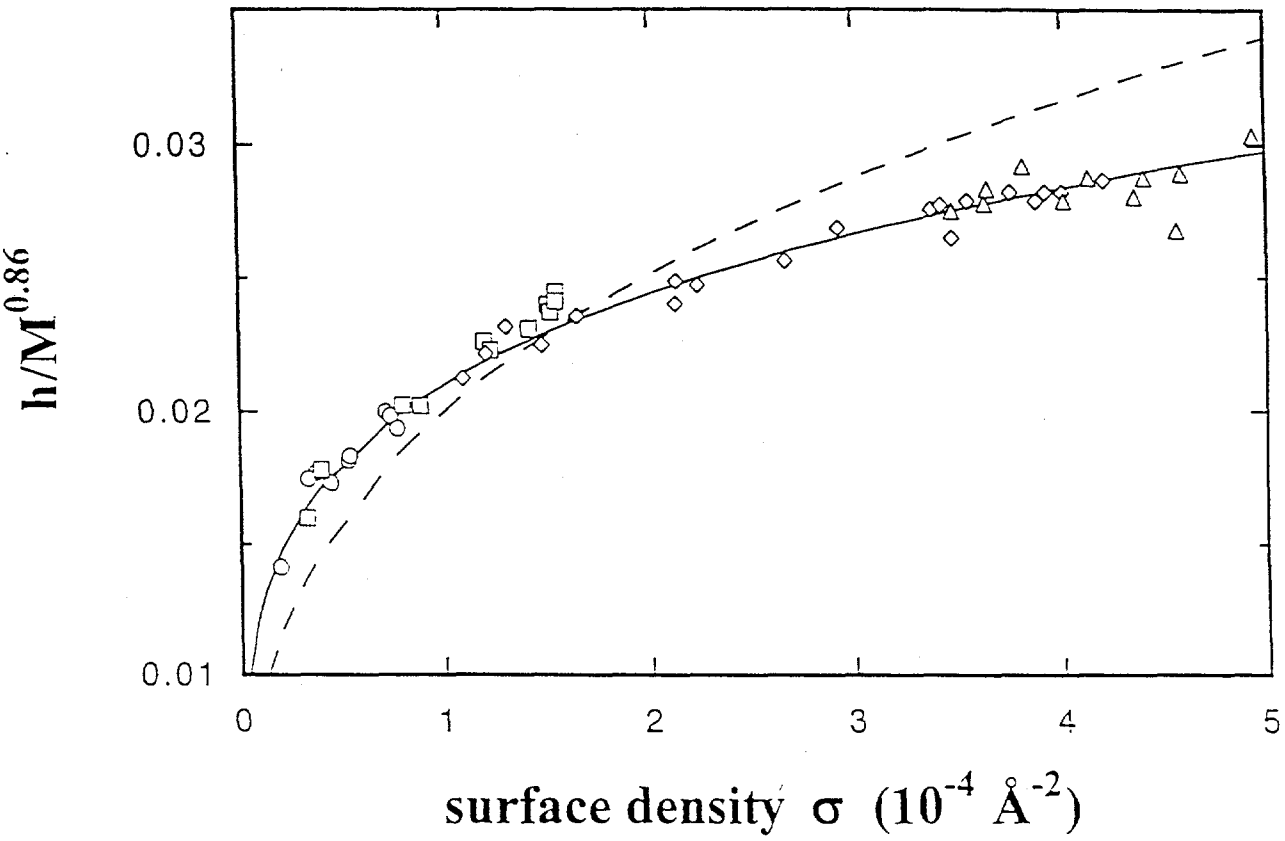
0.03
0.02
0.01
0
1
2
3
4
5
h/M^0.86
surface density σ (10^-4 Å^-2)

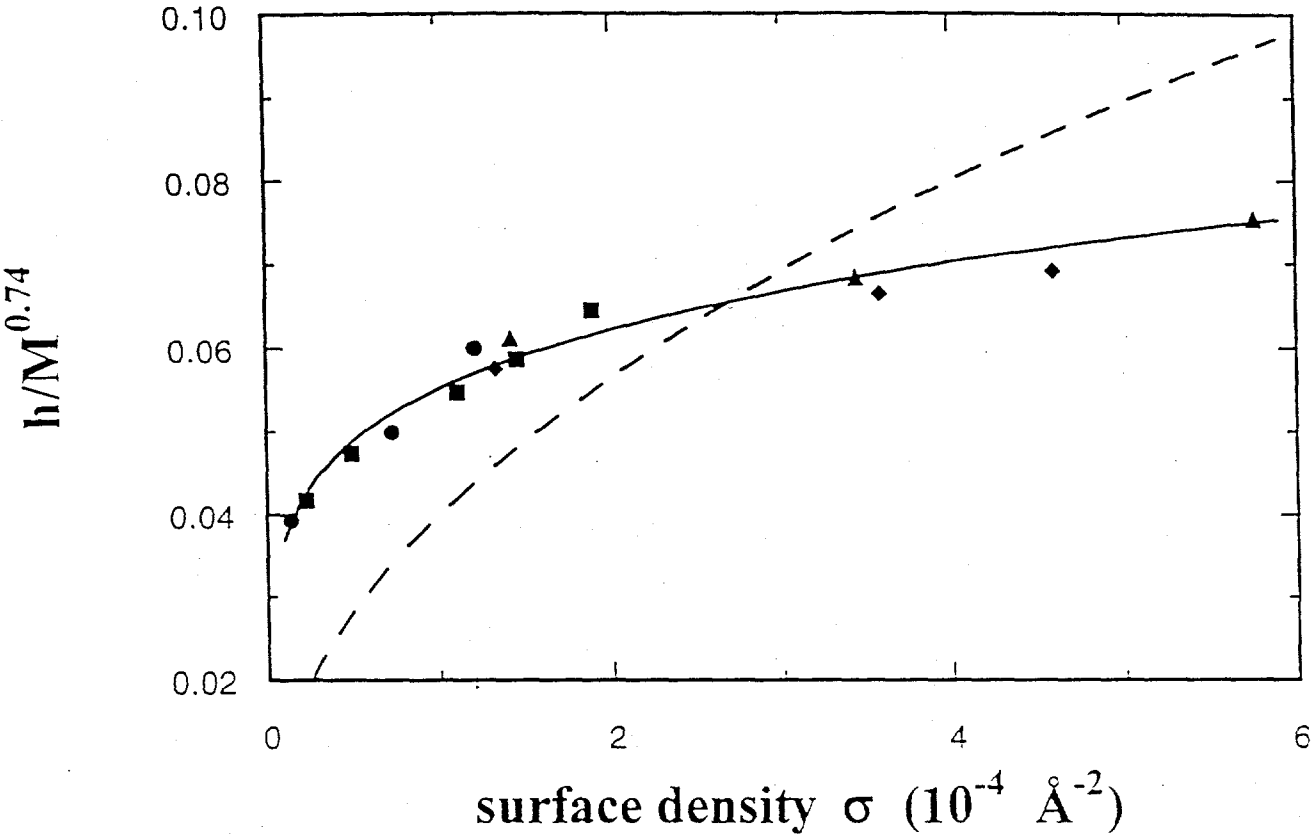
0.10
0.08
0.06
0.04
0.02
0
2
4
6
h/M^0.74
surface density σ (10^-4 Å^-2)

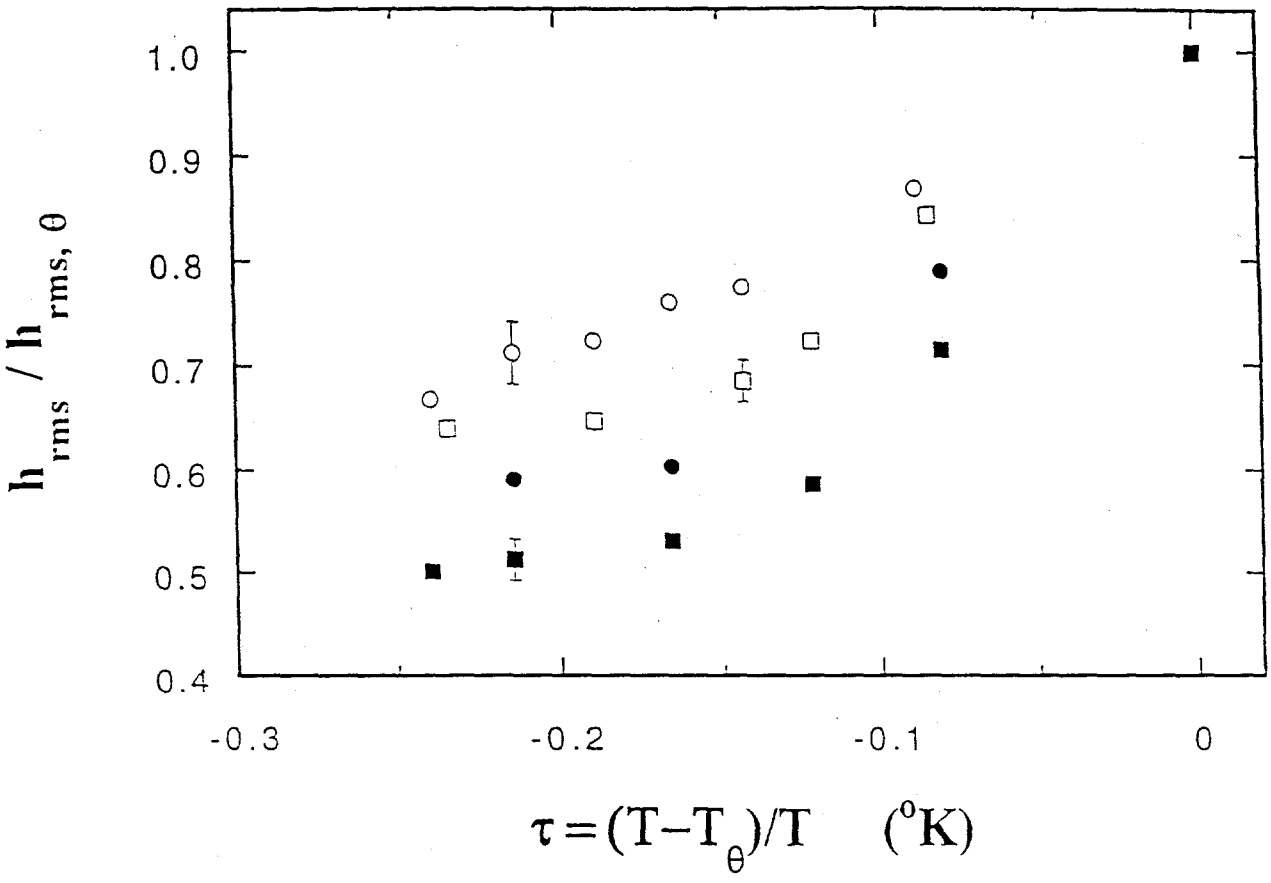
1.0
0.9
0.8
0.7
0.6
0.5
0.4
-0.3
-0.2
-0.1
0
$h_{rms} / h_{rms,\theta}$
$\tau = (T - T_\theta)/T \quad (^oK)$

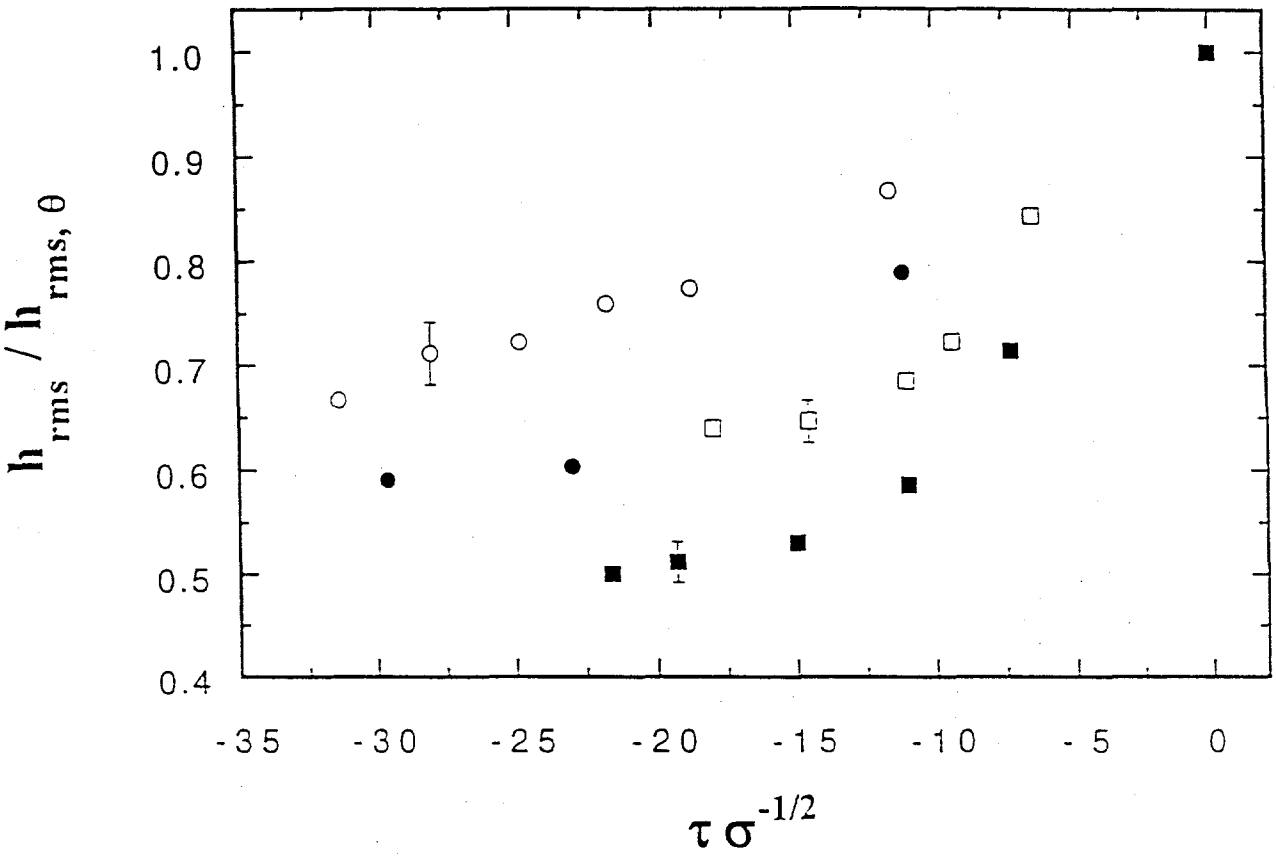
1.0
0.9
0.8
0.7
0.6
0.5
0.4
-35
-30
-25
-20
-15
-10
-5
0
$h_{rms} / h_{rms,\theta}$
$\tau \sigma^{-1/2}$

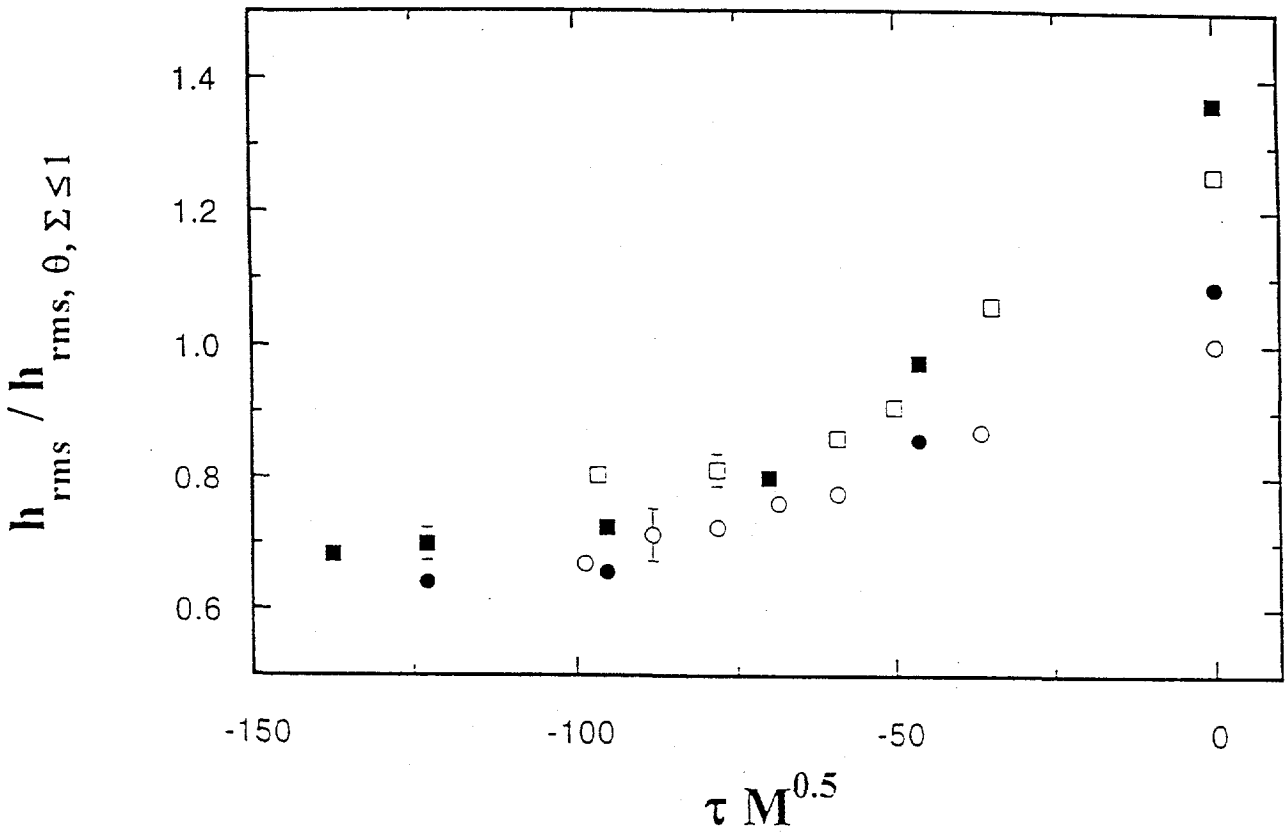
1.4
1.2
1.0
0.8
0.6
-150
-100
-50
0
$h_{rms} / h_{rms,\ \theta,\ \Sigma \leq 1}$
$\tau\ M^{0.5}$

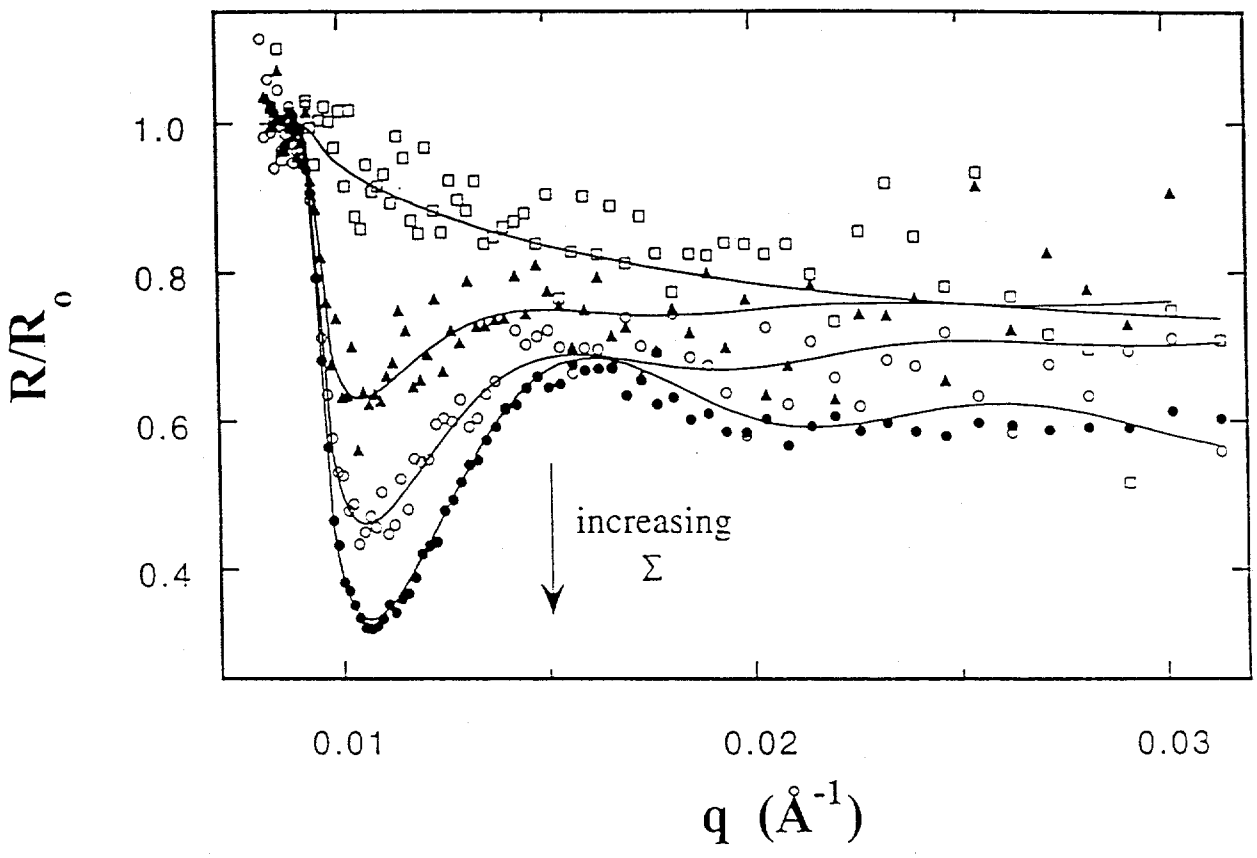
R/R0
1.0
0.8
0.6
0.4
increasing
Σ
0.01
0.02
0.03
q (Å-1)

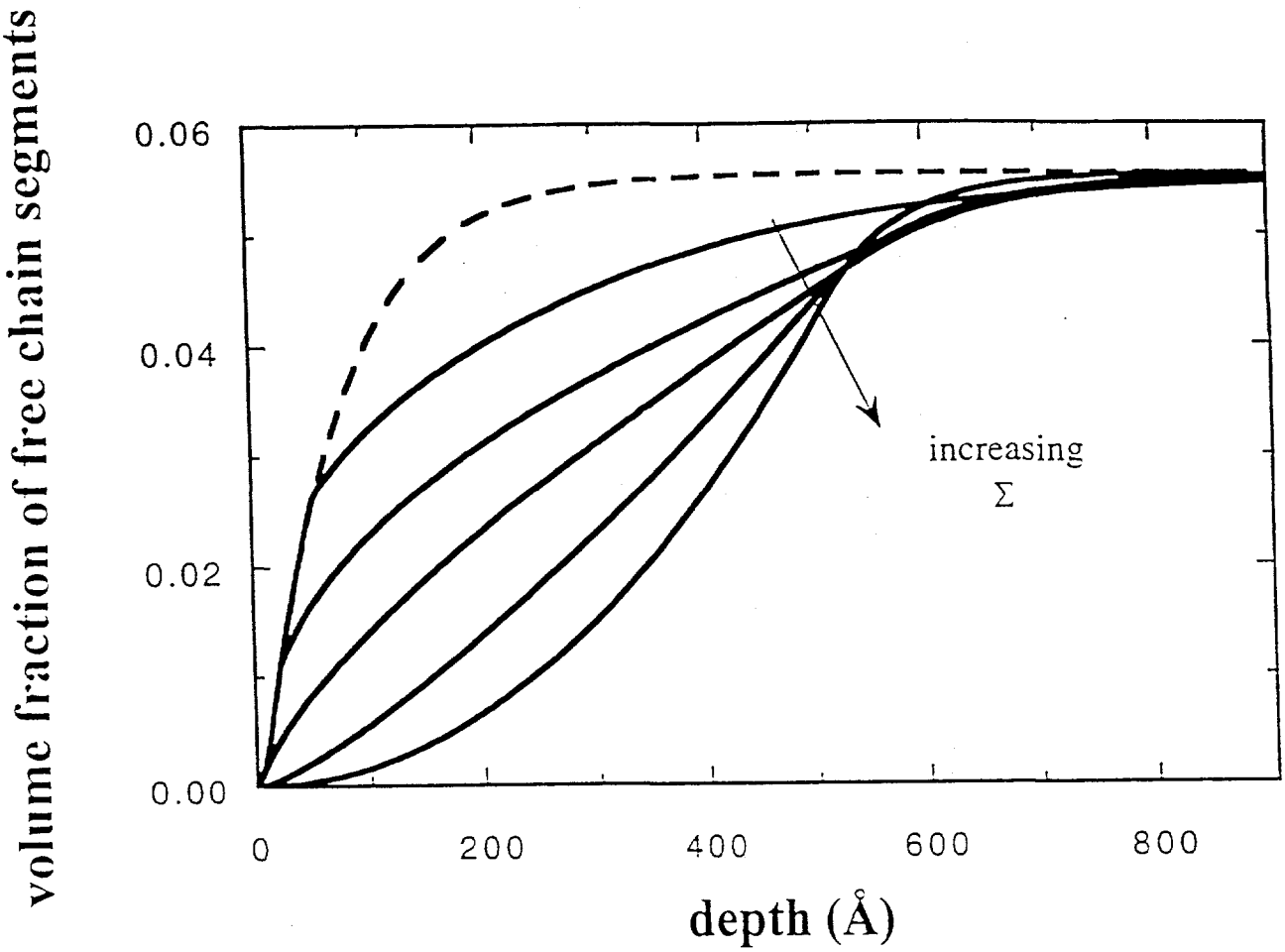
volume fraction of free chain segments
0.06
0.04
0.02
0.00
0
200
400
600
800
depth (Å)
increasing
Σ

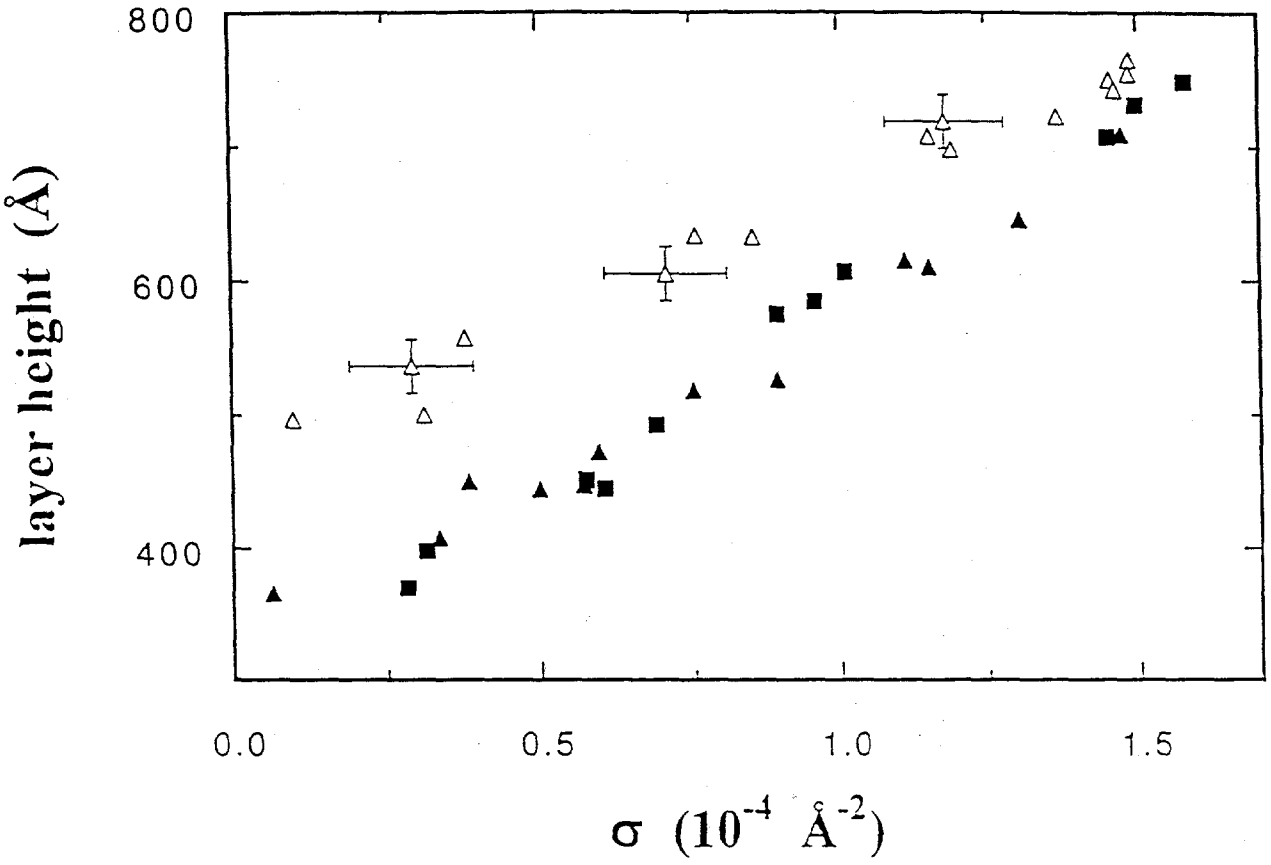
800
600
400
layer height (Å)
0.0
0.5
1.0
1.5
σ (10^-4 Å^-2)

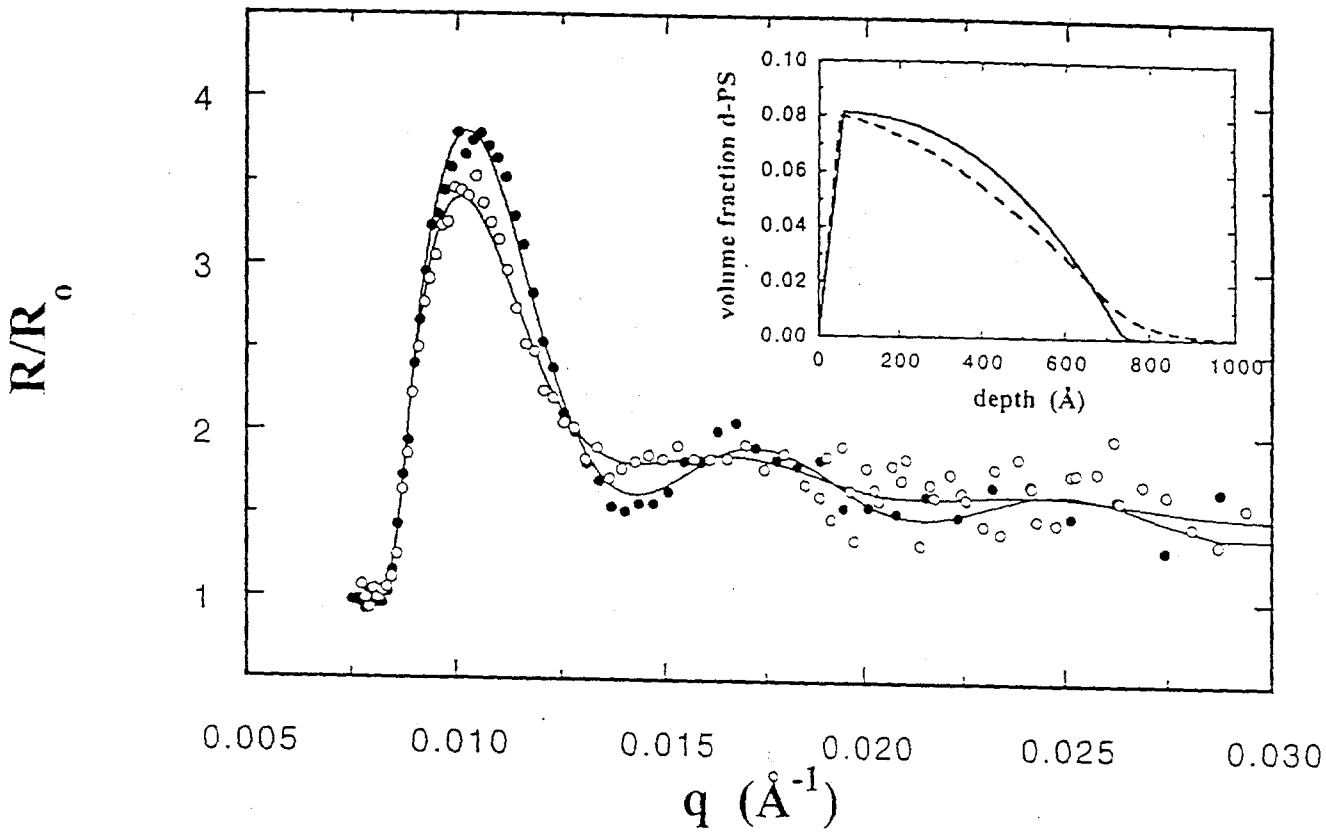
R/R0
4
3
2
1
0.005
0.010
0.015
0.020
0.025
0.030
q (Å-1)
volume fraction d-PS
0.10
0.08
0.06
0.04
0.02
0.00
0
200
400
600
800
1000
depth (Å)

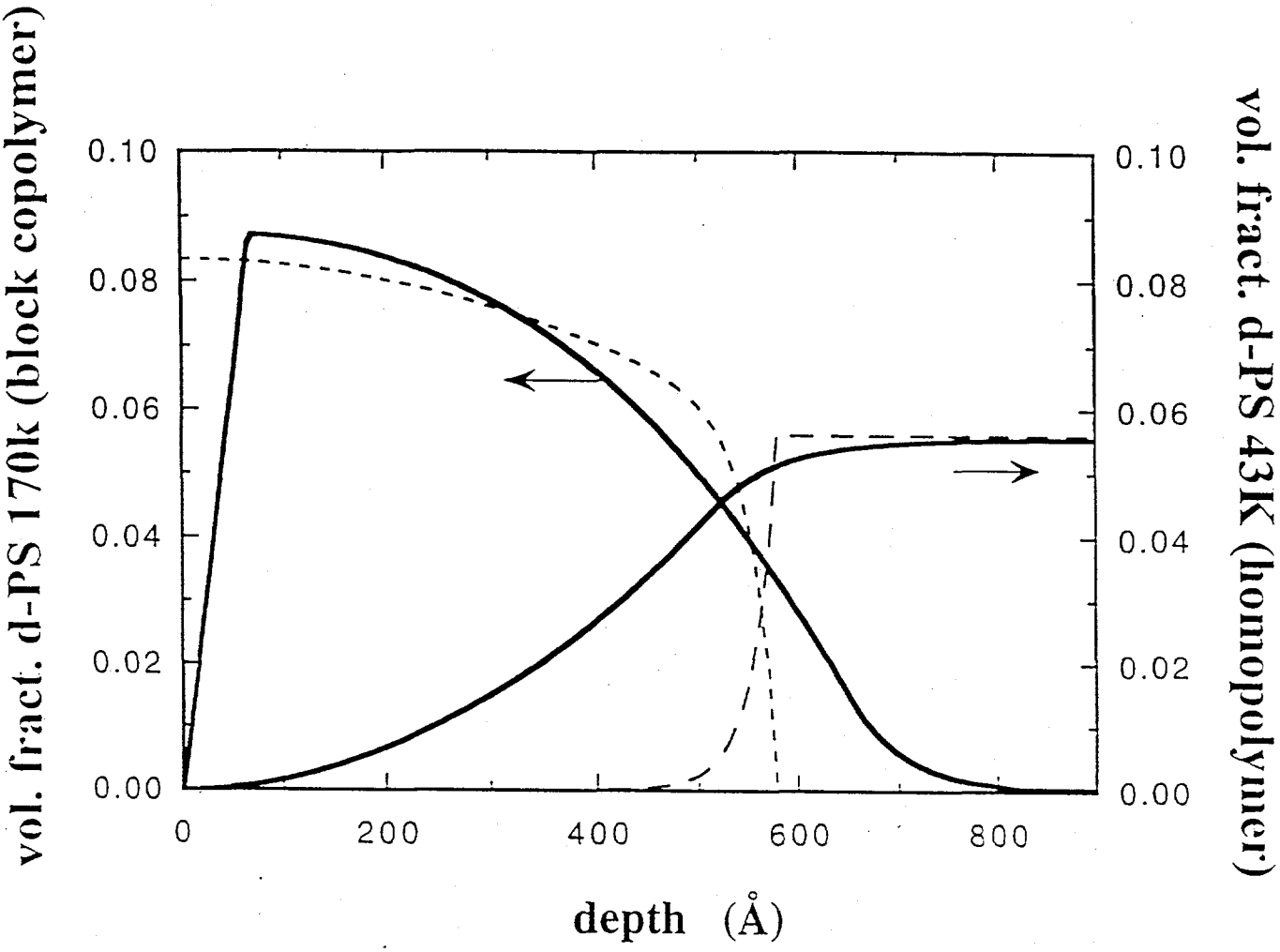
vol. fract. d-PS 170k (block copolymer)
vol. fract. d-PS 43K (homopolymer)
0.10
0.08
0.06
0.04
0.02
0.00
0
200
400
600
800
depth (Å)

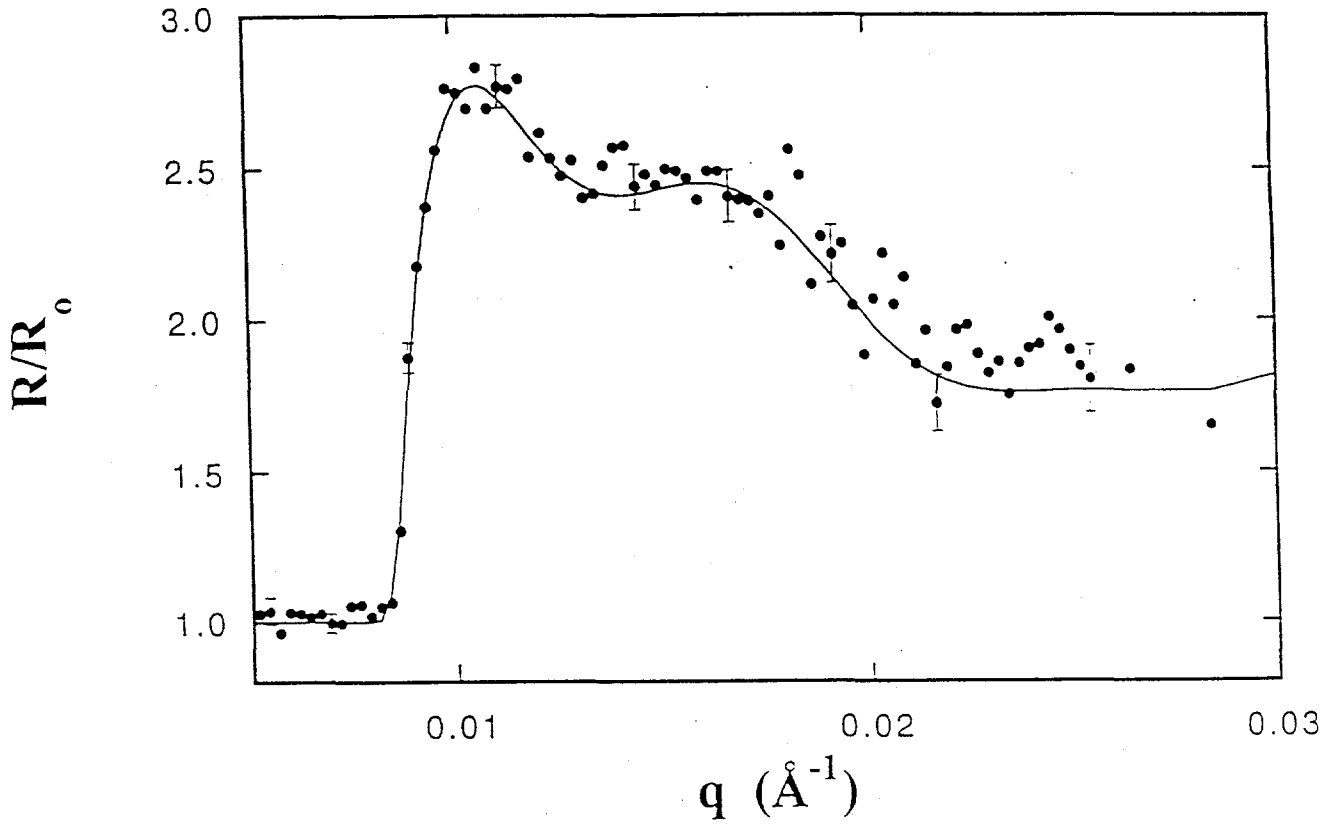
3.0
2.5
2.0
1.5
1.0
R/R$_o$
0.01
0.02
0.03
q (Å^{-1})

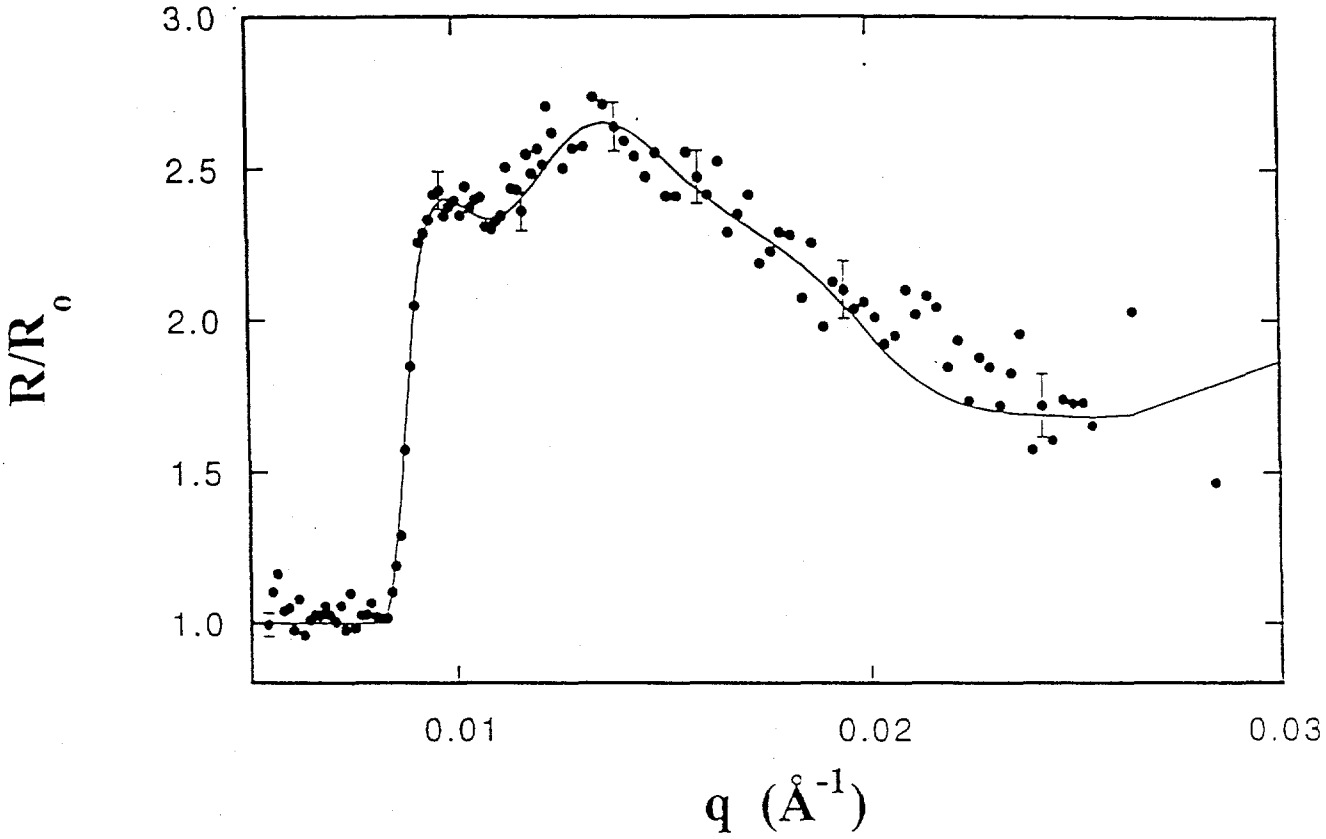
3.0
2.5
2.0
1.5
1.0
R/R$_0$
0.01
0.02
0.03
q (Å^{-1})

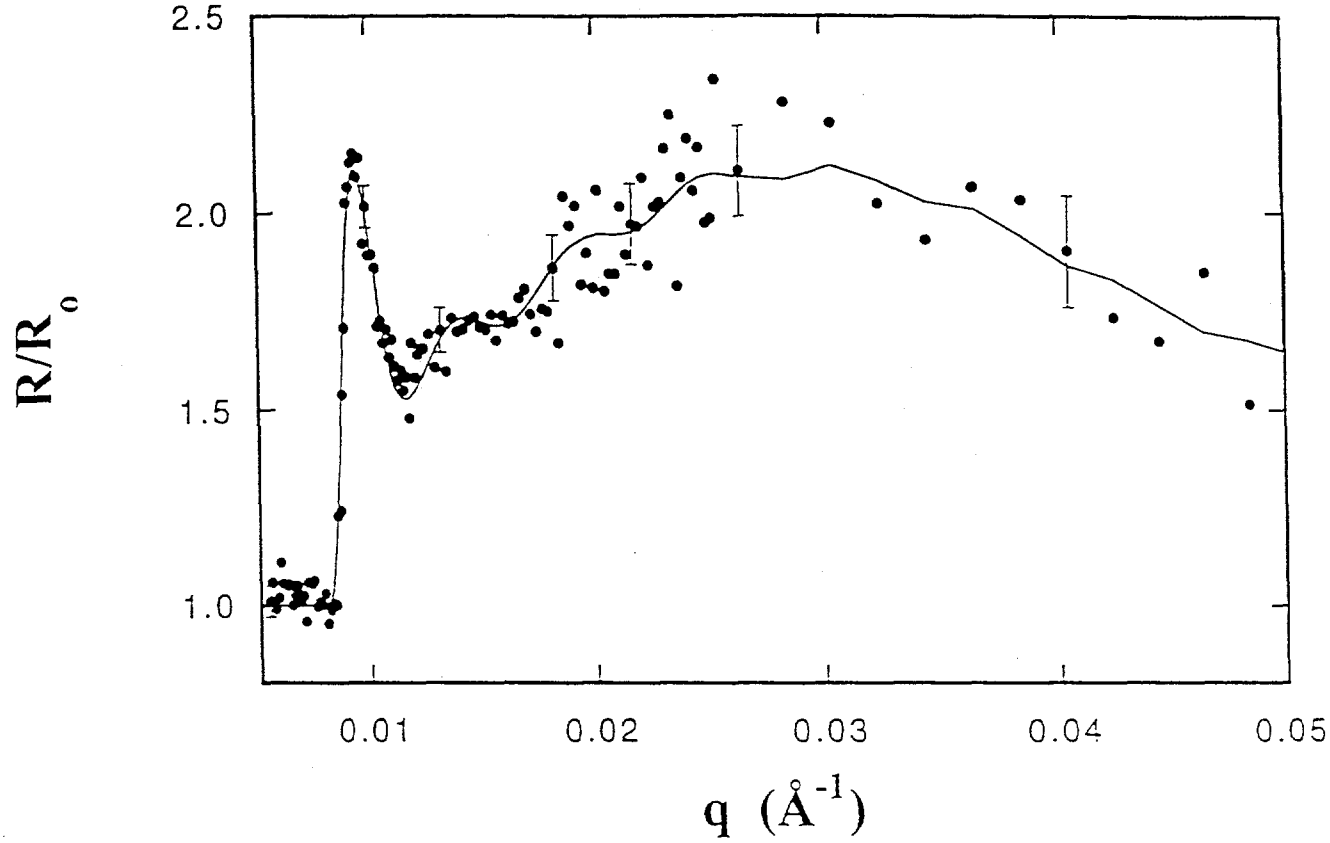
2.5
2.0
1.5
1.0
R/R$_c$
0.01
0.02
0.03
0.04
0.05
q (Å^{-1})

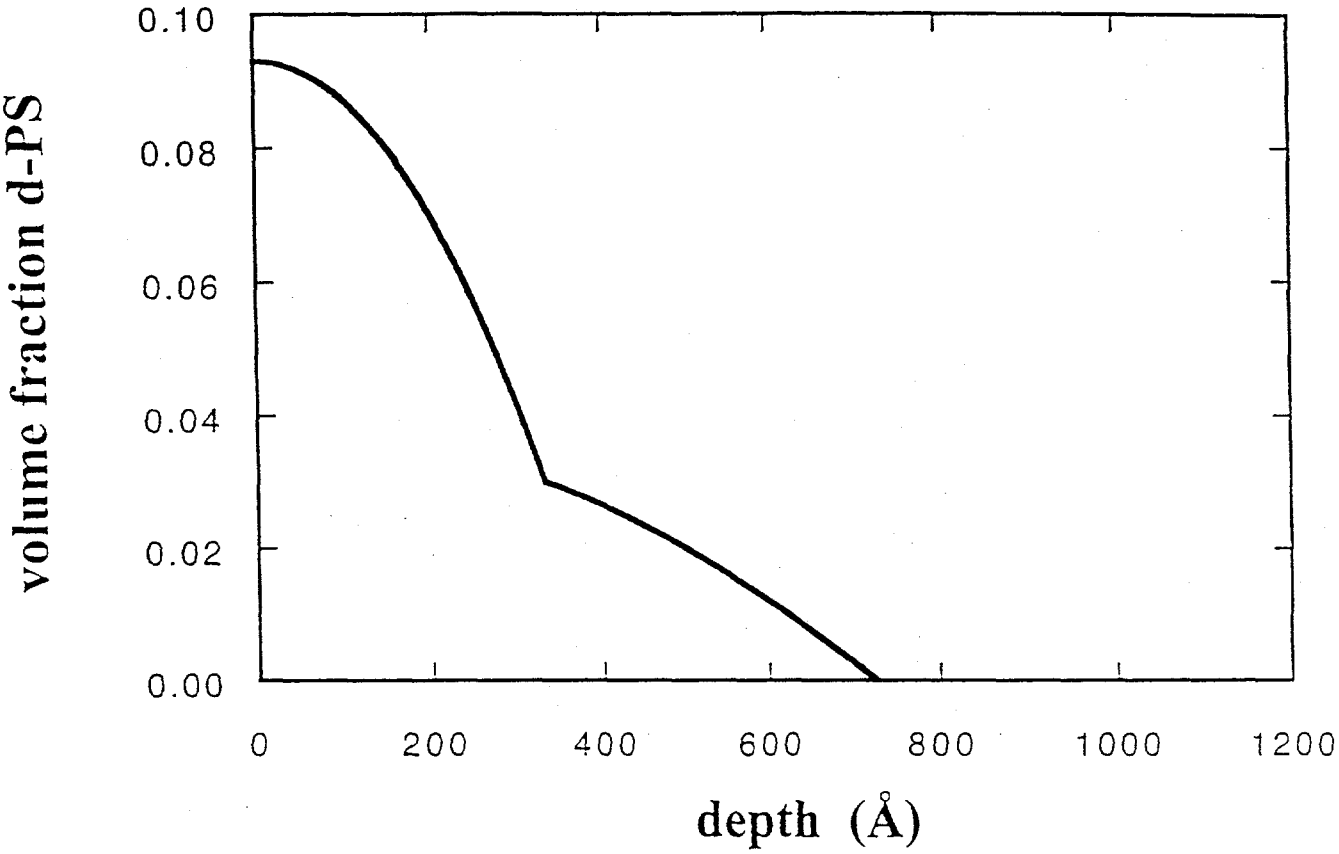
volume fraction d-PS
0.10
0.08
0.06
0.04
0.02
0.00
0
200
400
600
800
1000
1200
depth (Å)

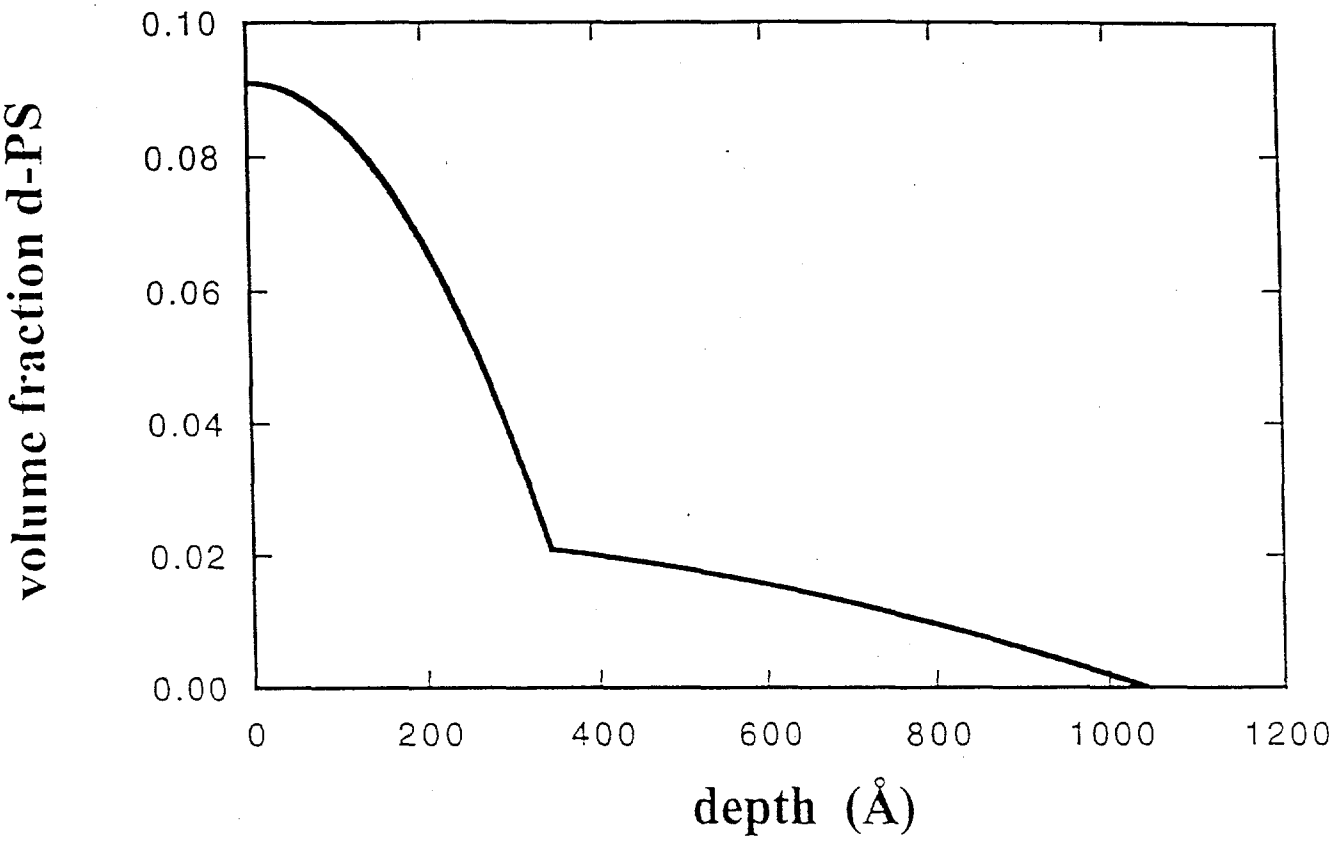
volume fraction d-PS
0.10
0.08
0.06
0.04
0.02
0.00
0
200
400
600
800
1000
1200
depth (Å)

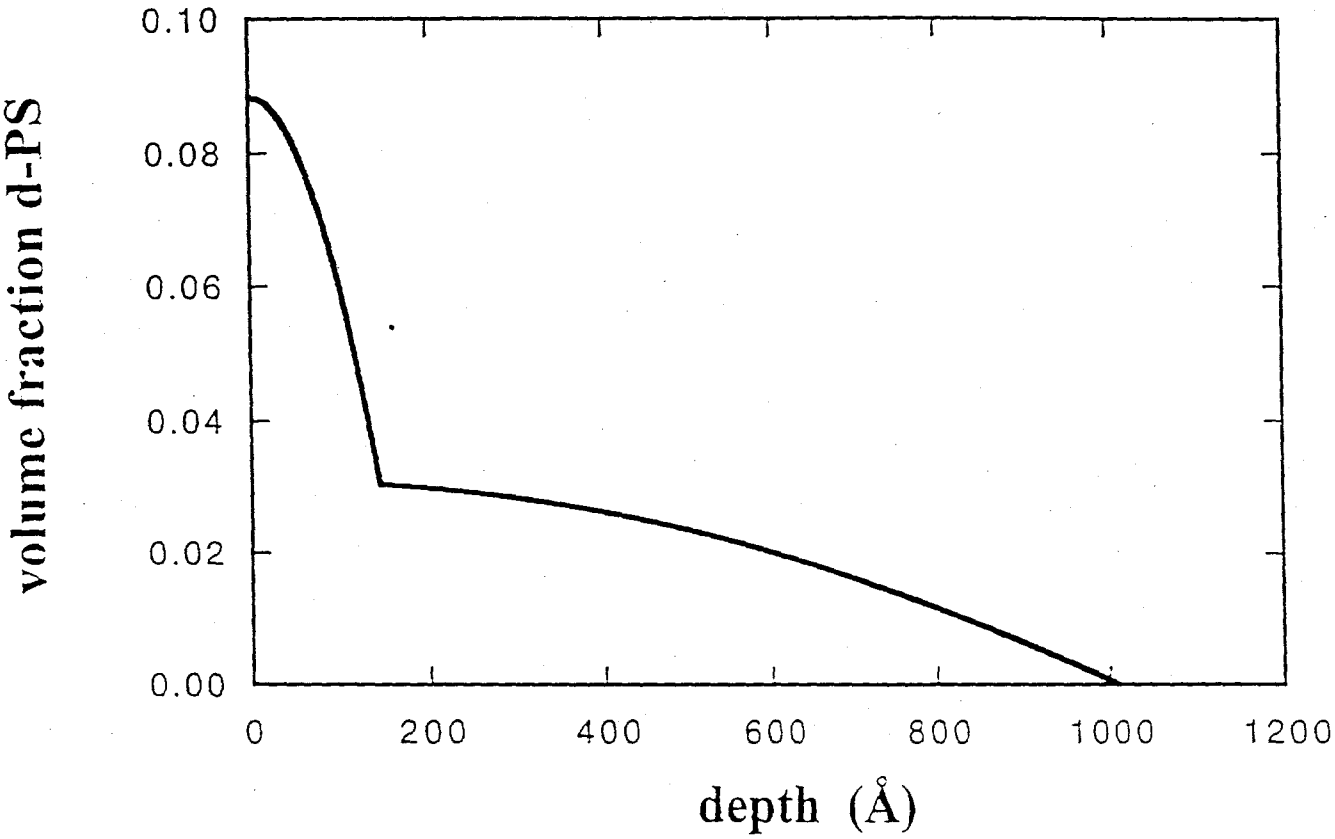
volume fraction d-PS
0.10
0.08
0.06
0.04
0.02
0.00
0
200
400
600
800
1000
1200
depth (Å)

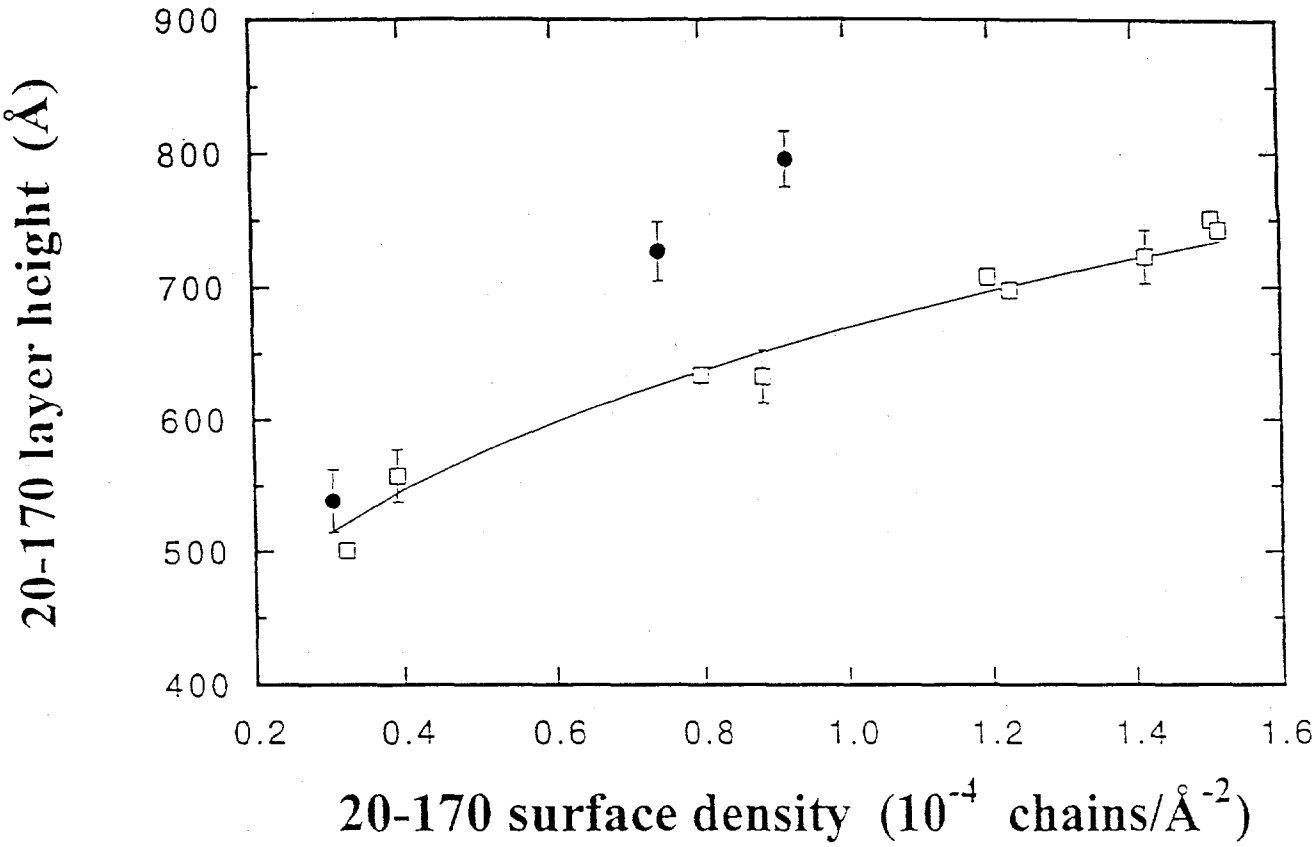
900
800
700
600
500
400
0.2
0.4
0.6
0.8
1.0
1.2
1.4
1.6
20-170 layer height (Å)
20-170 surface density (10^{-4} chains/Å^{-2})

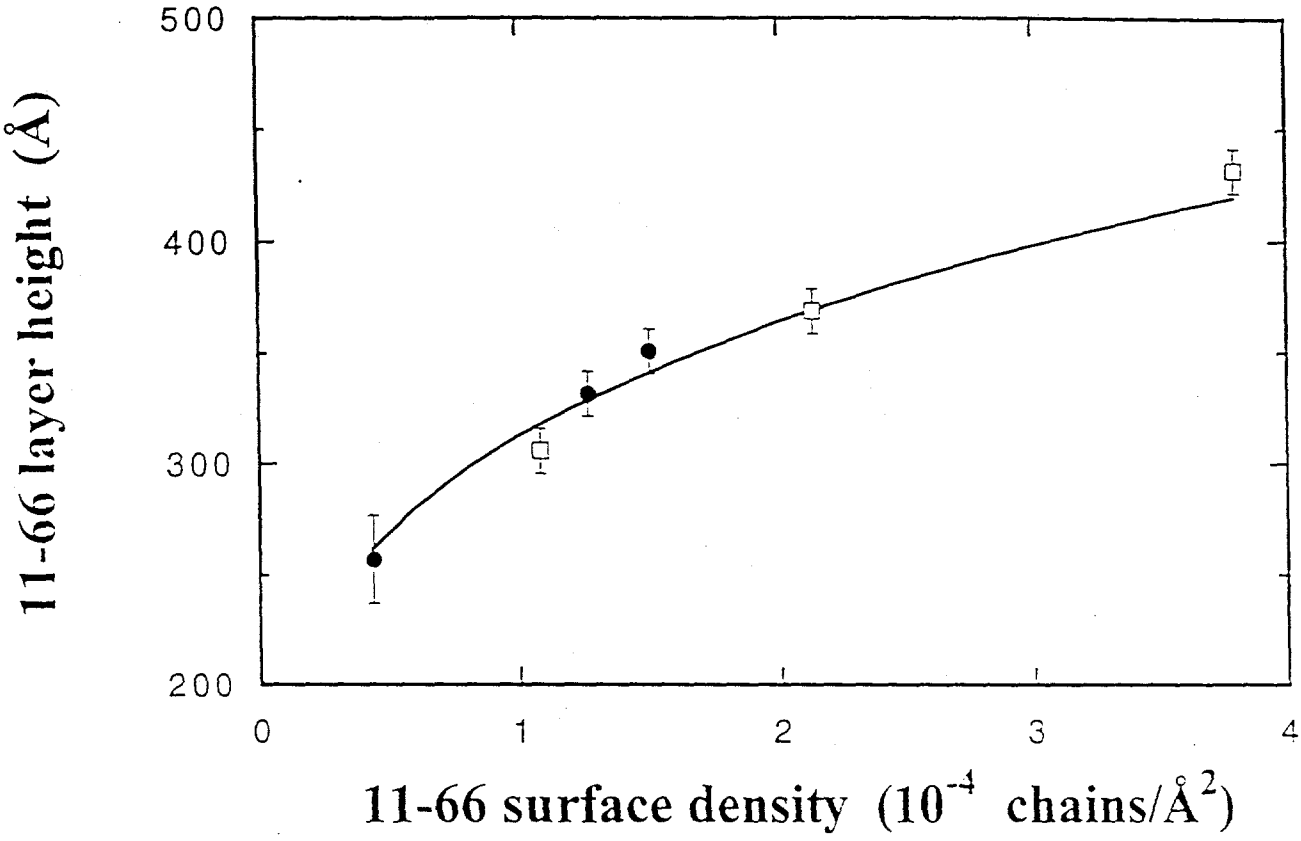
500
400
300
200
0
1
2
3
4
11-66 layer height (Å)
11-66 surface density (10^{-4} chains/Å^2)

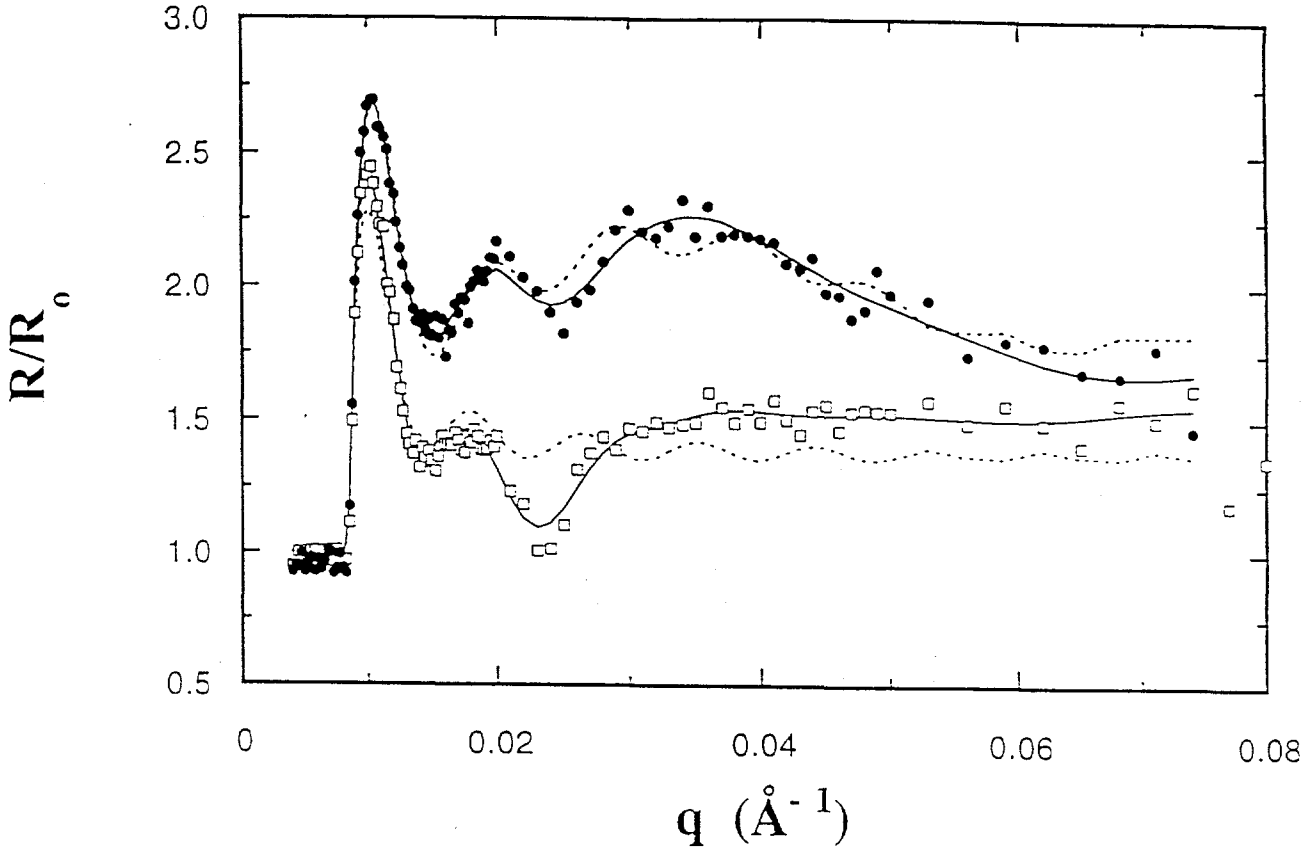
3.0
2.5
2.0
1.5
1.0
0.5
R/R0
0
0.02
0.04
0.06
0.08
q (Å-1)

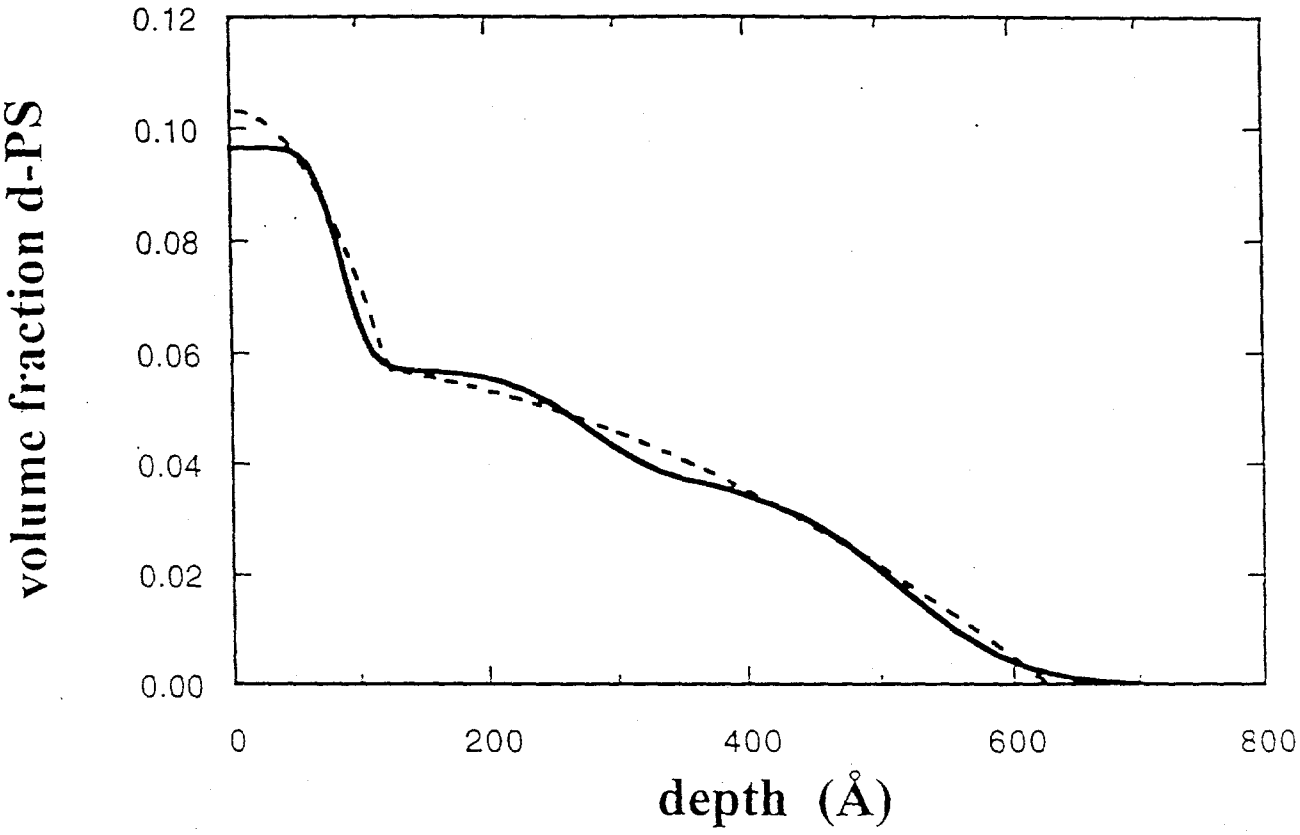
volume fraction d-PS
0.12
0.10
0.08
0.06
0.04
0.02
0.00
0
200
400
600
800
depth (Å)

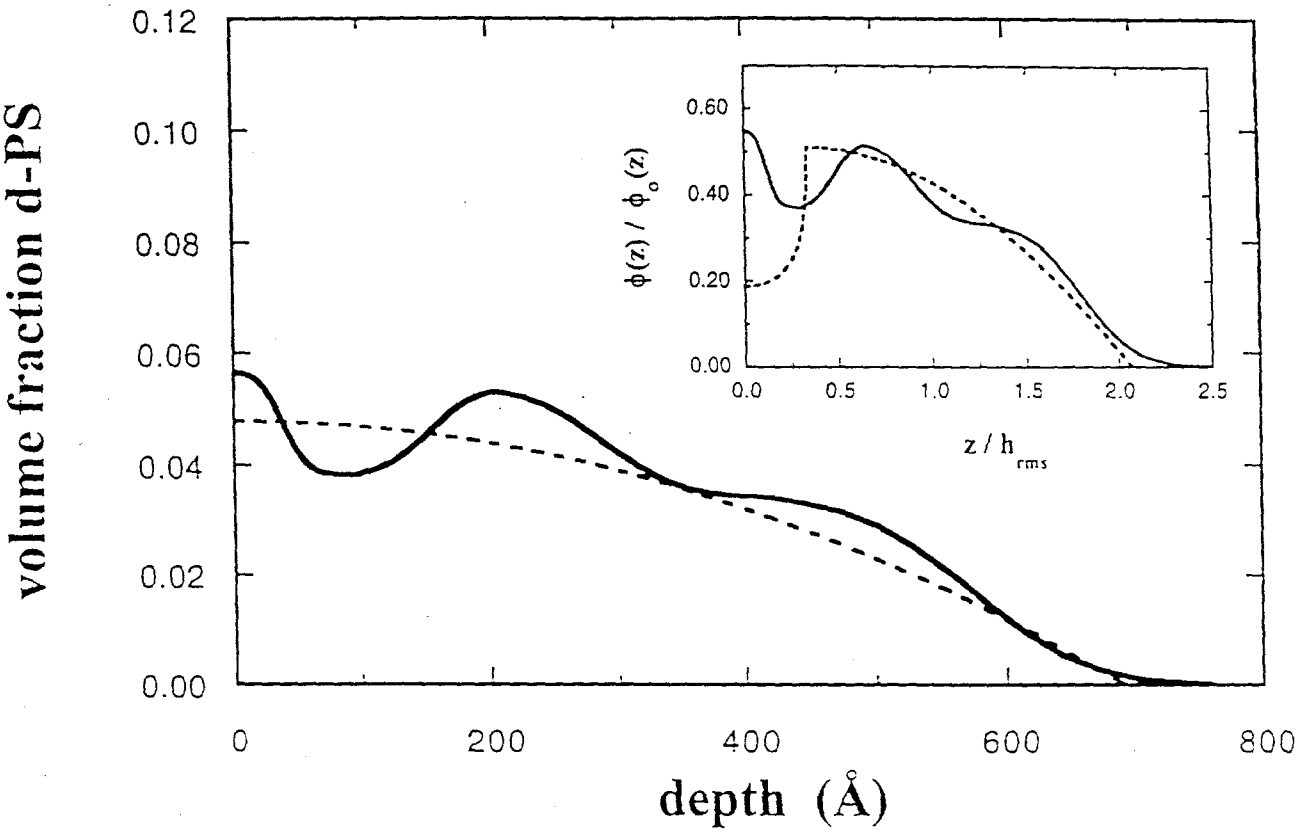
volume fraction d-PS
0.12
0.10
0.08
0.06
0.04
0.02
0.00
0
200
400
600
800
depth (Å)
φ(z) / φ_o(z)
0.60
0.40
0.20
0.00
0.0
0.5
1.0
1.5
2.0
2.5
z / h_rms

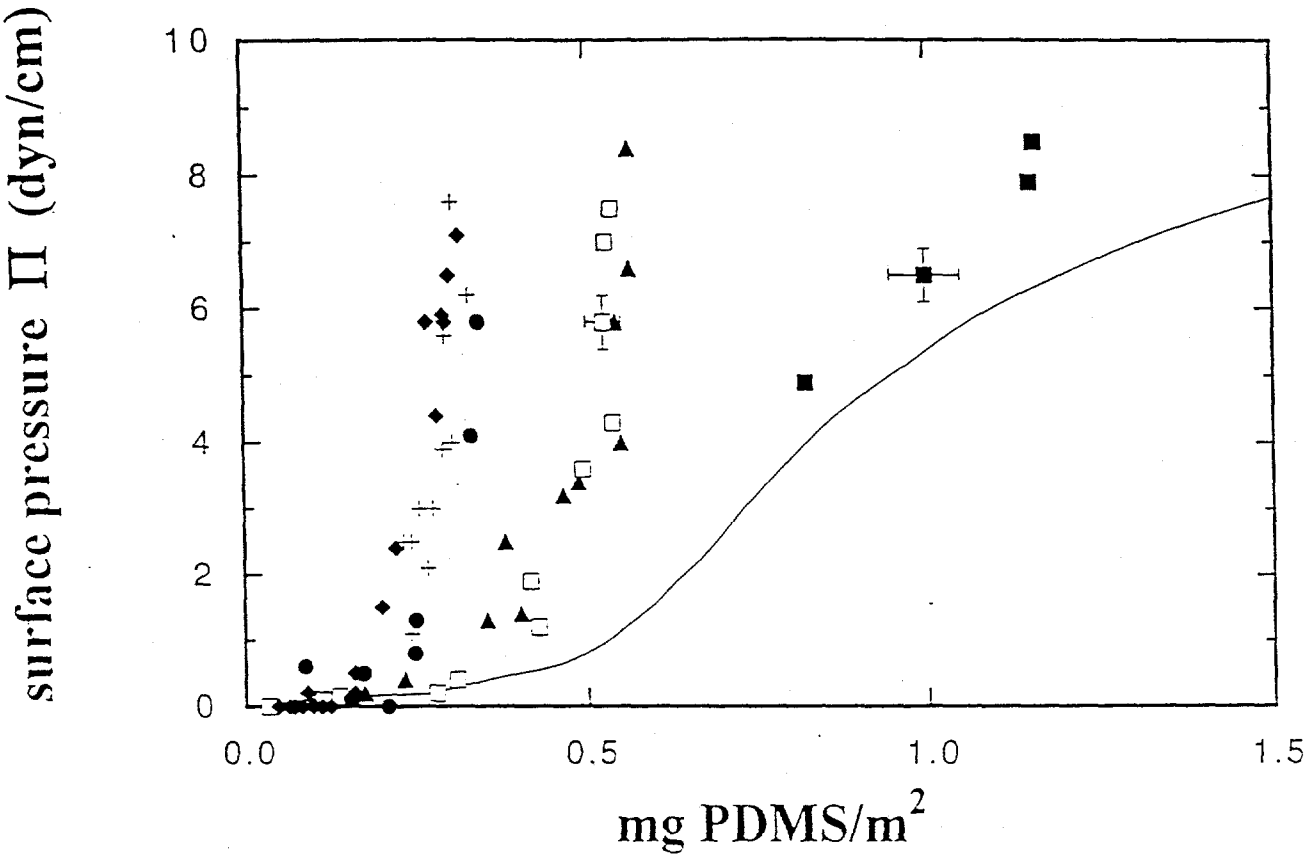
surface pressure Π (dyn/cm)
10
8
6
4
2
0
0.0
0.5
1.0
1.5
mg PDMS/m²

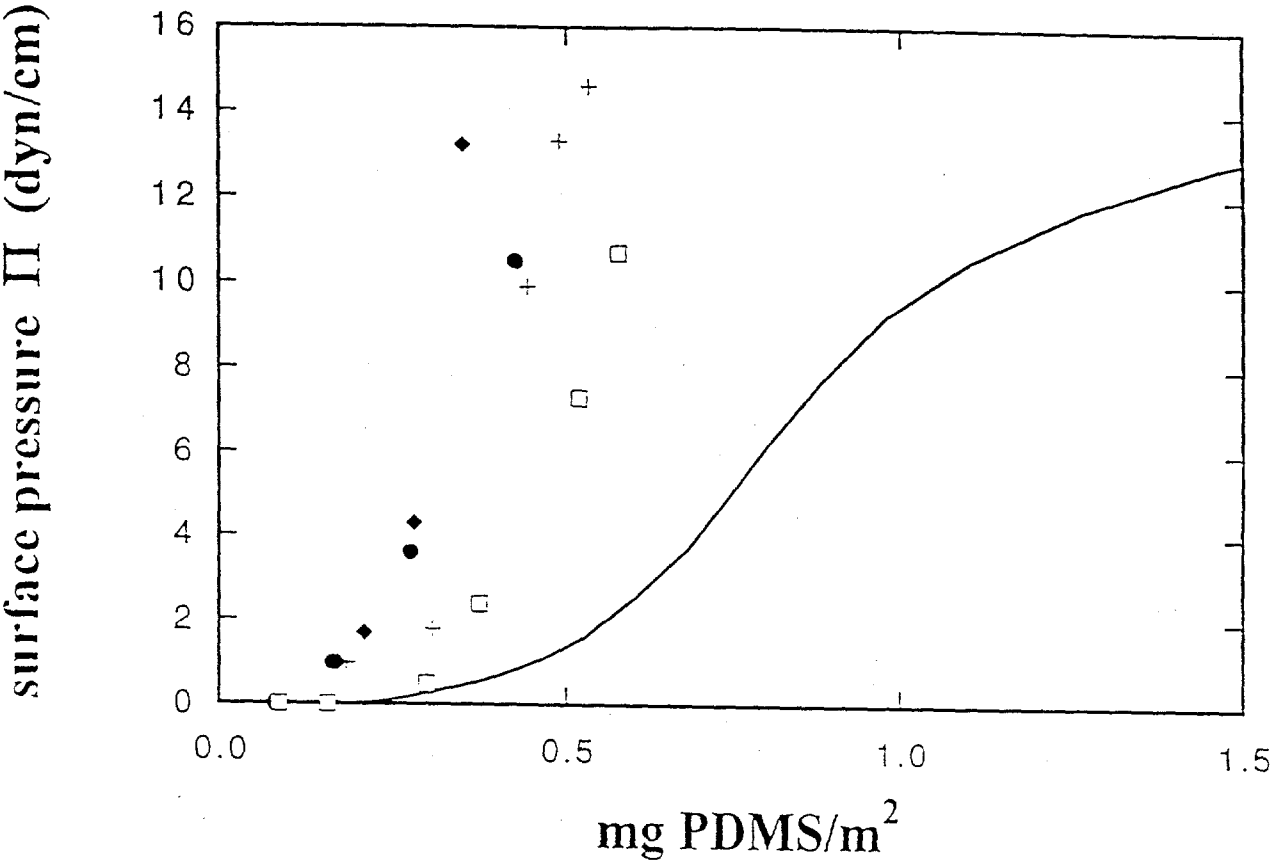
surface pressure Π (dyn/cm)
16
14
12
10
8
6
4
2
0
0.0
0.5
1.0
1.5
mg PDMS/m²

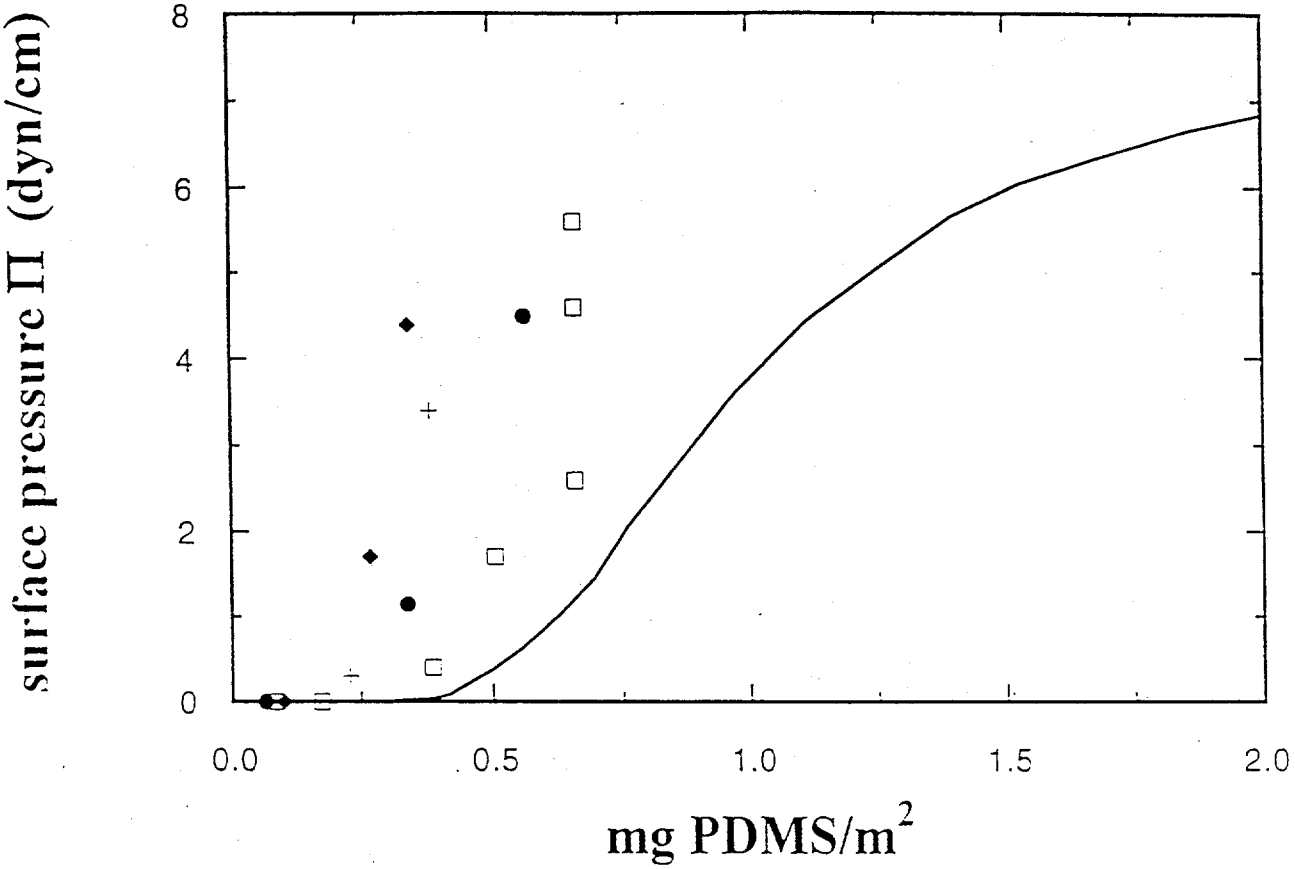
surface pressure Π (dyn/cm)
8
6
4
2
0
0.0
0.5
1.0
1.5
2.0
mg PDMS/m²

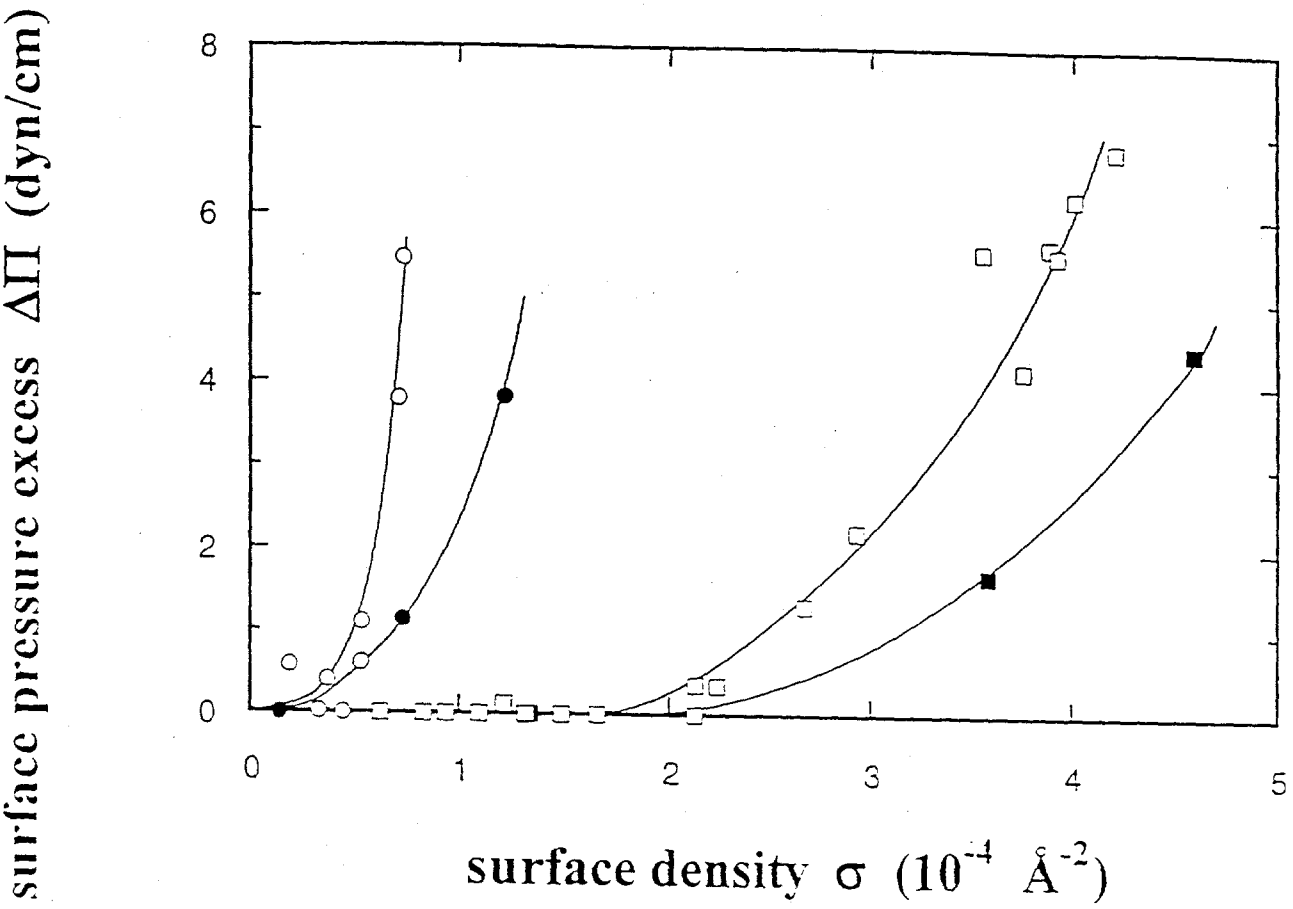
surface pressure excess ΔΠ (dyn/cm)
8
6
4
2
0
0
1
2
3
4
5
surface density σ (10^-4 Å^-2)

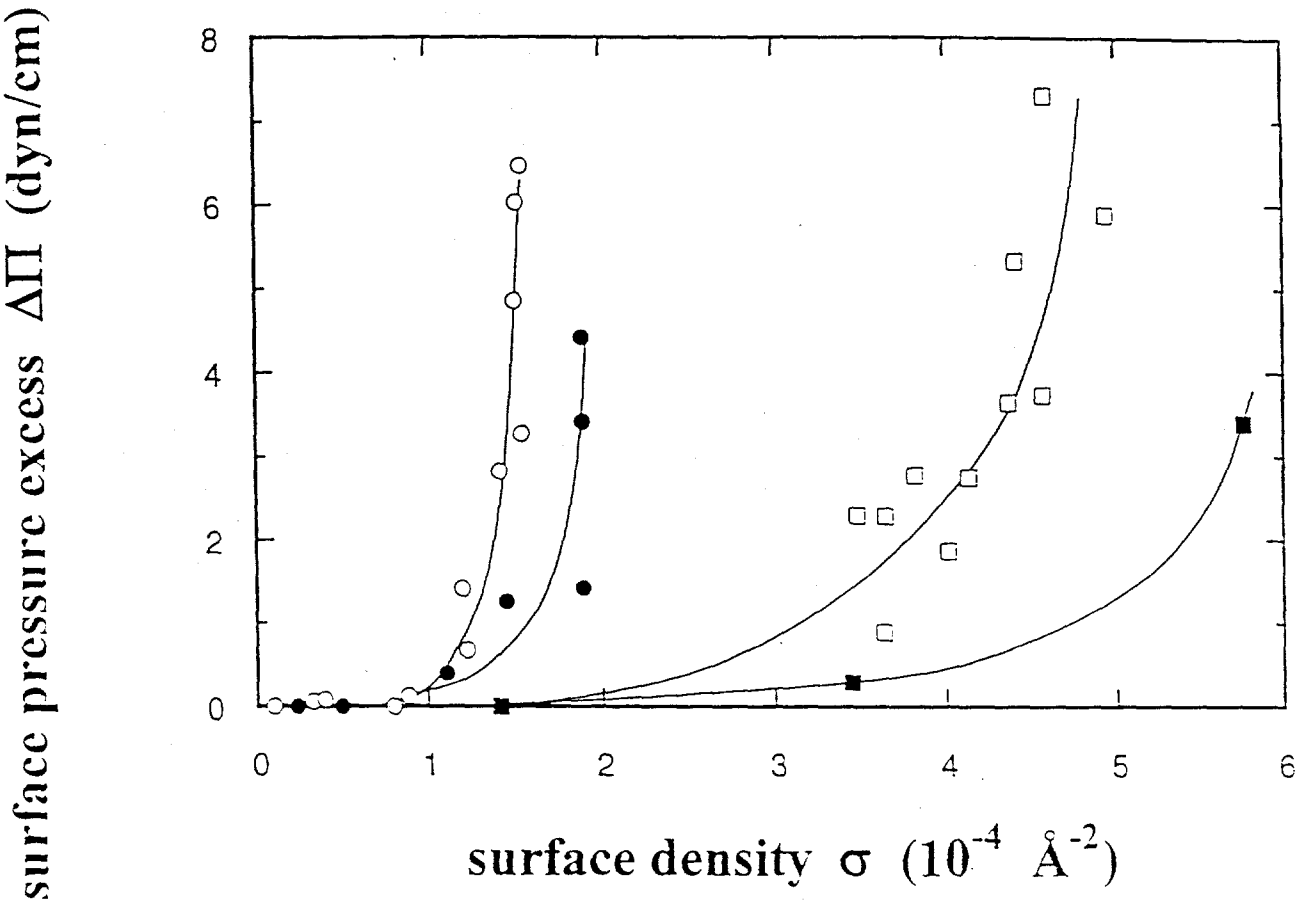
surface pressure excess ΔΠ (dyn/cm)
8
6
4
2
0
0
1
2
3
4
5
6
surface density σ (10^-4 Å^-2)

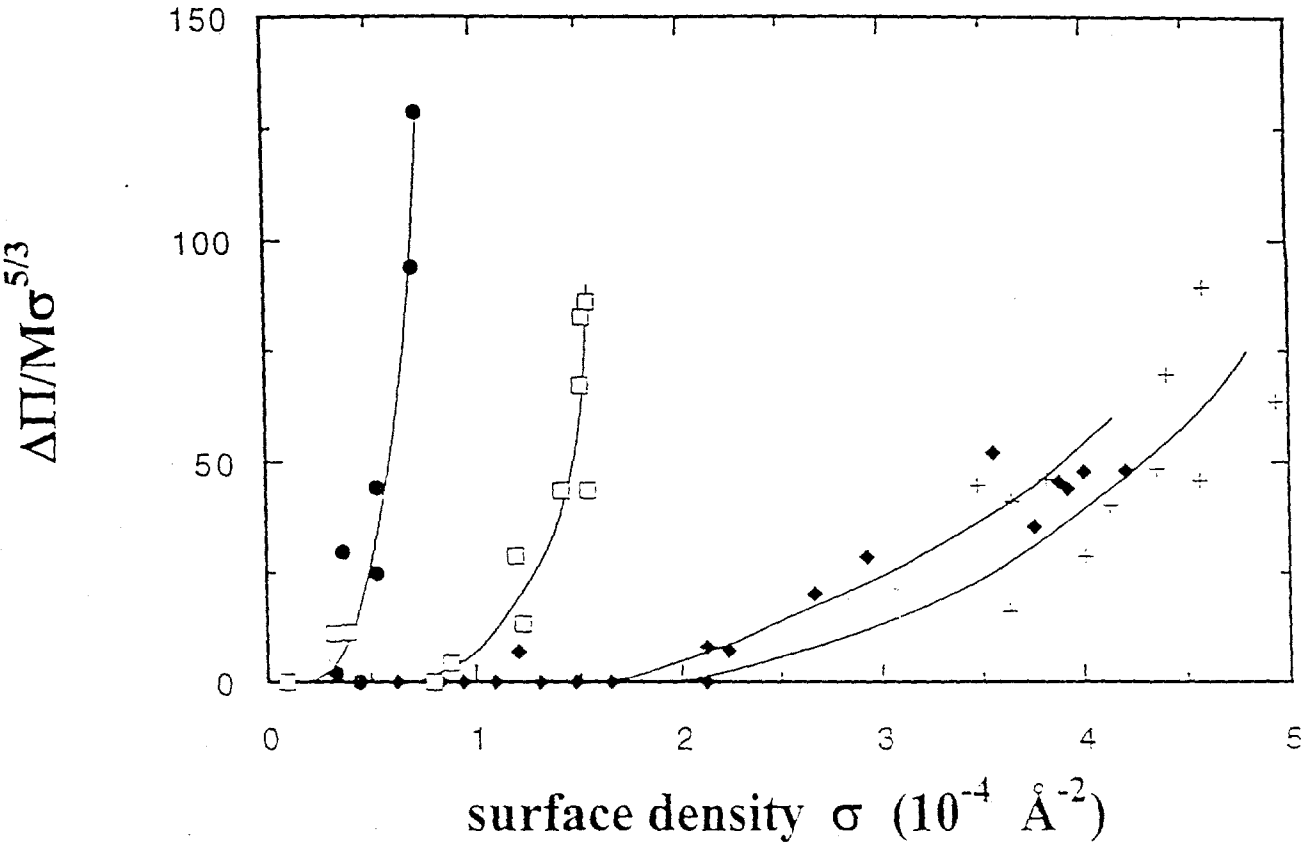
150
100
50
0
0
1
2
3
4
5
ΔΠ/Mσ^5/3
surface density σ (10^-4 Å^-2)

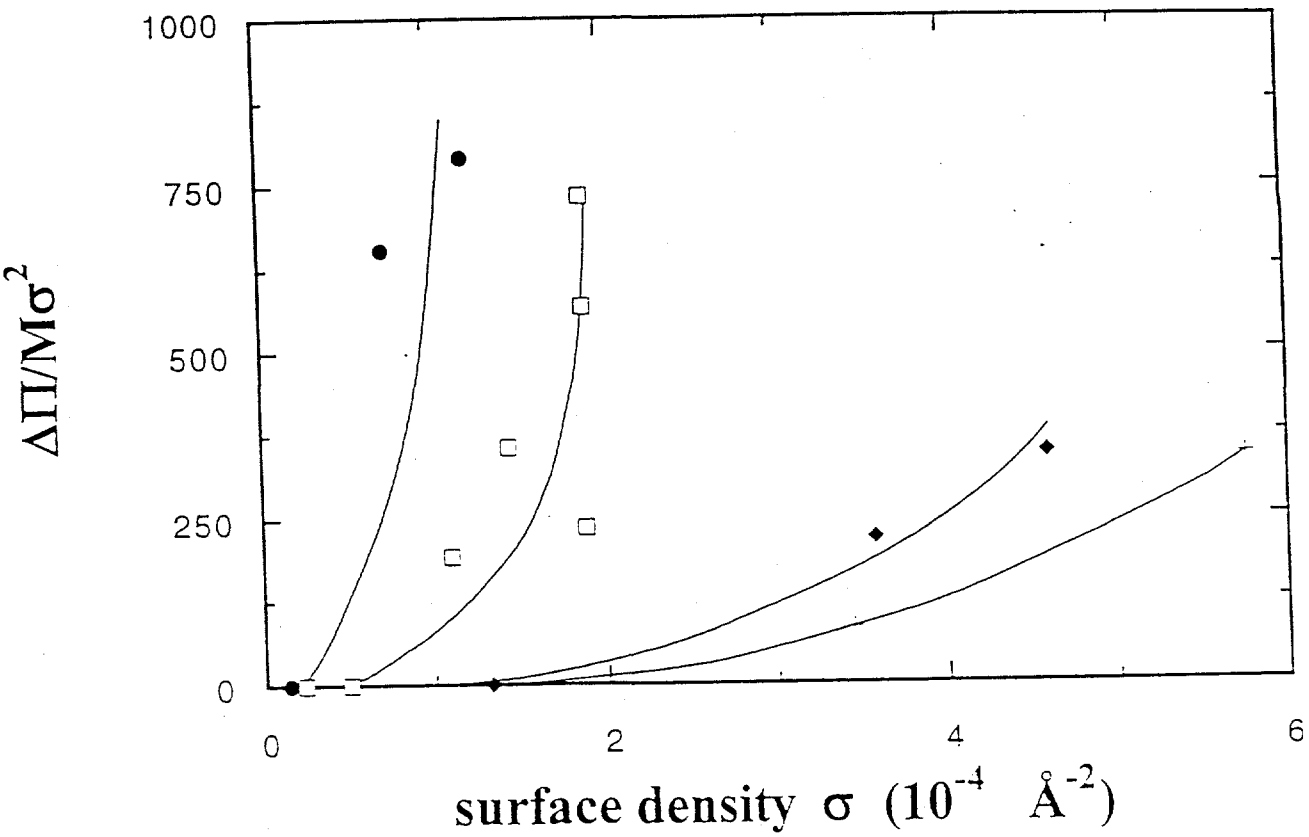
1000
750
500
250
0
0
2
4
6
ΔΠ/Mσ²
surface density σ (10⁻⁴ Å⁻²)

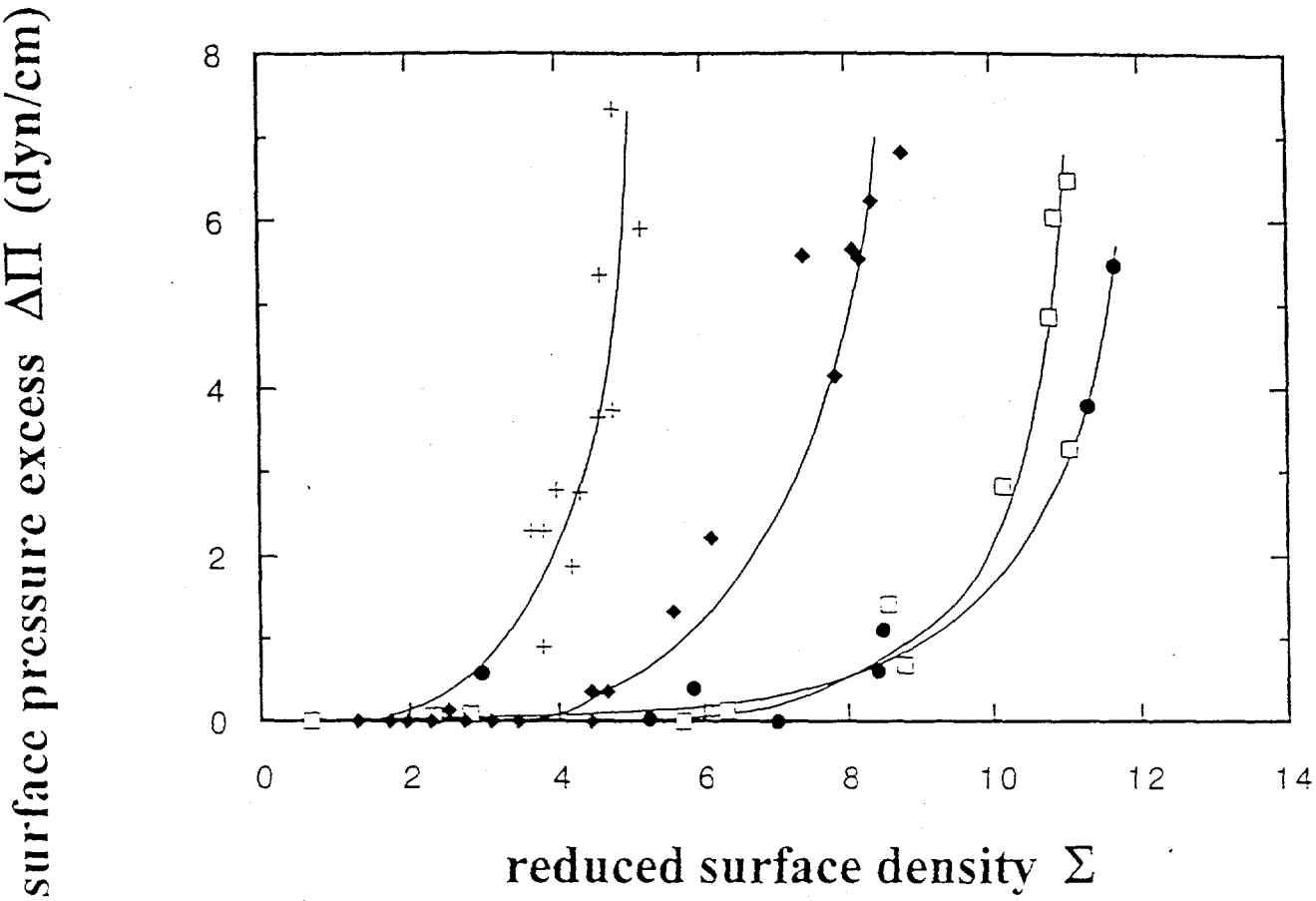
surface pressure excess ΔΠ (dyn/cm)
8
6
4
2
0
0
2
4
6
8
10
12
14
reduced surface density Σ

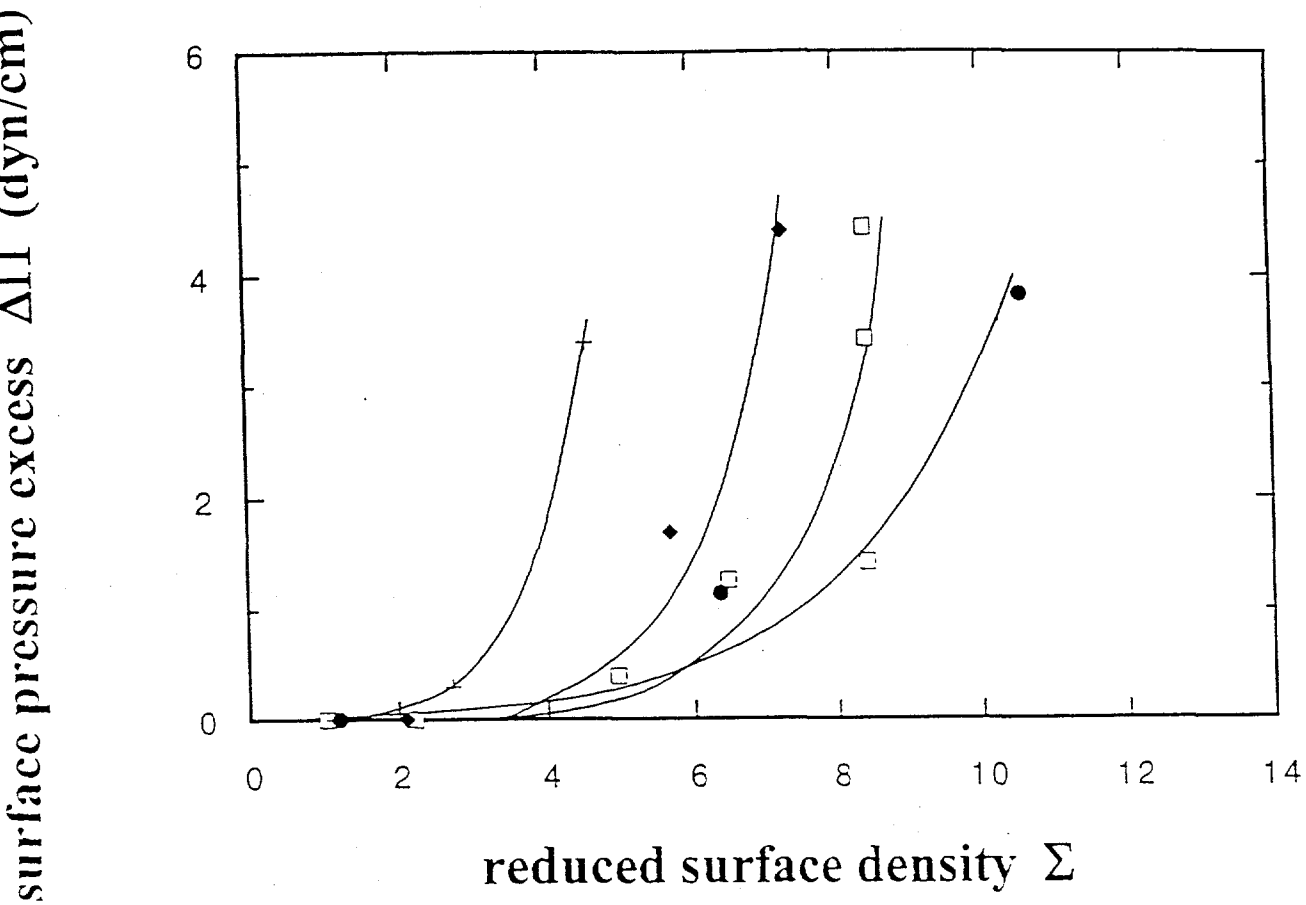
surface pressure excess ΔΠ (dyn/cm)
6
4
2
0
0
2
4
6
8
10
12
14
reduced surface density Σ

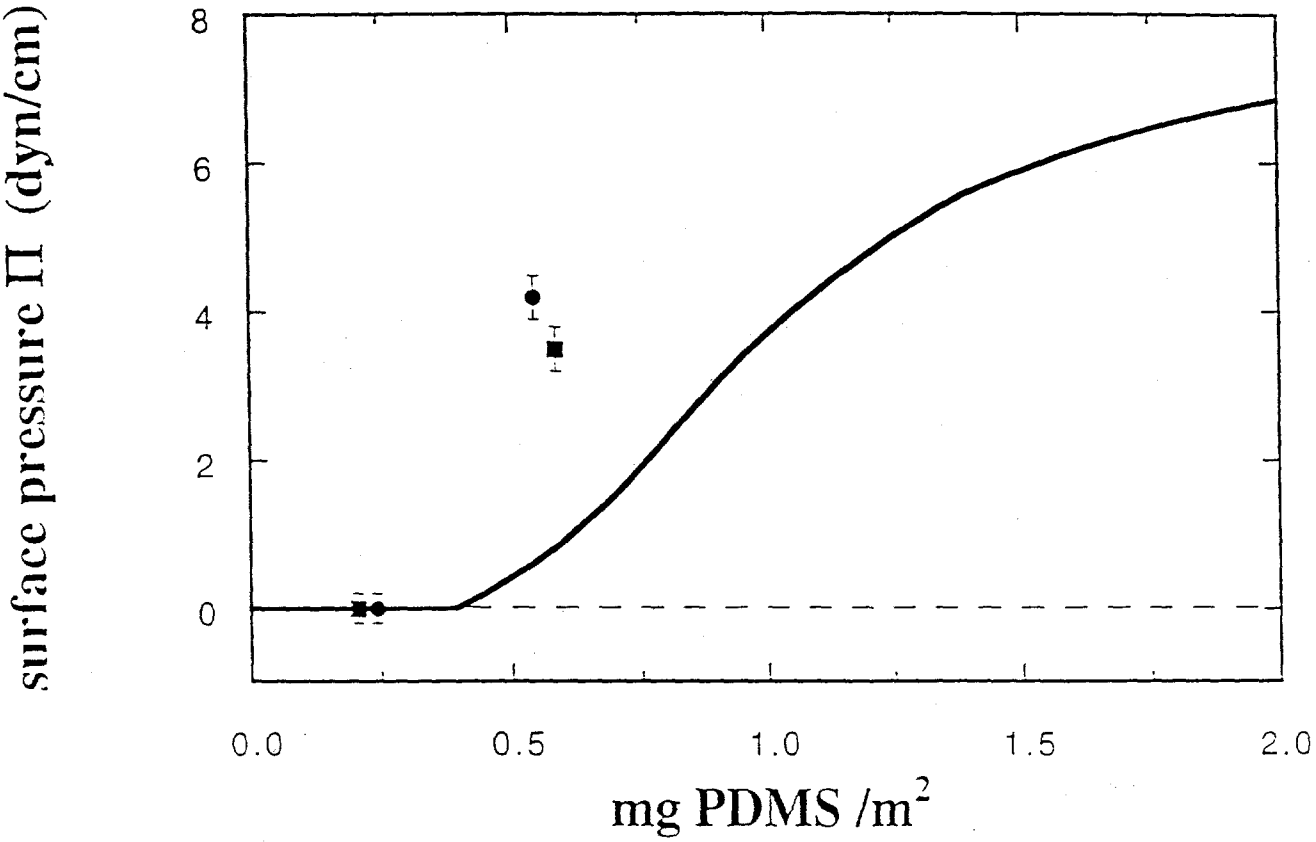
surface pressure Π (dyn/cm)
8
6
4
2
0
0.0
0.5
1.0
1.5
2.0
mg PDMS /m²

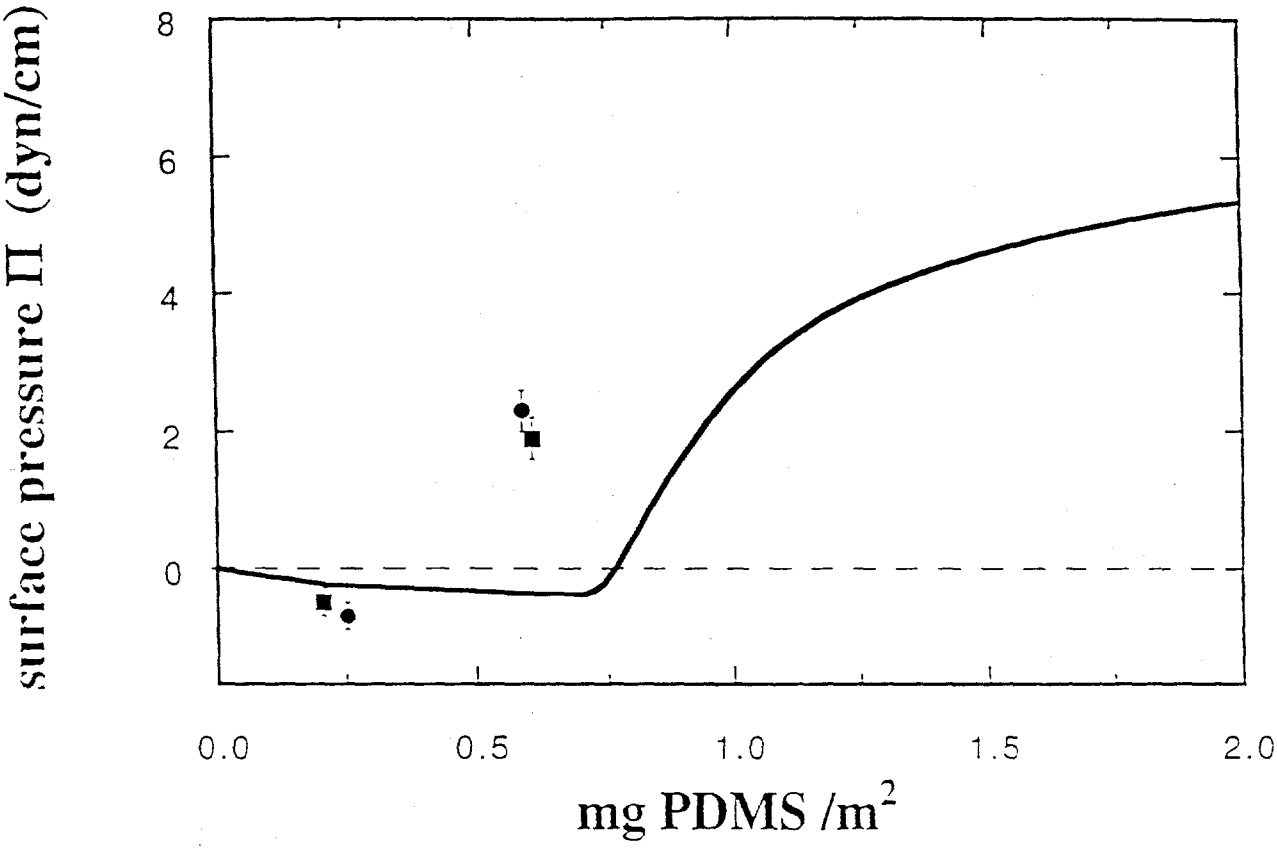
surface pressure Π (dyn/cm)
8
6
4
2
0
0.0
0.5
1.0
1.5
2.0
mg PDMS /m²

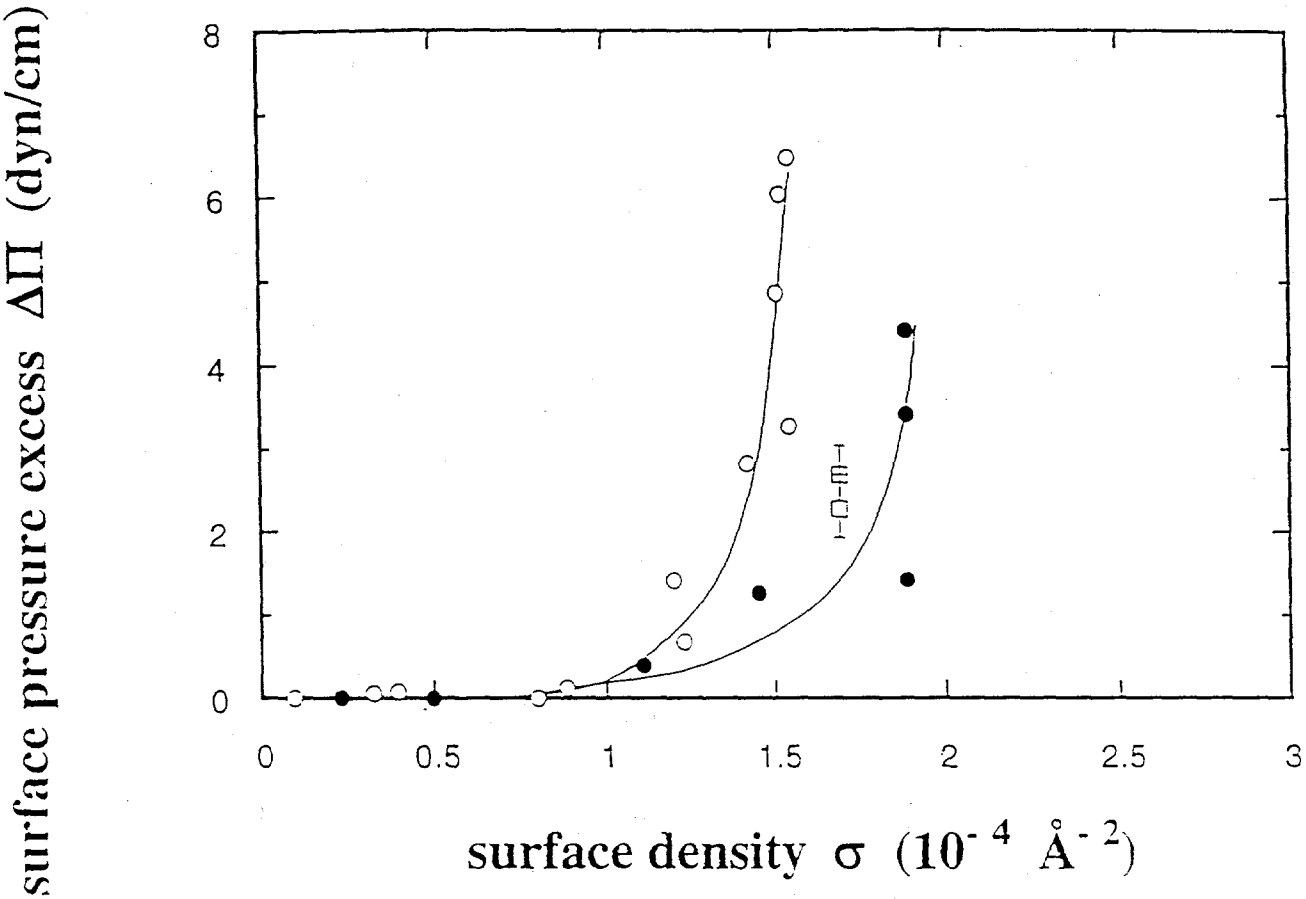
surface pressure excess ΔΠ (dyn/cm)
8
6
4
2
0
0
0.5
1
1.5
2
2.5
3
surface density σ (10⁻⁴ Å⁻²)
I-D-E-A-L

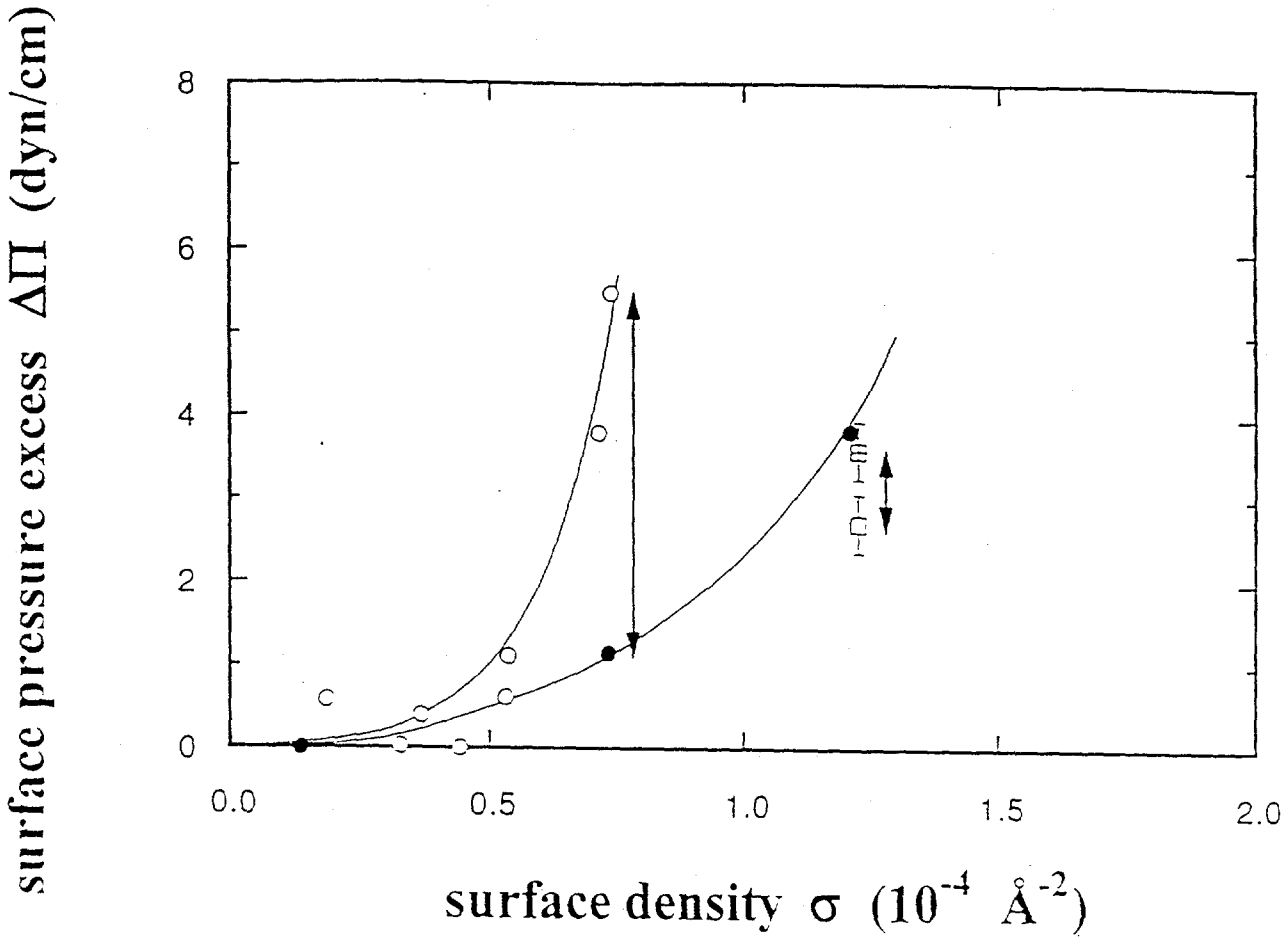
surface pressure excess ΔΠ (dyn/cm)
8
6
4
2
0
0.0
0.5
1.0
1.5
2.0
surface density σ (10^-4 Å^-2)

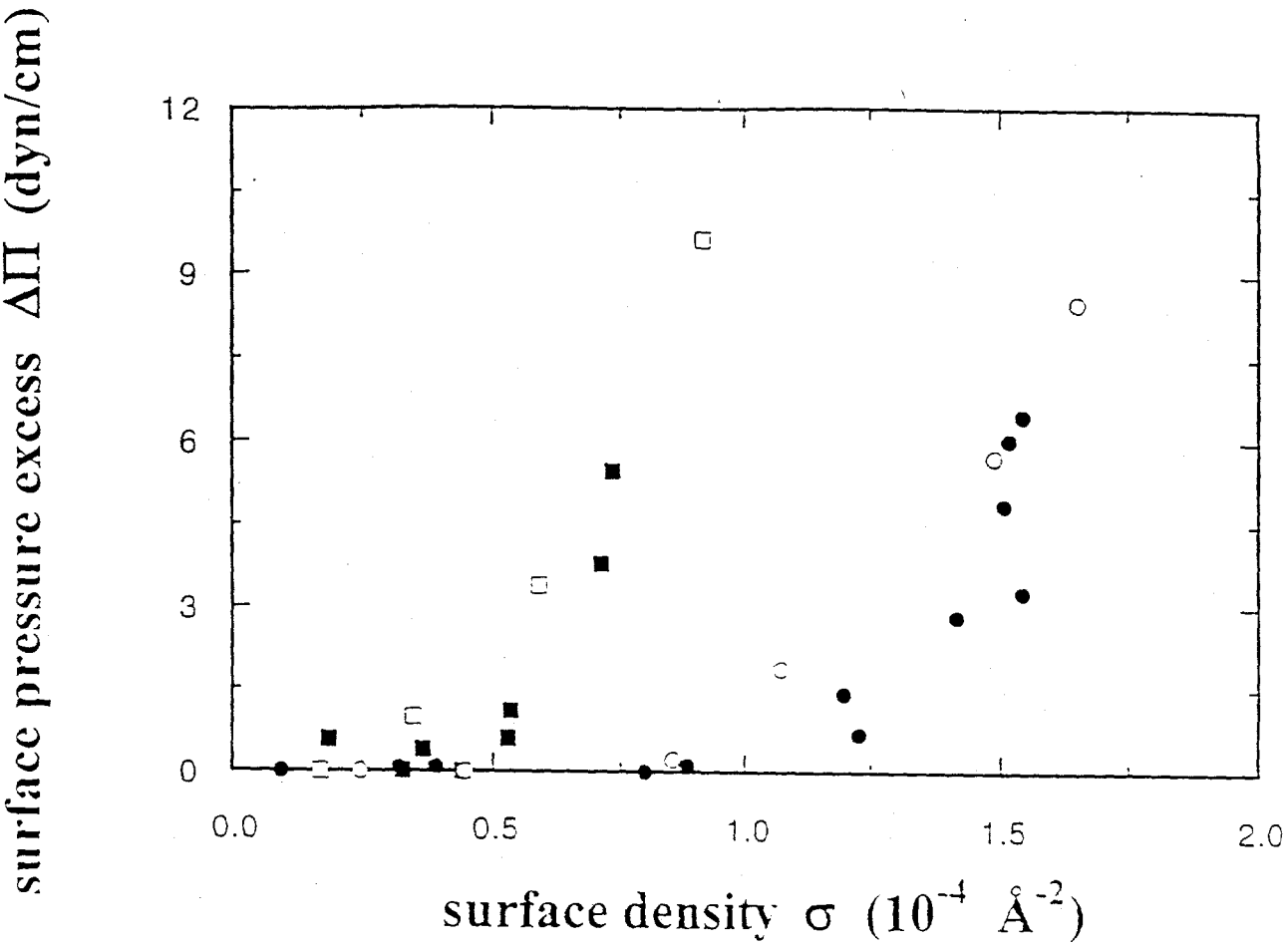
surface pressure excess ΔΠ (dyn/cm)
12
9
6
3
0
0.0
0.5
1.0
1.5
2.0
surface density σ (10^-4 Å^-2)